[OFFICIAL]

An investigation into wear of media in stirred media milling

Tinashe Arison Manzini
(1902685)

A dissertation submitted to the Faculty of Engineering and Built Environment, University of the Witwatersrand, Johannesburg, in fulfilment of the requirements for the degree of Master of Science.

Johannesburg, 2025.

Supervisor**: Professor Murray Mulenga Bwalya (University of the Witwatersrand)**

Abstract

The beneficiation of low grade and finely disseminated ores has increased the adoption of stirred media mills because of their superior energy efficiency compared to tumbling mills. However, the highly dynamic and energy intensive milling environment accelerates grinding media wear, affecting both process efficiency and operating costs. This study investigated the wear behaviour of ceramic grinding media in stirred media mills through combined experimental and numerical (Discrete Element Method, DEM) approaches. The work aimed to identify operating conditions and media interactions that promote wear and to evaluate the capability of DEM to analyse energy transfer mechanisms associated with media wear. Direct wear quantification was not possible due to limitations such as uncharacterised media, the absence of the slurry phase, and the inability to resolve separate normal and tangential forces required to compute shear impact energies.

Experimental tests were conducted using a laboratory-scale stirred mill with ceramic beads as grinding media. Specific energy input was varied at 5, 10, and 20 kWh/t, while feed sizes of -1180 + 850 μm and -650 + 425 μm were used to evaluate their influence on grinding performance and wear. Results showed that increasing specific energy input produced finer products, confirming the relationship between energy input and grinding efficiency. Coarser feed exhibited higher power draw and torque due to increased resistance and viscous losses, consuming more energy for the same milling duration. Wear tests performed on the coarse feed for 2 h and 4 h showed measurable bead degradation, with a linear wear-rate trend under the tested conditions.

DEM simulations revealed predominantly low-energy collisions through the collision energy spectra, consistent with abrasion dominated milling environments. Predicted power draw values were 13% to 34% lower than experimental measurements, primarily due to the exclusion of the slurry phase, which typically accounts for up to 34% of total power losses in stirred mills. Despite these constraints, DEM reproduced realistic energy transfer trends, complementing the experimentally observed trends. The study confirms that integrating experimental data with DEM analysis offers valuable insights into the mechanisms governing energy dissipation and media wear in stirred milling environments. Further work should employ DEM software capable of resolving stress fields for integration into energy-based wear models, include detailed characterisation of ceramic media properties, and incorporate breakage models to establish a more comprehensive representation of the grinding process.

Declaration

I declare that this dissertation is my own, unaided work. It is being submitted for the Degree of Master of Science at the University of the Witwatersrand, Johannesburg. It has not been submitted before for any degree or examination at any other University.

____

(Signature of candidate)

20 day of October 20 25 at University of Witwatersrand

____

(Signature of supervisor)

20th day of October 20 25 at Witwatersrand University

Dedication

I dedicate this work to my parents, Mr and Mrs Manzini, for their unwavering love, support, and devotion to my personal and career growth. Your belief in me has been a constant source of strength, and I am forever grateful for your sacrifices and guidance.

To my siblings, Allan and Rumbi, this is also for you. Your belief in me, even in moments when I stumbled, has always lifted me up. Thank you for always being there, offering support, and inspiring me to keep going.

A special thank you to my uncle, Omega, whose mentorship has played a pivotal role in my career development. You took me under your wing and showed me the ropes, and for that, I am deeply thankful.

May God continue to bless you all with long, happy, and fulfilling lives. I love you all.

Acknowledgements

I would like to express my deepest gratitude to my supervisor, **Professor Murray Mulenga Bwalya** for his insightful guidance and unwavering support throughout the research. His dedication and willingness to go above and beyond have been pivotal in helping me navigate challenges and refine my work.

I would also like to acknowledge the leadership and team members of the **Mintek Mineral Processing Department** for their invaluable support, particularly with providing equipment, resources, and assistance during my experimental work. Your contributions made a significant difference in the success of my research.

A special thanks to my research mate, **Oliver**, for your camaraderie and collaborative spirit. Your support and feedback have been invaluable throughout this journey.

CONTENTS

List of figures

List of tables

Abbreviations

Symbol/Abbreviation	Description	Unit
DEM	Discrete Element Method	-
PFC	Particle Flow Code	-
FISH	Flexible Interaction Script for Humans	-
JKR	Johnson-Kendall-Roberts	-
LSD	Linear Spring Dashpot	-
e	Coefficient of restitution	-
P_{80}	Product size at which 80% of the particles pass	μm
E_m	Specific energy input	kWh/t
$E(t)$	Total energy input	J
m_p	Mass of a product	kg
N	Rotational speed	rpm
T	Torque	Nm
SE	Stress energy	J
ρ	Density	kg/m³
Ψ	Grinding media filling ratio	%
v	Particle velocity	m/s
c	Solids concentration	%
HV_{GM}	Vickers hardness of grinding media	GPa
HV_P	Vickers hardness of product particles	GPa
Δ	Incremental change	-
F	Force	N
μ	Coefficient of friction	-
K_n	Normal stiffness constant	N/m
θ	Angular position	rad
I	Moment of inertia	kgm²
P	Power draw	W
ω	Angular velocity	rad/s
D_{50}	Median particle size (50% passing)	μm
D_{80}	Size below which 80% of the particles fall	μm

Chapter 1 Introduction

1.1 Background

Grinding is the last stage of comminution in which particles are reduced in size by a combination of impact, abrasive, and attrition forces in grinding mills. Grinding mills normally contain a charge of loose crushing bodies referred to as grinding media which act as a means of transferring energies required for comminution. Grinding mills can be classified on the basis by which energy is imparted to the charge, i.e., tumbling mills and stirred mills (Wills & Napier-Munn, 2006).

There has been a growing need to comminute ore particles to fine and ultrafine ranges in recent times in the mining industry context (Jankovic, 2003). Reason being majority of the ores that needed coarse grinding to liberate valuable minerals have been depleted. Concentrators now must treat ores that require grinding to finer sizes for adequate liberation of minerals and optimal recoveries (Ndimande *et al*., 2019). Stirred mills were adopted as the technology of choice in the finer size range of comminution, mainly due to being more energy efficient than tumbling mills. This technology was first introduced in 1953, and their use has steadily increased (Jankovic, 2003).

Energy consumption in tumbling mills (ball mills) rises sharply when grinding below 75 μm and below 30 μm, grinding using ball mills becomes uneconomical. Consequently, the use of stirred mills has become more prevalent in fine and ultra fine grinding because these mills deliver higher power intensity and better energy efficiency than tumbling mills (Lehto *et al*., 2016; Radziszewski, 2013; Altun *et al*., 2023). Notwithstanding the improved energy efficiency nature of stirred mills, the cost of grinding still represents a significant portion of concentrators' operating cost (Moema *et al*., 2009). This cost can be divided between energy (50%) and liner/grinding media wear (50%). Therefore, concentrators should always strive to continually optimise the grinding efficiency in general.

In the industrial application of stirred mills, it was established that characteristics of grinding media, mill geometry, and operating conditions have significant effects on the grinding efficiency. Studies showed that the tip speed of stirrer elements as well as the density and the size of grinding media affect the specific energy input (net energy input related to mass of product) required to achieve a certain product fineness (Kwade *et al*., 1996; Becker *et al*., 2001). From literature, it has been observed that grinding media characteristics play major role in achieving the desired product fineness, therefore it invariably represents a key optimisation opportunity.

In stirred mills, grinding media can be broadly classified by material and shape. Common materials include metallic media (steel, chrome steel, stainless steel) and non-metallic media (ceramics, alumina, zirconia, glass). Ceramic grinding media (ceramic beads) is mostly utilised within the stirred milling technology to maximise energy efficiency and reduction of product particles contamination (Kwade & Schwedes, 2007). However, the magnitudes of cost of energy and wear during milling invariably creates a need to continually improve the economics of the process. Wear in grinding process affects the desired physical and mechanical properties (size distribution and shape, hardness, and impact toughness) of ceramic beads. This will in turn impacts the comminution behaviour in the stirred mills. Wear of ceramic beads in the grinding process is an inevitable process; however, it is the way in which they wear which has impact on the grinding efficiency (Hassall *et al*., 2016).

Focus of current study is on predicting ceramic beads wear in stirred mills which is an area of study that is not well documented in literature. Accurate wear prediction capability provides an avenue to optimise grinding efficiencies in operation as far as ceramic bead selection is concerned and key operating parameters in general. To be able to predict the wear process, an understanding of the wear environment is required which is influenced by flow patterns, energy absorption and collisional environment (Radziszewski, 2002). Discrete Element Method (DEM) has been employed by various researchers to understand the particle flow dynamics and interactions within stirred mills (Cleary *et al*., 2015; Cleary *et al*., 2006; Sinnott *et al*., 2006; Ndimande *et al*., 2019). These studies have shown that grinding action is almost entirely dominated by abrasion and that energy dissipations associated with particle interactions is dominated by shear energies.

DEM predicted energy dissipations were used as basis for a total wear model showing encouraging results for the cases studied as compared with the Bond abrasion test (Radziszewski, 2002). Zhao proposed a shear impact energy model of erosion suitable for both dilute and dense particle flows based on the shear impact energy of particles in DEM simulations (Zhao *et al*., 2017). The shear impact energy model was later extended by Xie and Zhao (2022) to the milling environment to predict grinding media wear in a pilot planetary ball mill.

1.2 Problem statement

Operating costs in milling operations are mostly affected by energy consumption and wear. Grinding media wear is by far the most significant factor affecting operating costs within the tumbling and stirred mills' environments. Uncontrolled wear of ceramic beads in stirred mill affects the specific energy input and further exacerbates the costs of energy and wear itself. This uncontrolled wear will also affect product fineness and ultimately affect metal recovery. The mining industry is faced with severe challenge of economic media selection. Ceramic beads in stirred mills do offer a combination of low wear rate, high energy efficiency and low unit cost. While ceramic media can be beneficial in stirred mills for their efficiency in fine and ultra fine grinding, they can become uneconomical in certain situations due to factors like high cost and wear rates, especially in larger-scale operations. This has limited the application of such energy efficient grinding technology such as the Isa Mill and restricted its application to regrinding and ultra-fine milling only (Curry & Clermont, 2005).

Many ceramic bead producers have introduced several products to meet the industries growing demand. The range of formulations and technologies employed are rather broad. In fact, the only consistent factor is probably the size ranges offered; usually 2-3, 3-4, 4-5 and 5-6 mm. This range of formulation and chemistry has significant influence on the nature and behaviour of the bead. Although the formulations can vary significantly, fundamentally they are all based on three basic oxides, silica (SiO_2), alumina (Al_2O_3) and zirconia (ZrO_2). The large variety of available products, each with differing microstructures and mechanical properties, has made the selection of fit-for-purpose media increasingly difficult for operations. Identifying the most suitable media type through experimental testing alone is both time-consuming and costly. Developing predictive tools capable of rapidly evaluating different media types under varying process conditions has therefore become essential.

Predicting media wear is particularly challenging because of the dynamic and multiphase nature of stirred milling, where interactions occur between the grinding media, slurry, and mill surfaces. Existing approaches to estimate wear are either empirical or based on simplified correlations that do not adequately capture energy dissipation mechanisms at the particle level. Consequently, the development of models that can reliably link energy input to media wear is essential to improving process optimization. Numerical modelling techniques such as the Discrete Element Method (DEM) provide a potential framework to evaluate these relationships, offering the capability to simulate particle interactions and energy transfer processes at micro-scale if properly calibrated to represent the actual milling process.

1.3 Research objectives

The overall aim of this study is to investigate grinding media wear behaviour in stirred media mills using experimental and numerical (DEM) approaches. The study specifically focuses on identifying the operating conditions and dominant grinding media interactions that lead to wear. The insights obtained from this investigation provide a foundation for optimisation and design considerations in stirred media milling operations.

To achieve this aim, the study entails the following objectives:

- To employ DEM to analyse grinding media interactions and infer potential wear mechanisms by examining key parameters such as contact forces, collision energy spectra, and power dissipation.

- To use DEM generated stress and energy distributions to identify regions of high wear potential within the stirred media mill.
- To compare DEM results with experimental data to validate the feasibility of using DEM for grinding media wear analysis in stirred media milling.
- To evaluate how variations in operating parameters, such as energy input and feed size, influence both grinding performance and media wear.

1.4 Dissertation layout

This dissertation is structured into five main chapters, each of which builds on the previous to provide a logical and comprehensive information of the study on wear of grinding media in stirred media mills. Short summaries of what the chapters entail is given in the following subsections.

Chapter 1 Introduction

Introduces the research objectives and background of the study, outlining the significance of the investigation into the wear of grinding media and the key factors influencing the grinding process, such as specific energy and feed size.

Chapter 2 Literature review

Provides a review of relevant concepts and findings from the available wealth of stirred media milling literature, discussing the critical role of specific energy in the grinding process, and examining the effects of other parameters. This chapter also reviews previous research on media wear, energy dissipation, and the use of DEM simulations in grinding studies, setting the scene for the study covered in subsequent chapters.

Chapter 3 Methodology

Describes the methodologies and materials used for both the experimental studies and DEM simulations. It outlines the experimental setup, the key variables studied, and the calibration process used to align the DEM tool with the experimental data.

Chapter 4 Results and discussion

Analyse and discuss findings from both the experimental work and simulations. Key metrics such as specific energy, feed size, power draw, collision energy spectra, and wear are discussed. This chapter also highlights the challenges faced during the experimental work and the insights gained.

Chapter 5 Conclusions and recommendations

Provides conclusions, summarising the key findings from the study and discussing the implications of the results. The chapter also includes recommendations for future research to address the limitations faced in this study.

References

Lists all the sources cited throughout the work

Appendices

Contains additional information such as experimental data, pictures, and all other supplementary information gathered during the course of the study to complement the main parts of the dissertation.

Chapter 2 Literature review

2.1 Introduction

In mineral processing, fine and ultrafine grinding has become increasingly necessary in many operations to improve recovery and grade. The shift in minerology of ores from relatively coarse to fine-grained has necessitated the need to grind finer. To cope with very fine grinding to below a P_{80} of approximately 20 μm, stirred milling technology to a greater extent, is the size reduction technology of choice (Jankovic, 2003; Lehto *et al*., 2016; Ndimande *et al*., 2019; Sinnott *et al*., 2006; Taylor *et al*., 2020).

Stirred milling technology prevails in notable aspects such as energy efficiency and power intensity, where ball mills fall short (Jankovic, 2003; Radziszewski, 2002). The first of the many stirred mills configurations was introduced by Klein and Szegvary in 1928 (Kwade & Schwedes, 2007). Since then, various but equivalent configurations have come to the fore. In principle, stirred mills utilise stirrers consisting of a shaft with pins, disks or helical screw (see Fig 2.1 for illustration). They can be categorised by their shell orientations: vertical such as the Sala Agitated Mill (SAM) or horizontal such as the IsaMill (Radziszewski, 2013).

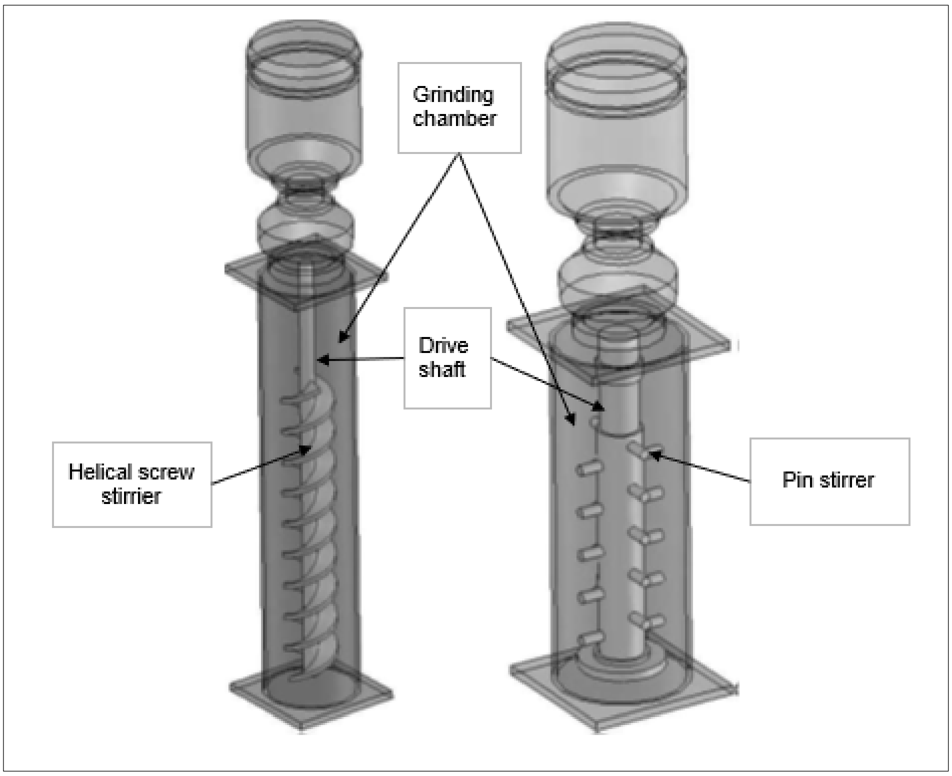

Figure 2.1. Schematic illustration of common stirred mill configurations showing (left) a helical screw stirrer and (right) a pinned stirrer (adapted from Sinnott *et al*., 2006).

Stirred mills utilise relatively small media to achieve fine and ultra fine product sizes due to the increased surface area. This is a fundamental limitation of ball mills which cannot employ smaller media sizes because of diminishing gravitational effect on tumbling media charge. In contrast, stirred mills overcome this limitation by applying momentum to the media with an impeller which enable utilisation of small beads on the scale of millimetres (Taylor *et al*., 2020). Characteristics of media used (physical and mechanical characteristics) are part of key determinants of efficient milling or grinding processes.

Due to the abrasive environment presented by the stirred milling process, grinding beads are bound to wear and in turn lose the required properties for efficient size reduction. Periodic replenishment of beads ensures a constant size distribution of beads is maintained in the mill. However, the wear nature if not controlled, the economics of the milling processes is heavily impacted. For this this reason, operational parameters need to be optimised to ensure an efficient and cost-effective operation. To be able to optimize both during design and operational stages, a good understanding of the motion and dynamic physical structures of charge during the milling process is important.

Development of numerical modelling tools such as Discrete Element Methods (DEM) has contributed immensely to the understanding of flow and dynamic interaction of particulate systems in mills aiding mill designers, operators, and media manufacturers to measure, analyse and control the various milling outputs more precisely and accurately.

In this literature review, the theory of stirred media mills and media wear is reviewed. Similarly, the numerical modelling of stirred milling process is also reviewed.

2.2 Stirred media milling

Metal resources, particularly base metal ores are becoming more fine-grained and refractory. Consequently, mineral liberation would require grinding to increasingly finer size ranges. To cope with very fine grinding to below a P_{80} of approximately 20 μm, stirred milling technology has been adopted from other industries (Jankovic, 2003).Typical ore quality has declined over the years, fine and ultrafine grinding become increasingly necessary in many operations to improve recovery and grade (Jankovic, 2003; Radziszewski, 2013).

This technology prevails in notable aspects such as energy efficiency and power intensity, wherein other technologies like the ball mill fall short (Jankovic, 2003; Radziszewski, 2013). Stirred mills utilises stirrer elements consisting of a shaft with pins, helical screw or disks. Stirred mills can be categorised by their shell orientations i.e. vertical or horizontal, such as the Sala Agitated Mill (SAM) or the IsaMill (Wills & Napier-Munn, 2006).These mills are used where a fine product is demanded and are energy efficient in the fine size range. The higher energy efficiency of stirred mills comes from efficient utilization of smaller grinding media (Taylor *et al*., 2020).

The first of the many stirred media mills configurations was introduced by Klein and Szegvary in 1928 (Kwade & Schwedes, 2007). Since then, various but equivalent configurations have come to the fore. A typical horizontal oriented stirred media mill is shown in Figure 2.2. Generally, stirred media mills can take any one of the 3 configurations with respect to stirrer design namely, disc agitator, pin-counter pin agitator and helical screw.

The simplest stirrer geometry being the disc geometry. They are distinguished by the designed power intensity. For tower mills, the power intensity is $20 - 40\ kW/m^3$; for a vertical pin stirrer mill it is $50 - 100\ kW/m^3$; and for horizontal stirred mills it is around $300 - 1000\ kW/m^3$. The energy intensity for horizontal stirred mills is an order of magnitude higher than that of vertical ones due to the simpler vertical mills design which does not require a pressurized seal (Wills & Napier-Munn, 2006).

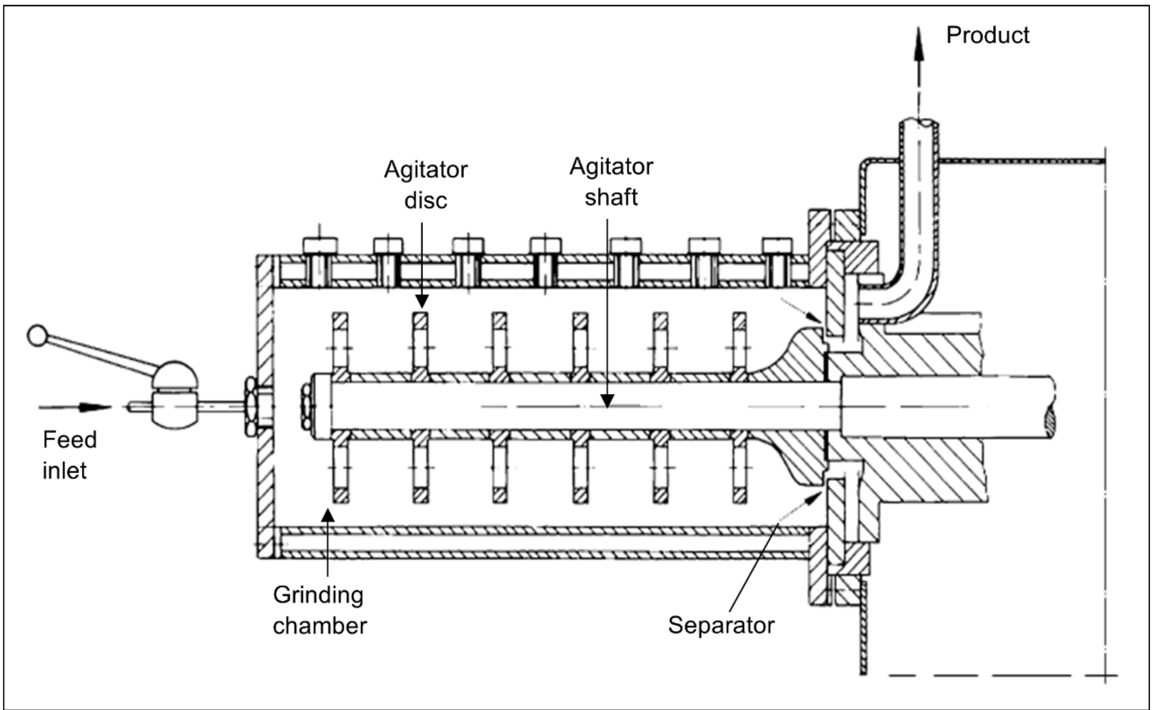

Figure 2.2. Schematic of a stirred media mill showing grinding chamber, agitator, inlet, outlet, and separator (adapted from Kwade & Schwedes, 2007).

2.2. 1 Principle of operation

Stirred media mills mostly operate wet since the water promotes mixing and disperses product particles to suppress re-agglomeration (Taylor *et al*., 2020; Theuerkauf & Schwedes, 2020). Up to 85% of the mill chamber volume is filled ceramic beads which effect grinding process (Blecher *et al*., 1996). Both ceramic beads and solid suspension(slurry) are mechanically transferred into the grinding chamber. The beads are typically in the size range of 1- 6 mm, depending on the mill type and operating conditions (Hassall *et al*., 2016).

Regardless of the nature of stirred media mill utilised, the underlying grinding mechanisms that occur are fundamentally similar. The stirrer transfers momentum to the grinding media closest to it, accelerating the media to a significant fraction of the stirrer tip speed (Cleary *et al*., 2006; Sinnott *et al*., 2006). Circumferential velocities of the stirrer-tips of up to $20\ m/s$ are used leading to centrifugal accelerations of more than 50 times the acceleration due to gravity (Kwade *et al*., 1996; Theuerkauf & Schwedes, 1999).

Grinding media circulates around the stirrer, and by collision transfers kinetic energy to other grinding media radially outwards, and so on until the chamber wall is reached, creating a shear rate distribution across the chamber radius (Cleary *et al*., 2006; Sinnott *et al*., 2006). Colliding ceramic beads with different velocities transfer momentum to particles trapped in between, with the intensity that the particle experiences dependent on the relative momenta of the media (Taylor *et al*., 2020).

The zone of highest energy density, called milling zone is said to be located close to the stirrer tip and has an assumed thickness of about approximately 25 mm (Cleary *et al*.,2006; Sinnott *et al*., 2006; Kwade & Schwedes, 2007). Approximately 90% of the energy applied is dissipated in 10% of the chamber volume, close to the stirrer tip (Blecher *et al*., 1996; Taylor *et al*., 2020). Figure 2.3 shows an example of a flowsheet including a stirred media mill. In this operation, 60–75% of the mill free volume is filled with ceramic beads, typically $1-6\ mm$ in size with a density of about $4\ \ g/cm^3$. The scalping cyclone directs the coarser cyclone underflow to the HIGmill for further grinding, while the finer overflow proceeds to the rougher concentrate. The HIGmill reduces particle size to improve mineral liberation, and the ground slurry is conditioned before entering flotation. This circuit configuration allows finer grinding without sacrificing overall throughput and enhances downstream flotation efficiency (Lehto *et al*., 2016).

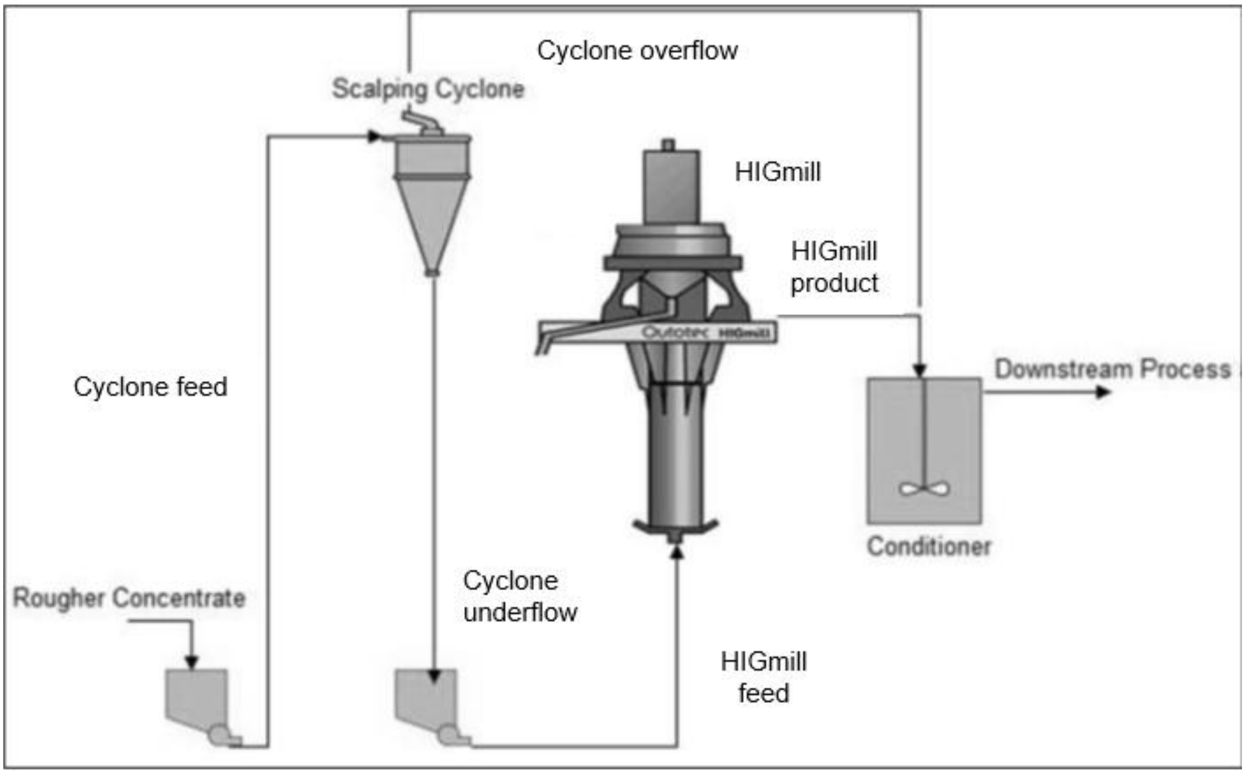

Figure 2.3.Typical flowsheet including a vertical stirred media mill showing scalping cyclone, HIGmill, conditioner, rougher concentrate, and downstream flotation process (adapted from Lehto *et a*l., 2016; Outotec, 2015)

2.2. 2 Stirred media milling parameters

There is a considerable number of parameters that influence grinding performance in stirred media milling. Albeit not all of them are of major importance. Jankovic (2003) cited that up to 44 parameters were identified to influence the grinding process from previous work. For any application, there is a certain set of parameters which gives the optimum grinding outcome or product fineness. To find the parameter set which is the most favourable for any grinding application, usually experiments using a laboratory or other small-scale mill are conducted (Kwade & Schwedes, 2007).

The more important parameters as identified by various authors, includes specific and stress energy, mill design, grinding media characteristics, stirrer speed, solids concentration, media filling and product particle characteristics (Yang *et al*., 2017; Ohenoja & Illikainen, 2015; Jankovic, 2003; Becker & Schwedes, 1999). The parameters are discussed in the following sub-sections.

a) Specific energy and stress energy

Specific energy is the net energy input related to mass of product and was identified as the main influencing parameter on comminution result for a wide range of operating parameters (Becker *et al*., 2001; Kwade & Schwedes, 2007). Specific energy describes the influence of mill size, tip speed of stirrer, solids concentration and density of grinding media as shown in Figure 2.4. The figure demonstrates that across a range of parameters tested, specific energy input and product fineness show a linear relationship, reinforcing the significance of specific energy input in stirred milling optimisation. Kwade and Schwedes (1996) stated that the production capacity is proportional to the power input into the grinding chamber and inversely proportional to the specific energy required for the demanded product quality. This makes it a primary metric for optimizing milling operations, aiming to reduce energy consumption while achieving the desired product size. Specific energy input, E_m , for a grinding process is determined by equation 2.1, assuming negligible grinding media wear.

$$E_m = \frac{E(t)}{m_p} = \frac{\int_0^t N(\tau)d\tau}{m_p} = \frac{\int_0^t (T(\tau) - T_0)2\pi n d\tau}{m_p} \tag{2.1}$$

Where $E(t)$ is the mechanical energy input, m_p is the mass of the solid ground product, N the power input, t the comminution time, T the torque measured during comminution, T_0 the no load torque, n the number of revolutions of stirrer and τ is instantaneous time variable.

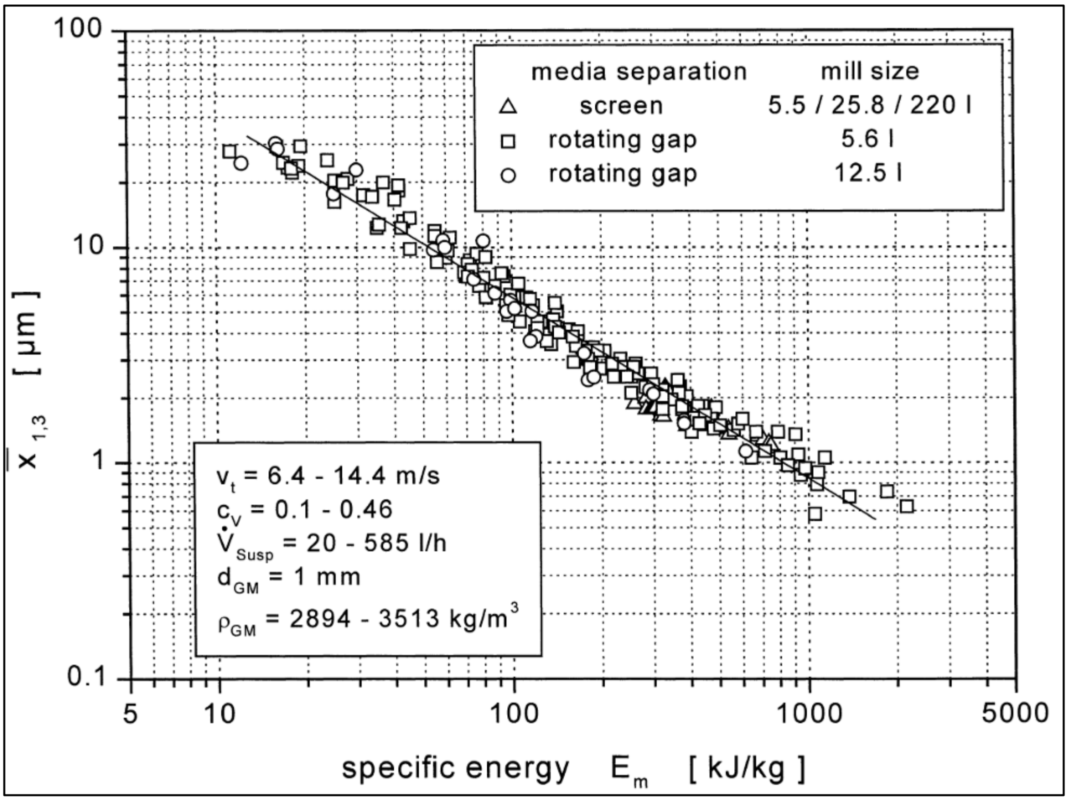

Figure 2.4. Relationship between product fineness and specific energy input for limestone comminution under different media separation methods (screen and rotating gap) and mill sizes. Increasing energy input leads to finer product size under the reported test conditions (reprinted from Kwade & Schwedes, 2007).

Another parameter closely related to specific energy is stress energy. While specific energy represents the total energy consumed, stress energy specifically focuses on the energy transferred to the particles during collisions. Stress energy of the grinding media, SE_{GM}, describes the effect of the three parameters, namely, stirrer tip speed, grinding media density and grinding media size in combined form. Stress models were developed to better describe the physical processes in the stirred media mills and stress energy is key consideration in these models (Kwade & Schwedes, 2007). Becker (2001) stated that comminution result is mainly determined by the stress energy at each stress event. Stress energy is estimated as,

$$SE \propto SE_{GM} = d_{GM}^3 . \rho_{GM} v_t^3 \qquad (2.2)$$

Where SE is the stress energy, SE_{GM} is stress energy of the grinding media, d_{GM} and ρ_{GM} are grinding media diameter and density respectively and v_t is stirrer tip speed.

b) Mill design

The main structure of the stirred media mill includes power source, a cylinder shell, and a stirrer or agitator, which drives the slurry and grinding media inside the mill to grind the product particles. With respect to power, the amount of installed power must be sufficient to achieve the desired grinding result. However, the installed power must be efficiently utilised. A key consideration in improving the efficiency or power draw is the design of the cylinder shell. Ford and Naude (2021) showed that adding a disc liner on the shell when operating with pin and disc type stirrers significantly improved the mill power draw. Altun *et al*. (2014) presented results from a horizontal pilot scale stirred mill which showed an improvement in energy efficiency when diameter of mill was increased.

As highlighted earlier, another important design consideration is the stirrer design. Altun *et al.* (2014) also investigated the effects of stirrer design on the grinding performance, which varied with change of stirrer type. Cayirli *et al*. (2024) highlighted that disc designs are effective for horizontal mill orientation, while pin designs are effective for vertical mill orientation. Sinnott *et al*. (2006) found that media flow patterns within a tower and pin mill are very different as are their distribution of energy absorption which control comminution of product particles. The extensive literature on mill design factors underscores their importance in achieving an efficient grinding process.

Table 2.1. Different stirred mills available in the market (adapted from Ndimande *et al*., 2019).

Mill Type	Manufacturer	Orientation	Agitator Type
Vertimill	Metso	Vertical	Helical screw
SMD	Metso	Vertical	Impellers
Tower mill	Kubota	Vertical	Helical screw
Isamill	Xstrata	Horizontal	Rotor discs
HIGmill	Outotec	Vertical	Rotor discs

A list of the main stirred mills currently available, showing their manufacturers, orientations, and agitator types is shown in Table 2.1.

c) Stirrer velocity

Stirred media mills are advantageous for their high stirrer speeds of up to $20\ m/s$, (Kwade & Schwedes, 2007), which results in high power intensities within the grinding chamber: for tower mills, the power intensity is $20 - 40\ kW/m^3$; for a vertical pin stirrer mill it is $50 - 100\ kW/m^3$; and for horizontal stirred mills it is around $300 - 1000\ W/m^3$ (Wills & Napier-Munn, 2006).There exist an optimum velocity for every application within the optimum parameter set. Stirrer velocity hugely influences stress intensity and the same is true for the overall grinding performance.

Jankovic (2003) studied the effect of stirrer speed on Pilot Tower mill, High Speed Netzch and Pilot SAM all showing different responses to increase in speed. In a study conducted by Yang (2017) on a vertical stirred mill, relatively lower speed was determined to be better appropriate for the evaluated operating conditions. Guo *et al*. (2022) showed that the mean power of the motor demonstrated a good correlation with stirrer tip speed. Cleary *et al*. (2015) showed how variation in stirrer speed impacted the media flow structures in a Isamill which influences the grinding result.

The influence of stirrer speed on relation of product fineness and specific energy is illustrated in Figure 2.5. At constant specific energy inputs, the particles become coarser with increasing stirrer tip speed which is a result of a change in stress intensity (Kwade & Schwedes, 2007). Based on the demonstrated work in literature, stirrer speed is a pivotal factor in determining the efficiency and outcomes of the grinding process in stirred media mills. The specific impact of stirrer speed varies depending on the type of mill and the operating conditions (Cleary *et al*., 2015). While higher stirrer speeds can enhance stress intensity and improve grinding performance, they must be carefully optimized to avoid over-grinding or energy inefficiency. The correlation of stirrer speed, power consumption, and product fineness underscores the importance of identifying the optimal speed for each application (Sinnott *et al*., 2006), ensuring that the grinding process is both energy-efficient and effective. Kwade and Schwedes (2007) concluded that stirrer velocity must be determined in a way that the power input is as high as possible for the grinding media size chosen.

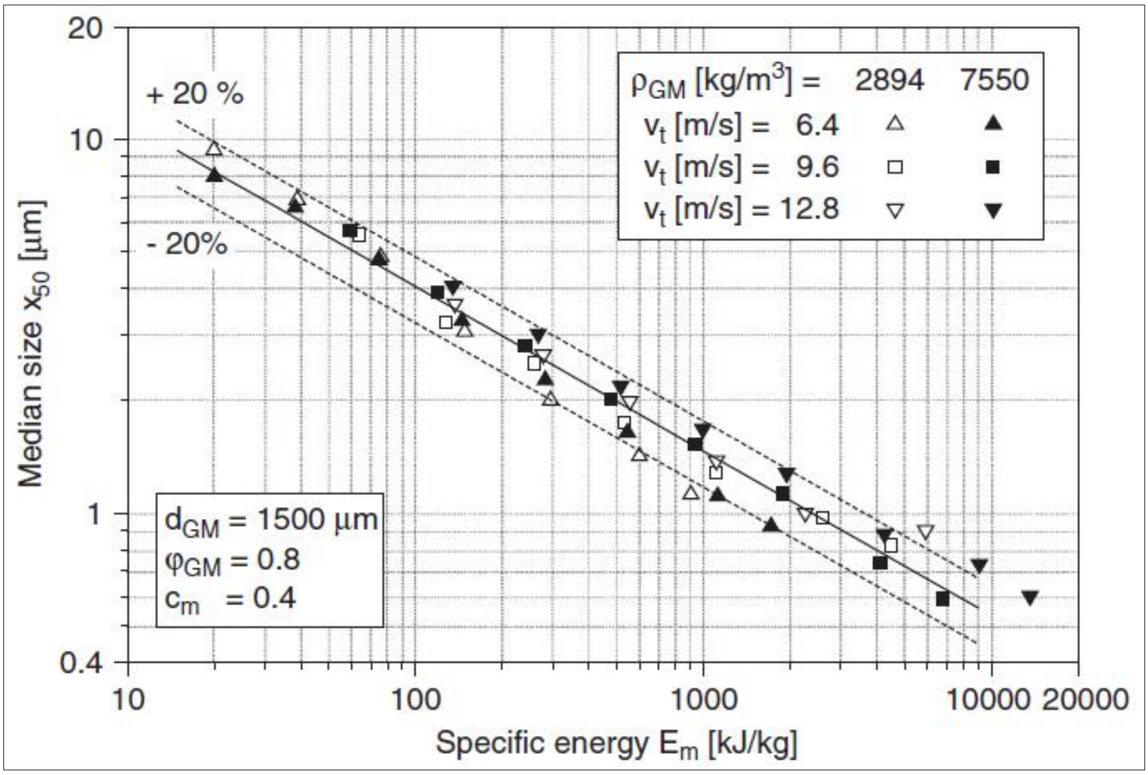

Figure 2.5. Effect of stirrer tip speed on the relationship between product fineness and specific energy input for different grinding media densities. Higher stirrer speeds shift the curve towards finer sizes at the same specific energy (reprinted from Kwade & Schwedes, 2007).

d) Product particles characteristics

Product particles characteristics such their physical properties play an important role in the stirred media milling outcome as noted by (Kwade & Schwedes, 2007). The harder the ore particles the more energy required to achieve the demanded product quality. The impact of ore hardness on ceramic media wear was investigated was by Becker and Schwedes (1999). Grinding media wear was found to be most significant when the ratio of media hardness to product particles was lowest (HV_{GM}/HV_P). With respect to modulus of elasticity, Becker *et al*. (2001) found that for product materials with a high Young's modulus e.g., fused corundum, the transferred energy strongly depends on the Young's modulus of grinding media, whereas the transferred energy is nearly independent of the Young's modulus of grinding media for weak product materials. An area that is not extensively covered is the size of the feed particles which facilitates efficient grinding. Kwade and Schwedes (2007) noted that the media size need to closely match with feed particles, or else much of the energy will be lost in interactions that does not affect actual grinding.

e) Solids concentration

Solids concentration, or slurry density, also plays a critical role in the outcome of the stirred media milling process. It was observed that for pilot Tower and Netzch mills, the grinding efficiency increased with slurry % solids over the range tested (Jankovic, 2003). The finding was attributed to decrease in power draw caused by buoyancy effects and the increase in the number of particles in the mill resulting in an increase in probability that a particle will be broken. Solids concentration also influences movement of grinding media and therefore stress number and especially the stress intensity. But, if the suspension is too high, the grinding efficiency drops, because the movement between the grinding media and the suspension decreases to a minimum, and parts of the grinding chamber cannot be activated by the stirrer anymore.

f) Grinding media filling ratio

The grinding result is also influenced by the ratio of grinding media filling. According to Kwade and Schwedes (2007), as the filling ratio rises, there are more media interactions and less spaces between the individual grinding media, which improves the grinding outcome. However, too narrow distances between the grinding media and their correspondingly reduced freedom of motion cause the grinding result to deteriorate beyond a specific filling ratio. There is an ideal filling ratio for each type of mill and grinding operation (Kwade & Schwedes, 2007).

Kwade and Schwedes (2007) also stated that for every filling ratio there is a distinct relation between the product fineness and the specific energy as shown in Figure 2.6 and that at a given specific energy with increasing filling ratio of the grinding media a finer product is achieved until an optimum is reached. In general, higher specific energies are required for lower filling ratio to obtain the size reduction that higher media filling ratio achieves (Altun *et al.*, 2013).

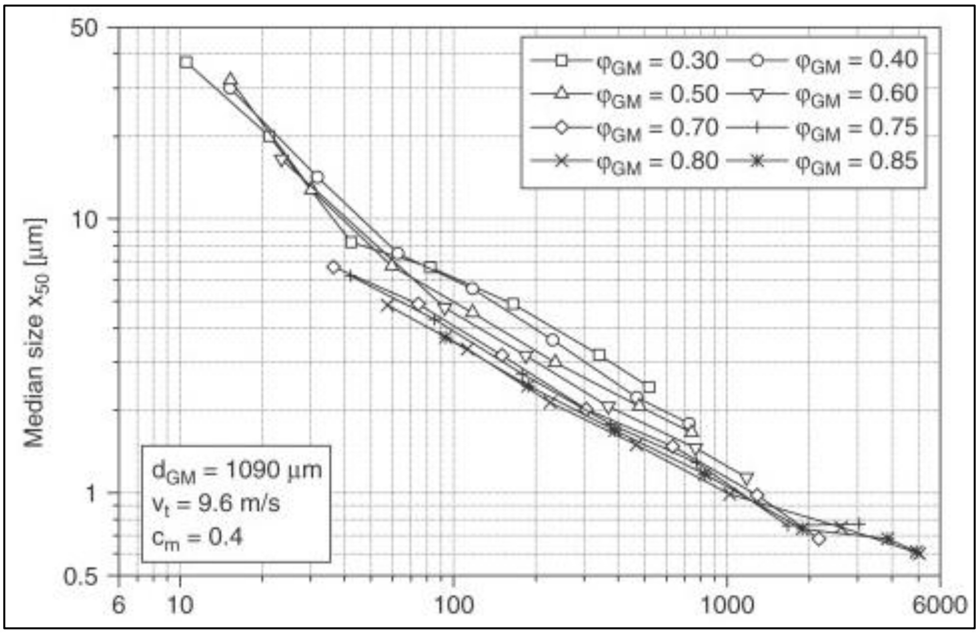

Figure 2.6. Effect of grinding media filling ratio on the relationship between product fineness and specific energy input. Higher filling ratios generally improve grinding efficiency,

resulting in finer product sizes at the same specific energy (reprinted from Kwade & Schwedes, 2007).

Larsson *et al*. (2020) further supported the notion that grinding result improves with increasing solids concentration when they observed that for grinding media fill rates of 40, 60 and 80%, increased fill rate results in fewer low energy collisions and increased contact frequency of grinding media. Sadler *et al*. (1975) observed a similar behavior in their study. They found that better grinding performances were achieved when the mill was operated at higher media fillings. In general, the mills are recommended to be operated at maximum media fillings due to the improved grinding performances.

g) Grinding media characteristics

Proper selection of grinding media type and size are two of major critical success factors for any stirred media milling application. Key characteristics such as hardness, fracture toughness, modulus of elasticity, density and size all affect milling efficiency and apart from size, these characteristics will vary across media types. Denser media improve energy transfer, while the size of the media influences the balance between grinding efficiency and product fineness. Smaller media allow for finer grinding but may reduce stress energy, while larger media relatively provide higher stress energies with a coarser product. The effect of these parameters on stirred media milling is reviewed in the following sub sections.

i. Effect of media size

As mentioned before in leading sections, grinding of particles in a stirred media mill is a result of continuous stressing of product particles by grinding media. For breakage to occur at a stress event, adequate stress energy should be transferred by the grinding media (Kwade & Schwedes, 2007).In the stress model of grinding media proposed by Becker *et al*. (2001), which has been successful in optimising the grinding conditions, size of media is one of the key parameters that influence amount of stress energy available at stress events.

Experimental tests conducted by Becker *et al*. (2001) showed that media size has a strong influence on the relationship between product fineness and specific energy input (Figure 2.7). With increasing grinding media size, the mass of a media increases and in turn the stress intensity also increases. However, the number of grinding media in the grinding chamber decreases simultaneously and thus the number of stress events increases too (Becker *et al*., 2001).

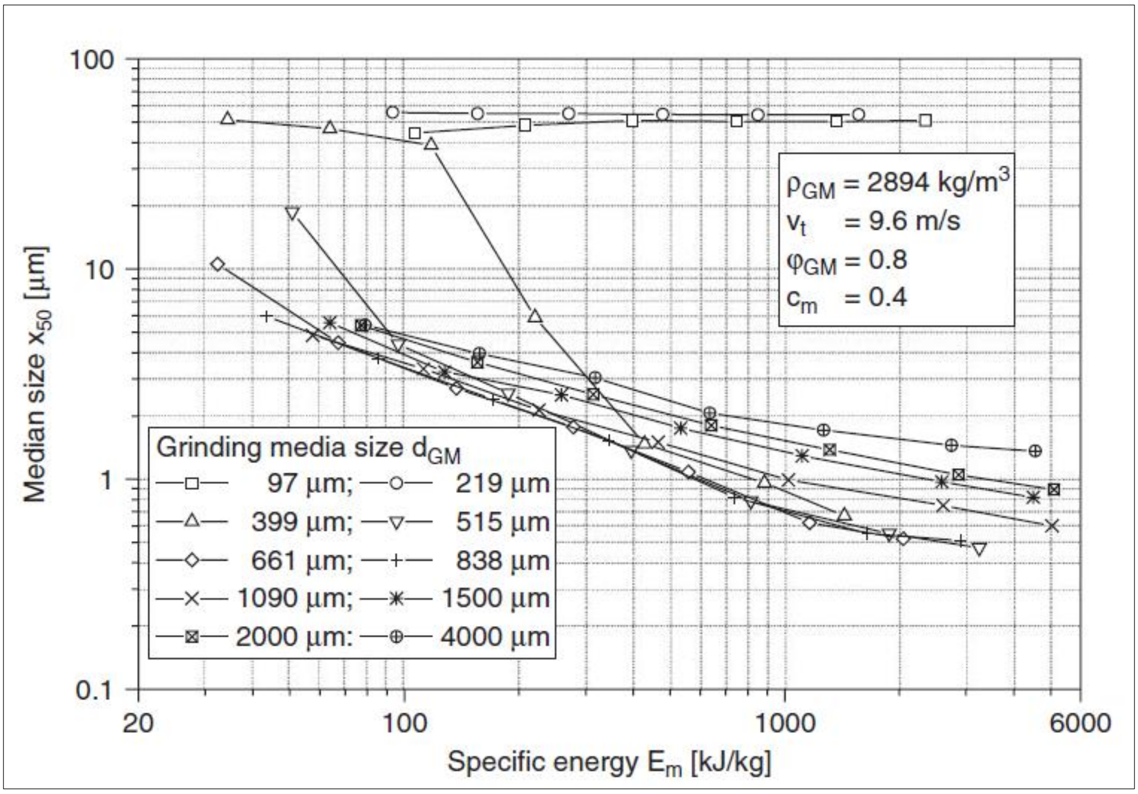

Figure 2.7. Effect of grinding media size on the relationship between product fineness and specific energy input. Smaller media sizes produce finer products at the same specific energy, while larger media sizes show reduced grinding efficiency (reprinted from Kwade & Schwedes, 2007).

A similar finding was observed by Mankosa *et al*. (1986), concluding that grinding kinetics are significantly affected by the media diameter/particle diameter ratio in the mill. For ore grinding, media size ranges from $2 - 6\,mm$ (Hassall, Nonnet, Keikkala, Komminaho, & Kotila, 2016).

ii. Effect of media density

Density was the first characteristic property of media that was explored. It is one of the key variables that impacts stress intensity from the stress model proposed by Becker *et al*. (2001) .For the same media size, the higher density media required less specific energy input for the same product fineness (Becker *et al*., 2001). A similar finding was obtained by Altun *et al*. (2023) , with alumina and steel beads. The results proved that the bead density affect the product fineness for a given specific energy or, the other way around, affect the specific energy which is required to produce a certain product fineness.

In their investigation, Ohenoja *et al*. (2013) observed that a media type with the highest density did not achieve the target product fineness, proving that every process has an optimum media density required for efficient grinding. In ore grinding environment, literature cites densities ranging from a low of 2.7 g/cm^3 to a high of 6.2 g/cm^3 are predominantly used, however a mid-range of densities are preferred (Hassall *et al*., 2016; Rule *et al*., 2008).

iii. Effect of Young's modulus

The modulus of elasticity or Young's modulus is key when assessing the material's deformation under stress as it measures its ability to resist deformation. Stirred media milling is a high stress environment, which requires media to be competent enough for a specific grinding process. Becker *et al*. (2001) observed that for the grinding of fused corundum, the transferred energy strongly depended on the Young's modulus of grinding media, whereas the transferred energy was nearly independent of the Young's modulus of grinding media for limestone.

The reason for the different grinding results when using grinding media with different modulus of elasticity is because energy which is transferred from the grinding media to the product particles depends on the modulus of elasticity. For the particles to break, sufficient energy must be passed from the grinding media to the product particles. If the energy transferred during each stress event is too low to break the particles, they will need to be subjected to multiple stress events for the breakage to occur (Kwade & Schwedes, 2007).

iv. Effect of media hardness

Hardness is described as a measure of the resistance of a material against plastic deformation. It an important mechanical property of media. Hardness and fracture toughness indicates media's wear resistance (Kotzé, 2012). Size reduction in stirred media milling is well understood to be affected via stressing of ore particles at stress events (Becker & Schwedes, 1999). During the stress event, not only the product particles are reduced in size but also the surface of the grinding beads is stressed and damaged. The rate at which the grinding beads surface wear is heavily depended on their hardness. Hardness is determined via indentation techniques namely the Vickers, Rockwell or Knoop tests.

v. Effect of fracture toughness

Grinding beads toughness is described as a measure of their resistance to fracture. Together with hardness, these two mechanical properties are major determinants of wear behaviour of grinding beads during the grinding process since media wear is a combination of surface plastic deformation, i.e. hardness, and surface micro-fracture, i.e. toughness (Kotzé, 2012). Correctness of fracture toughness measurements on media via indentation techniques is contested in literature, though valuable in comparable tests.

vi. Effect of composition and microstructure

Composition and microstructure play a significant role in wear behaviour of ceramic beads in tribological environments. Various compositions of ceramic beads exist, albeit fundamentally they are all based on three basic oxides, silica (SiO_2), alumina (Al_2O_3) and zirconia (ZrO_2) (Hassall *et al*., 2016). None of the media are based on the pure forms, either due to suitability, ease of processing or cost. Ceramic media of the same type are available in various compositions which affect their performance in similar application environment. As an example, Dogan and Hawk (1999) investigated performance of a range of Alumina ceramic beads with varying Alumina contents from 85% to 99.9999% and reported varying physical properties and wear performance. Moreover, grinding performance of ceramic beads can be improved by additions of certain dopants. It has been found that addition of a trace amount of Lu_2O_3 to alumina can evidently improve wear resistance by grain refinement and enhancing density (Wu *et al*., 2016).

The final microstructure of ceramic beads heavily affects its physical properties and wear performance. When selecting media type, microstructure must be considered. It is well founded in the literature that media types with fine grain sizes exhibit superior physical properties and wear characteristics. Dogan and Hawk (1999) concluded that in order to optimize abrasive wear resistance, the alumina grain size must be small, regardless of the alumina content. In addition, if second phases are present at the boundaries, they should be amorphous, with a composition high in alkaline earth constituents to reduce their softening point. Microstructure of ceramic media is determined via scanning electron microscopy (Reed, 1995).

2.3 Grinding media wear in stirred media milling

In stirred media mills, grinding media wear is by far the most significant wear problem (Toraman *et al*., 2019). Media wear is a key optimisation consideration in mining industry with regards to cost (Kotzé, 2012). Quantification of wear at plant scale is problematic due to dynamic operating conditions, continuous media replenishment, and challenges in accurately tracking media loss. For this reason, small-scale grinding tests are utilised.

Microstructure, composition, physical and mechanical properties of media such as size, density, sphericity, hardness, toughness etc. can be utilised to predict wear albeit to some extent. However, these parameters alone do not fully account for complex wear mechanisms such as impact, abrasion, and chemical interactions in slurry conditions, making direct wear quantification difficult. Media mass loss in grinding application which represents wear can be quantified based on equation (2.3) below (Kotzé & Bedesi, 2015).

$$w_{tot} = \frac{\Delta m_{GM}}{m_{GM}} \qquad (2.3)$$

Where w_{tot}, is total mass loss (%), Δm_{GM} is the difference between the starting and final media masses (g) and m_{GM} is initial media mass (g).

2.3. 1 Mechanisms of media wear in stirred media milling

The wear mechanisms of grinding media in stirred media mills are primarily dictated by the shear-dominant collisional environment, as demonstrated by studies carried out by various researchers (Larsson *et al*., 2020; Ndimande *et al*., 2019; Sinnott *et al*., 2006; Cleary *et al*., 2006). Grinding media follow a toroidal flow pattern, where particles experience low-energy, high-frequency collisions rather than high-impact breakage events as described by Sinnott *et al*. (2006) through a DEM simulation study.

Abrasion is the primary wear mechanism which occurs due to persistent surface contact between media, ore particles, and mill internals, causing gradual material removal (Sinnott *et al*., 2006). Attrition, which results from repeated low energy collisions, leads to surface fatigue and chipping over time (Ndimande *et al*., 2019). Unlike in ball mills, impact wear is secondary, as normal contact forces in stirred mills are significantly lower, with shear forces playing a more dominant role. The presence of slurry can lubricate interactions, reducing direct friction, but in some cases, it may accelerate chemical wear through tribochemical reactions (Sinnott *et al*., 2006). These insights are critical for optimising media selection and operational conditions to minimize wear and enhance grinding efficiency.

2.3. 2 Experimental and computational studies on media wear

Experimental studies on ceramic media wear in stirred media mills have been conducted through laboratory and pilot scale trials. A 100-hour wear test in the M100 Isa Mill showed significant differences in wear rates based on media composition, bulk density, and fracture toughness. Fine-grained ceramic media exhibited lower wear rates than coarser grains, reinforcing the importance of microstructural integrity (Magamatha *et al*.,2014). Comparisons between zirconia and alumina-based beads indicated that zirconia offers superior wear resistance, making it the preferred choice for high-intensity stirred milling applications (Toraman *et al*., 2019).

Computational studies using DEM simulations provide deeper insights media wear mechanisms. DEM models confirm that shear forces dominate, leading to abrasion and attrition as the primary wear mechanisms (Edwards, 2016). Quantified normal and tangential forces, showed that high tangential forces accelerate surface degradation. Stress intensity modeling predicts the impact of stirrer speed, media size, and slurry density on wear rates, allowing for better optimization of media selection and operational efficiency (Lisso, 2013).

2.3. 3 Factors affecting media wear in stirred media milling

The wear rate of grinding media in stirred media mills is influenced by a combination of operational parameters and media material properties. These factors determine the extent of abrasion, attrition, and impact wear experienced by the media, ultimately affecting grinding efficiency and cost.

Parameters such stirrer speed, media material properties and size, and slurry density play a critical role in determining wear rates. Higher agitation speeds increase shear forces and media collisions can lead to enhanced surface wear through abrasion and attrition if other operational parameters are not set appropriately (Massola *et al*., 2016). Other parameters such as slurry chemistry and pH can contribute to wear, as corrosive environments accelerate surface degradation of media. Studies also show that feed particle hardness influences wear, with harder ore leading to greater media degradation (Becker & Schwedes, 1999). Given the harsh nature of stirred media milling's tribological environment, media selection is one of the most critical decisions in stirred milling operations.

The choice of media directly impacts wear rates, milling efficiency, and overall operational costs. Ceramic media is preferred in stirred mills due to its high wear resistance, superior hardness, and ability to maintain its shape over extended grinding cycles (Rule *et al*., 2008) . Unlike steel or natural media (e.g. silica sand), ceramic beads offer a controlled size distribution, lower contamination levels, and enhanced energy efficiency, making them ideal for fine and ultrafine grinding (Becker & Schwedes, 1999). Modern advancements in ceramic media manufacturing, have further improved energy efficiency and reduced media consumption, reinforcing ceramic media as the optimal choice for high intensity stirred milling (Hassall *et al*., 2016; Rule *et al*., 2008; Wu *et al*., 2016).

2.4 Ceramic media processing

Ceramic media properties' suite of composition, microstructure and physical and mechanical properties are influenced by their manufacturing or processing methods. The processing of ceramic materials these days is more of an advanced engineering operation, but there certainly remains an element of the artisan or craftsman (Hassall *et al*., 2016). There are various processes in which ceramic media is produced and this accounts for their difference in properties. A typical evolution of ceramic microstructure through the stages of processing is illustrated in Figure 2.8, raw materials in powder being prepared for forming (left); the mixture after homogenisation at elevated temperatures (middle); ceramic material after high-temperature sintering (right). The following paragraphs give an overview of different processing steps involved.

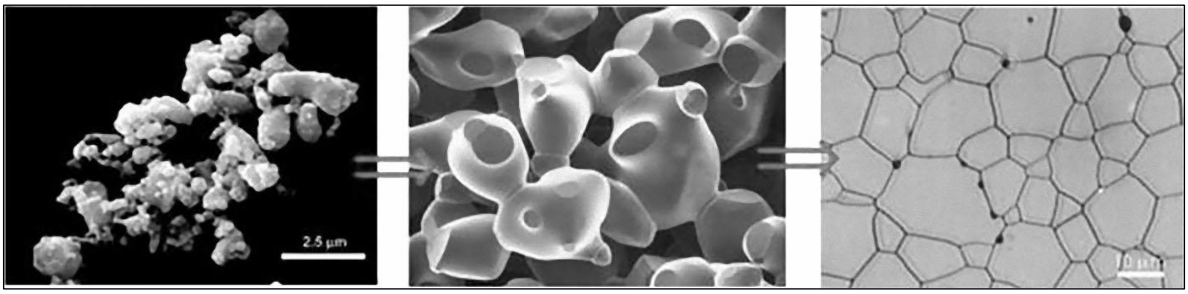

Figure 2.8. Microstructural evolution of magnetic garnet ceramic at different stages of its manufacturing process (reprinted from Kotzé, 2012).

2.4. 1 Raw material selection and preparation

The selection of type and quality of raw materials used in the manufacturing of ceramic media is determined by the desired properties of the final product (Kotzé, 2012) as well as cost of material (Reed, 1995). Size ranges of raw materials is critical as it determines the final grain sizes of the ceramic bead microstructure.

2.4. 2 Forming processes

Forming is responsible for the compacting and shaping of ceramic beads. There are three forming methods applied in the production of ceramic beads: the sol-gel process, granulation and pressing (Weber & Langlois, 2010). Sol-gel processing involves mixing colloidal particles or molecules with a liquid, which causes them to join into a continuous network, called a gel (Reed, 1995). The gel is then cast into droplets which are subsequently dried before sintering. Sol-gel is limited to the production of small bead diameters: usually less than 5mm (Kotzé, 2012).

In granulation, the prepared raw materials are added in powder form to small seed granules in a rotating drum. The seed granules progressively grow by addition of layers from the powder. Once the desired size range is reached, the granules are removed, dried and sintered.

Pressing involves filling a die cavity with prepared ceramic powder, normally spray-dried powder and compacting it at high pressure. This method is usually employed when making larger ceramic balls, i.e.,10mm and larger (Kotze, 2012; Hassall *et al.*, 2016).

2.4. 3 Sintering process

This process involves densification of ceramic beads at high temperatures in a furnace which renders them their final mechanical properties. The green product has little or no mechanical strength and has a bulk density of around 45-60% of the theoretical one (Kotzé, 2012). The necessary temperature range and temperature schedule of the sintering process depends on the material formulation and can vary, for example, from 1350°C to 1700°C (Weber & Langlois, 2010).

2.4. 4 Fusion Process

Alternative to the forming and sintering process route, fusion is another method of producing ceramic beads. Fusion involves smelting and homogenization of prepared raw materials in a kiln at high temperatures of up to 2000°C. Droplets are generated from the molten material and sprayed or granulated into the atmosphere. During their travel path, they cool down and solidify into stable beads. Beads thus produced are reported to tend to create micropores due to rapid cooling, air entrapment within the droplets, two or more beads sintering together after colliding in mid-air and/or in homogenization of the bead during cooling (Weber & Langlois, 2010).

2.5 Discrete Element Method

The Discrete Element Method (DEM) makes it possible to simulate how all particles collide with one another and their surroundings. It provides qualitative and quantitative information which includes visualization of charge flows, estimates of wear rates and distributions, collisional force and work distributions, dynamic loads on boundaries, power consumption, torques and flow rates. In addition, mixing and separation rates can be calculated (Cleary, 1998).

Following the pioneering work of Cundall and Strack (1979) who obtained sufficient validation when using DEM to simulate mechanical behavior of granular assemblies, Mishra and Rajamani (1992) extended the concept to ball mills, their work representing a crucial role in applying DEM to understand and optimize the ball milling process. After the foundational work of Mishra and Rajamani (1992), Cleary (2001) enhanced the understanding of ball milling dynamics, improving simulation techniques, and expanding the scope of DEM applications. DEM was further extended to the stirred media milling context, to provide useful information that was not initially possible via experimental work (Cleary *et al*., 2015; Cleary *et al*., 2006).

2.5. 1 Fundamental principles

Bwalya in his thesis concisely reviewed the fundamental concepts of DEM (Bwalya, 2005). It applies Newton's laws to model particle motion and uses a surface response method to handle collisions. Cundall (1988) soft contact approach permits overlap between colliding entities, where the contact force depends on the overlap distance and material stiffness. The primary components of DEM are detailed in the subsequent subsections.

a) Particle shape representation

In DEM simulations, both moving and stationary elements interact at their boundaries. For milling applications, the internal geometry is represented by solid lines or planes connected by nodes (Bwalya, 2005). The movement of the mill wall is determined by its initial speed and is unaffected by collisions. Particles are typically represented by discs or spheres, particularly in mineral engineering applications. The spherical particle shape allows for the largest number of particles for any given central processing unit (CPU) execution time budget and significantly streamlines simulations (Lane *et al*., 2010). These shapes are chosen because their properties simplify algorithms for tasks such as contact detection.

While spherical representations are effective for simulating balls in ball mills, they can be inaccurate for ore particles with irregular shapes, leading to unrealistic dynamic behavior. For this reason, significant attention has been given to developing geometric constructs that best represent non-spherical shapes. Popular DEM software uses sphere clusters, including that created and sold by Itasca and DEM Solutions Ltd (Lane *et al*., 2010). The three-dimensional ellipsoid and the two-dimensional ellipse are other common particle types (Liu & Zhao, 2020; Xie *et al*., 2020; Zhao *et al*., 2019). Polyhedra is another geometric construct implemented to achieve more realistic particle shapes modelling (Xie *et al*., 2020). Consequently, particle shape is an important, if not even the most important parameter to be considered in DEM simulations and, thus, must be captured accurately if DEM is to be used as a predictive tool (Lu *et al*., 2015). Recent commercial advances, such as those implemented in RockyDEM software, have enabled efficient simulation of irregular particle shapes with improved computational performance compared to traditional DEM approaches (Xie *et al*., 2020; Boikov *et al*., 2021).

b) Contact detection

Contact detection is an essential step in DEM simulations, serving to determine which particles are interacting within the system. Algorithms have been developed to implement contact detection models (Cundall, 1988; Feng, 2021; Nezami *et al*., 2004). The complexity of contact detection algorithms escalates with the intricacy of particle shapes, from simple spheres - where contact is identified if the distance between centers is less than the sum of their radii - to more complex shapes like ellipsoids, spherocylinders, and general polyhedra, which necessitate more advanced algorithms for accurate modeling.

Despite the prevalence of spherical particles in simulation studies, these represent a minority in natural settings. Therefore, there is a growing shift towards simulating more realistic shapes like ellipsoids and polyhedra, though this introduces significant computational challenges. For example, simulating large granular assemblies of tens of thousands of non-spherical particles can be exceedingly time-consuming, often representing just a small fraction of real-world granular materials, such as a teaspoon of powdered sugar containing approximately 50,000 grains (Lane *et al*., 2010).

Contact detection for non-spherical particles involves various models and algorithms tailored to specific particle shapes. For ellipsoids, advanced methods like the geometric potential algorithm are used (Lin & Ng, 1997). Polygons and polyhedra utilize the common plane (CP) algorithm for effective contact detection (Cundall, 1988; Nezami *et al*., 2004). Superquadratics employ the discrete function representation (DFR) method (Williams &

O'Connor, 1995). Combined spheres use multiple overlapping spheres, benefiting from existing frameworks but often leading to unphysical behavior. The composite spheres method is frequently used due to its simplicity and compatibility with established DEM frameworks.

c) Contact resolution

Newton's equations of motion govern the particle positions and velocities in DEM. Contact resolution is the process of using Newton's equations of motion to calculate the forces and moments at particle contact points. The simplest case involves spherical or disc-shaped elements, where overlap determination is straightforward. Various approaches and challenges are associated with resolving contacts for non-spherical particles. For instance, so far, there is no common agreement on the definition of a contact point for non-spherical particles.

i. Overlap calculation

Figure 2.9 illustrates geometric details of a ball-to-ball contact example. For two spherical or disc-shaped elements, the overlap distance Δ_n is given by:

$$\Delta_n = (r_i + r_j) - \sqrt{(x_j - x_i)^2 + (y_j - y_i)^2} \quad (2.4)$$

Where r is the radii of elements i and j, and x and y represents Cartesian coordinates of their centers. For non-spherical particles the definition of overlap is rather complex (Bwalya, 2005).

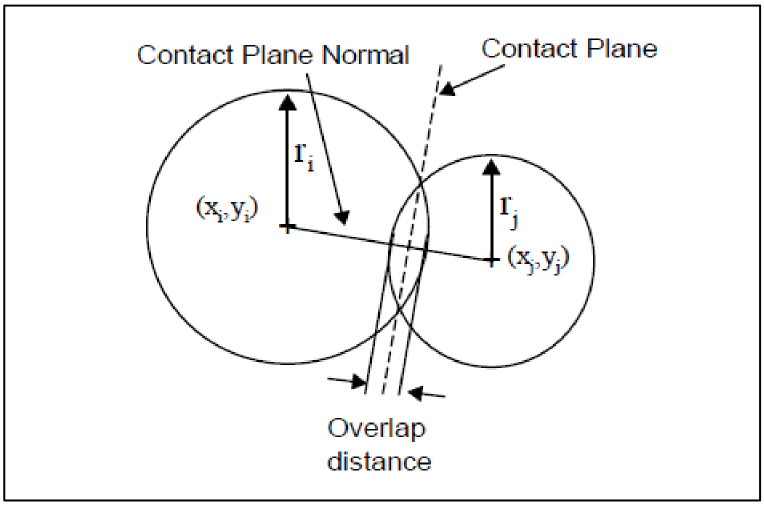

Figure 2.9. Illustration of ball-to-ball contact showing overlap distance, contact plane, and force vectors used in DEM modelling (reprinted from Bwalya, 2002).

Calculating the overlap between a disc and a wall is more complex as contact can occur at the edge, at the corner (where two walls meet), or simultaneously at both the corner and the edge. This issue has been addressed by several authors (Cundall, 1988; Mishra, 2003).

Once the overlap is established for two contacting elements, the forces (normal, shear, and angular) at the contact point can be calculated. The normal force is modeled as visco-elastic, comprising both an elastic (spring) component and a viscous damping (dashpot) component. For spherical particles, the normal contact force cannot induce any moment and, thus, rotation. However, for non-spherical particles, the situation is much more complicated. The tangential (shear) force includes a slider to model friction. The contact forces are represented by the following equations:

$$F_n = K_n \Delta_n + C_n V_n \tag{2.5}$$

$$F_n = K_s \Delta_s + C_s V_s \tag{2.6}$$

When

$$F_s \leq \mu F_n$$

Otherwise

$$F_s = \mu F_n$$

Where F is the force, K is the stiffness, Δ is the overlap change, and V is the relative velocity at the contact point. Subscript n and s denote normal and shear directions, respectively.

d) Motion physics

The computed resultant forces acting on the elements are then used to update their position and orientation via the linear and angular accelerations. These accelerations are determined by the following equations:

$$F_i = m\ddot{x}_i \tag{2.7}$$

Where F is the force acting in the specified directions x, y for 2D simulations or x, y, z for 3D simulations, $\ddot{x}$ represents the corresponding acceleration, and m is the mass of the particle.

$$T = I\ddot{\theta} \tag{2.8}$$

Where T is the torque, I is the moment of inertia, and $\ddot{\theta}$ is the angular position.

The velocities and displacements of the particles are calculated through successive numerical integration of the accelerations. The positions of the particles are then updated by adding these displacements to their previous positions. This iterative process allows for the dynamic simulation of particle motion over time.

2.5. 2 Challenges and improvements

Non-spherical particles present additional challenges as the contact normal does not typically pass through the particles' centers of gravity, inducing moments and rotations. Addressing these requires sophisticated algorithms. Multi-point contact models help mitigate the unphysical behavior seen with single-point contacts (Fraige *et al.*, 2008). Improvements in computational efficiency, such as the common plane (CP) algorithm, enhance contact detection and resolution by bisecting the space between contacting particles and iteratively adjusting the plane to find the maximum (Cundall, 1988; Nezami *et al*., 2004).

2.5. 3 Conclusion

The DEM is highly valued for its use of fundamental physical laws to predict the behavior of particulate systems. It allows for the accurate prediction of interparticle forces and energy dissipations, which are essential in understanding particle fracture and other phenomena. Despite its strengths, it is clear from this review that several areas of DEM require further research and development. Users must be aware of these limitations when employing DEM for their simulations.

Chapter 3 Methodology

3.1 Introduction

Study of media wear in the past usually used experimental methods only, due to the limited development of numerical simulation technology. Notwithstanding the demonstrated accuracy of results obtained via experiments, the process can be time consuming. Increasingly, researchers have begun to use numerical technology to investigate media wear in recent times. Numerical simulation if applied successfully, potentially provides a quick optimisation route of the grinding process. Most importantly it provides detailed information of the multi-physics involved at a particle level, information that cannot be obtained through experiments.

The typical strategy in literature is to correlate results from experimental studies and simulation to validate proposed wear models. This chapter details the experimental and simulation work carried out to produce comparative data for analysis. Consequently, the methodology involves two research approaches, namely, experimental tests using a laboratory stirred mill and numerical simulation based on DEM.

3.2 Experimental tests

Experimental work was conducted to get macrodynamic information which was key in drawing insights from the grinding process. The information would also be used to calibrate the DEM program which was also key to obtaining a wholistic view of the grinding process considering the parameters tested. The test work includes grinding tests on silica ore that was acquired from Wits' Chemical and Metallurgy department using a batch vertical stirred mill.

3.2. 1 Sample preparation

Sample preparation is crucial for ensuring accurate and reliable experimental tests results. The prepared sample should accurately represent the bulk of material being studied during experiments. This entails making certain that the sample is drawn from a representative portion of the bulk material and that it includes all relevant particle size fractions. This includes obtaining a representative sample size and composition that reflects the characteristics of the bulk material. The initial particle size distribution of the sample can significantly influence the grinding process and the properties of the final product. Proper sample preparation allows for controlling and standardizing the particle size distribution before the grinding experiment begins.

Proper sampling also ensures sample homogeneity which is essential to obtain consistent and reproducible results. Inhomogeneous samples can lead to variability in grinding performance and therefore quality of results. Proper sample preparation allows researchers to control experimental variables and conditions more effectively. This includes factors such as sample mass, initial particle size, and moisture content, which can significantly influence grinding outcomes. Consistent and well-prepared samples help minimize variability between experimental runs, improving the reliability and reproducibility of the results.

In the current study, care was taken to as far as possible to ensure representative samples were extracted from bulk. Rotating samplers were used for this purpose. These samplers are considered the most precise in obtaining representative samples from powdered or dry granular materials (Wills & Napier-Munn, 2006). The variant used, make use of a vibrating feeder to transfer the bulk into several containers as shown in Figure 3.1. The received sample was in the size range of -1150+850 µm which required further size reduction to obtain the -600+425 µm size range required for fine feed tests. This was conducted in a separate rod mill at Mintek as well.

Figure 3.1. Rotary samplers that were used to extract representative samples from the bulk.

a) Feed material

Silica sand also known as quartz sand was selected as the feed material for the test campaign owing to its high availability and high relative Mohr's scale hardness of seven (refer to appendices for images). In this study, a sample was available at Wits University already mono sized in the range of -1180+850 µm. The density of silica sand varies between 2.60 - 2,65 g/cm^3. The molecular formula and weight are SiO_2 and 60,08 g/mol respectively. The material was not analysed for chemical composition as this information was not relevant to the overarching objective of the study.

b) Ceramic bead

Alumina based ceramic bead type was made available by Mintek for the experimental tests. Bead sizes used for the tests were 4 mm, 5 mm and 6 mm beads in equal masses for each test run. The initial weight of each bead size was similar, measured by an electronic balance with an accuracy of 0.01 g and it goes without saying that the smaller bead sizes would have a high count of individual beads in every sample prepared. The beads had a density of approximately 4.0 g/cm³, typical of alumina grinding media used in fine grinding. Its chemical composition was not analysed in this study, however, comparable composition data for high purity alumina-based grinding media used in previous Mintek and literature studies are presented in Table 3.1.

Table 3.1. Representative chemical composition of alumina-based grinding media (Becker & Schwedes, 1999; Hassall *et al.*, 2016; Kwade & Schwedes, 2007).

Component	Al_2O_3 (%)	SiO_2 (%)	MgO (%)	CaO (%)	Fe_2O_3 (%)	Na_2O (%)
Range	94 – 97	1 – 3	0.5 – 1.5	< 0.5	< 0.2	< 0.5

3.2. 2 Laboratory Tests

The purpose of experimental test work campaign was to generate data that we would attempt to replicate with DEM and also to draw important insights from stirred milling process. The influence of two operating parameters on grinding result was investigated i.e. Specific energy input and feed material size. The effect of these parameters on grinding result is best described by the relation of specific energy input and product fineness. Therefore, particle size analysis was a major part of the test work. A summary of the test work campaign is given in Table 3.2.

Table 3.2. Experimental matrix description.

Test No	**Mill Geometry**	**Mono-sized silica sand size (μm)**	**Stirrer speed (m/s)**	**Energy input (kWh/t)**	**Bead size (mm)**
1	Smooth chamber + pin stirrer	-1180+850	2.5	5	4,5,6
2	Smooth chamber + pin stirrer	-1180+850	2.5	10	4,5,6
3	Smooth chamber + pin stirrer	-1180+850	2.5	20	4,5,6
4	Smooth chamber + pin stirrer	-600+425	2.5	5	4,5,6

5	Smooth chamber + pin stirrer	-600+425	2.5	10	4,5,6
6	Smooth chamber + pin stirrer	-600+425	2.5	20	4,5,6
7	Smooth chamber + pin stirrer	-1180+850	2.5		4,5,6
8	Smooth chamber + pin stirrer	-1180+850	2.5		4,5,6
9	Smooth chamber + pin stirrer	-1180+850	2.5		4,5,6

a) Laboratory scale stirred media mill

Batch wet grinding tests were carried out using a laboratory scale stirred media mill at Mintek shown in Figure 3.2 and Figure 3.3. The mill was fitted with a stirrer depicted in Figure 3.4, with pins attached to a shaft that is rotated by an electric motor with a power rating of 3 kW. A smooth mill chamber shown in Figure 3.4 without a liner was used for the tests. For cooling purposes, the grinding chamber is equipped with a water jacket. A speed sensor and load cell formed part of the configuration to measure shaft speed and torque which are recorded on a computer system (Figure 3.3). Power draw is then calculated in real time using equation (3.1). A similar mill was utilised by Ford and Naude (2021) and Lisso (2013) to carry out their grinding studies.

$$P = \frac{2\pi T\omega}{60} \tag{3.1}$$

Where:

P represents the mill power draw in Watts (W), T is the shaft toque (Nm) and ω is the angular velocity of the shaft in revolutions per minute (rpm). The power draw for a second interval is used to calculate incremental energy input in kWh to the mill during a test run. Accumulated energy input per mass of solids in kWh/t is then tracked over the duration of a test run. A detailed schematic of the mill dimensions is given in below.

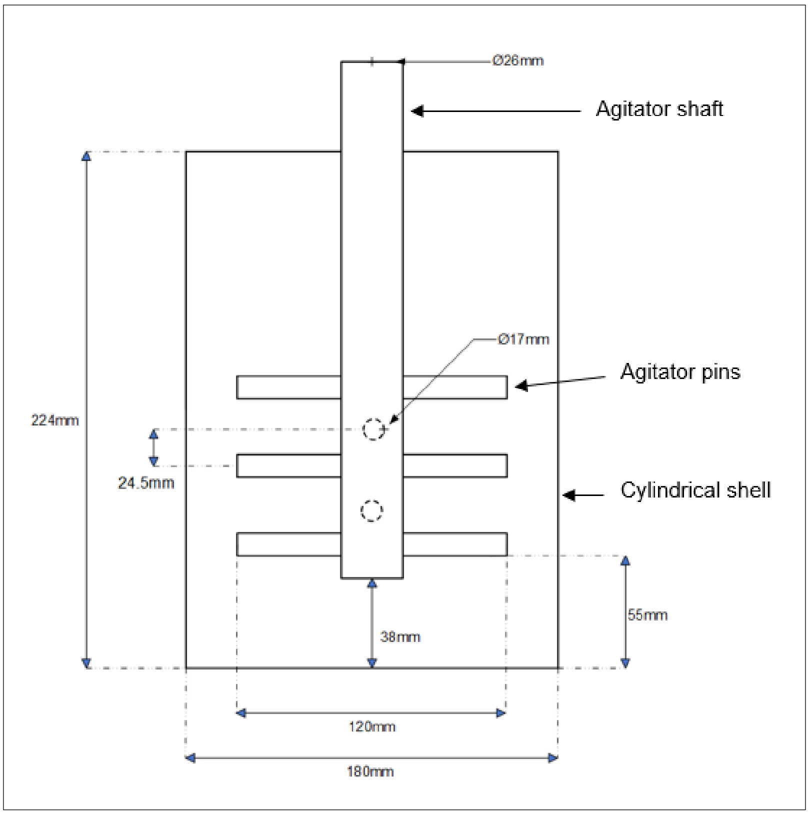

Figure 3.2. Schematic diagram of the laboratory stirred mill used, showing the structure and dimensions of the main components.

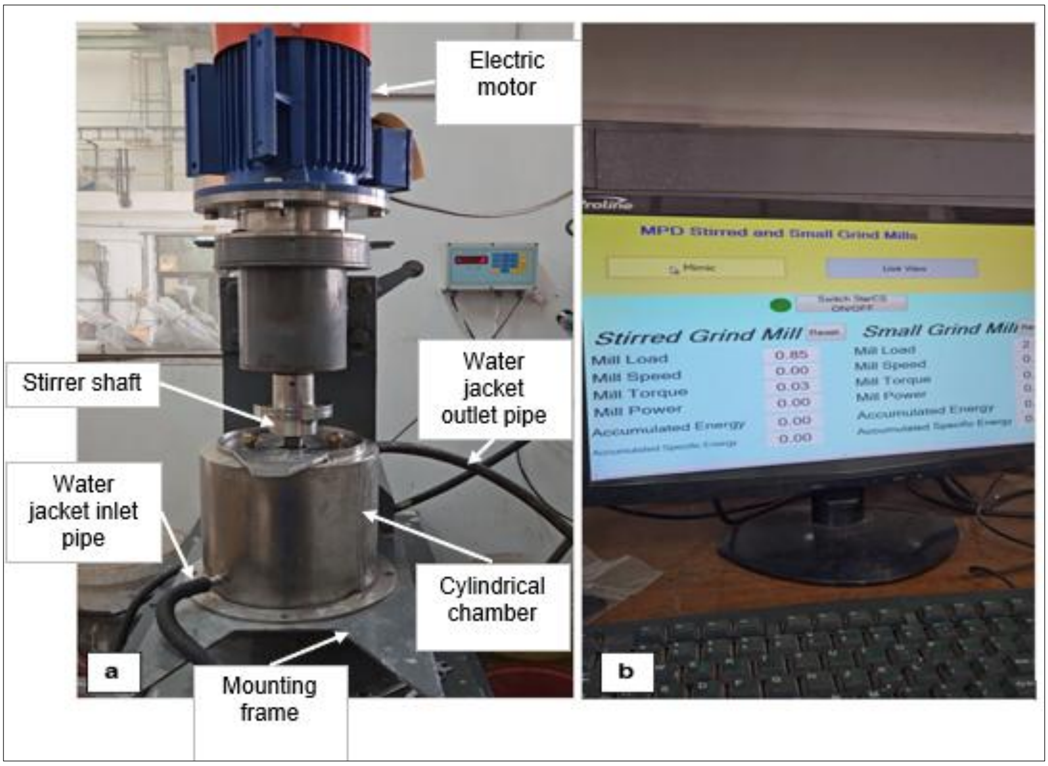

Figure 3.3. Laboratory stirred mill utilised for the grinding tests (a) stirred mill computer program (b)

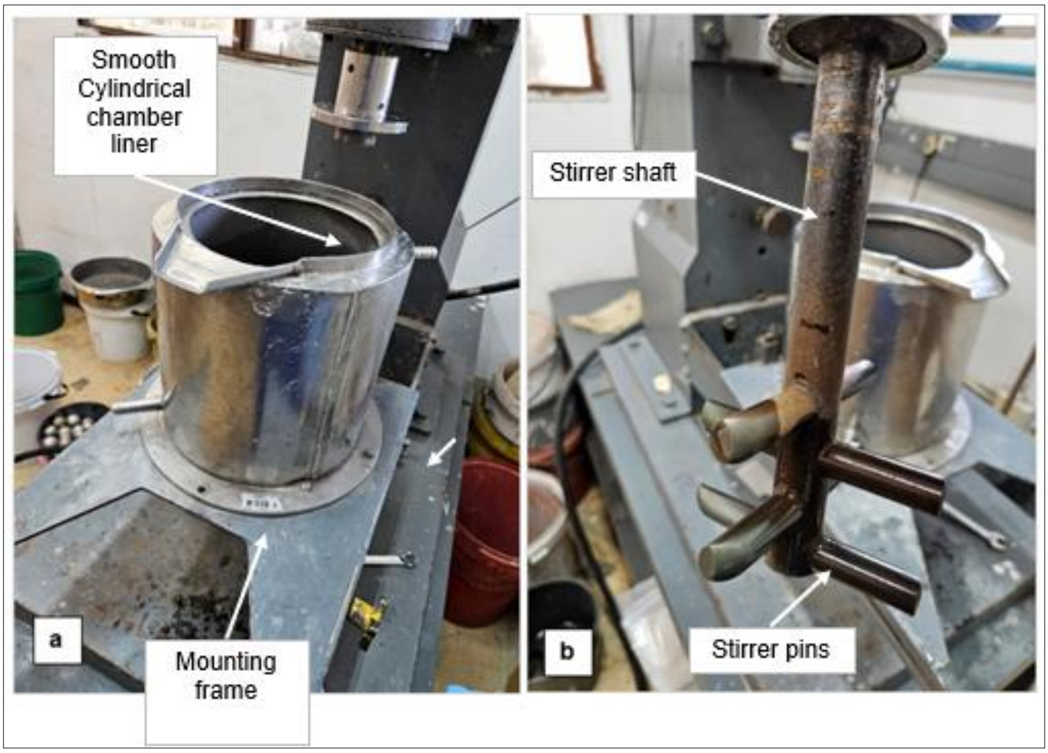

Figure 3.4. Smooth cylindrical chamber without a liner (a) Stirrer with pins (b).

b) Test procedure

Grinding tests were conducted following laboratory safety procedures as far as possible. The first step of procedure involved sample preparation of both feed material and ceramic beads. Silica sand as received was mono-sized at -1180+850 µm and a finer fraction of -600+425 µm was obtained by milling the coarser material in a laboratory rod mill. Great care was taken to ensure representative samples of individual silica sand and ceramic beads masses were extracted using rotary samples and a recently calibrated analytical balance to measure required weight. Test work conditions are shown in Table 3.3.

Table 3.3. Test work conditions.

Operating Parameters	**Value**
Water s.g. (g/cm^3)	1
Silica sand mass (g)	850
% solids	50
Water mass (g)	850
Slurry mass (g)	1700
Silica sand s.g. (g/cm^3)	2.67
Slurry s.g. (g/cm^3)	1.46
Slurry volume (cm^3)	1168.35
Mill Dimensions	
Diameter (cm)	18
Height (cm)	23
Mill volume (π/4. D2/L)	5852.79
% Loading fraction	0.50
Ball volume (cm^3)	1752.53
Ball s.g. (g/cm^3)	4
Ball mass (g)	7010

The next step was to ensure that all equipment was clean and free of material from previous experiments, especially in the stirred mill chamber. Adding contents inside the mill chamber involved decoupling the stirrer from the rotor, so great care had to be taken to ensure all mill components were properly assembled at start of each test run. Once all contents were added and mill properly assembled, the desired rotational speed was set before starting the mill. It was important to ensure that the stirred mill computer program (Figure 3.3) was reset at start of each test run.

The computer program, while the mill is running, generates data of the measured operating parameters at every second including mill load, mill speed, mill torque, mill power, accumulated energy and accumulated specific energy. This data is downloadable in excel format at the end of each test run for analysis. Tests were conducted in accordance with the test matrix given in Table 3.1. The milling operation of each test run was monitored and stopped at predetermined specific energy input i.e. 5,10,20 kWh/t for tests 1-6, and at 1 hr, 2 hrs and 4 hrs for tests 7-9. Tests 7-9 were long runs to allow for considerable wear of ceramic beads.

At the end of each test run, the mill was dissembled to remove the contents which were carefully separated via sieving into ceramic beads and silica sand mass fractions. Freshly prepared ceramic beads were used in each test run. The wet silica sand product was dewatered first using pressure filters and then dried in ovens at 80 degrees Celsius. Once dry and cool, representative samples were extracted and sized using both sieve analysis and laser diffraction techniques. Data from these operations were recorded for analysis. For ceramic beads, the mass after each test run was recorded for determination of grinding wear.

3.3 Discrete Element Modelling

A three-dimensional (3D) DEM software developed by Itasca Consulting Group, Particle Flow Code (PFC), was used for the simulation work. The software can model many industrial processes with less programming effort (Bwalya, 2005). The software includes an integrated programming language, Flexible Interaction Script for Humans (FISH), which allows users to create custom scripts for simulating particulate systems.

The DEM-PFC-3D program operates through command-line inputs or structured scripts written in FISH. These scripts, saved with a “Dat” extension in the same directory as the PFC software, can be executed using the "call" command followed by the script name. Before running, the program loads and compiles all defined functions and variables. Multiple scripts can be executed in a single session, provided they do not conflict, allowing data from one script to be used in subsequent simulations.

3.3. 1 Mill simulation program design

The development of the PFC-based mill simulation program was structured around two scripts: a variable script and a permanent script. The variable script is generated based on user input, allowing for flexibility in defining simulation parameters. The permanent script extracts the data from the variable script and transforms it into commands that appropriately drives the PFC program. This approach was adapted from the mill simulation program developed by Bwalya (2005), ensuring a structured and automated process for simulating mill operations.

a) The variable script

Bwalya (2005) developed a Windows Graphic User Interface (GUI) tool that enables users to specify the distribution of various sized particles within the mill charge and depict the interior geometry of the mill. The table below provides a comprehensive list of all user-specified parameters (Bwalya, 2005).

Table 3.4. List of parameters specified by the user.

Parameter	Description
Mill Geometry	Internal mill diameter and Length
	Stirrer dimensions
Ball and Wall Contact Parameters	Ball and wall stiffness in both shear and normal directions
	Wall and ball coefficients of restitution
	Wall and ball coefficient of friction
Simulation Parameters	Mill Speed
	Ball voidage and mill filling
	The number of revolutions prior to sampling
	Sampling revolutions number
	Simulation frames to be collected

b) Permanent script

Loading the variable script initiates a series of predefined steps that the simulator follows, using the permanent script to interpret the input data and execute the necessary instructions. This ensures that the simulation runs according to the specified parameters, as outlined in the flow diagram below.

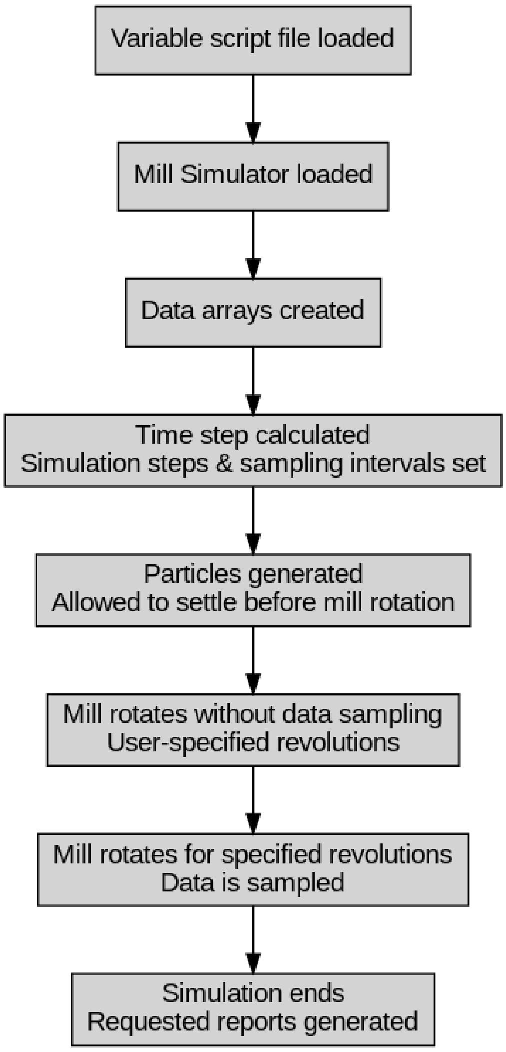

Figure 3.5. Sequence of tasks accomplished by the DEM simulation program (reprinted from Bwalya, 2005).

i. Data array creation

The goal of this procedure is to allocate sufficient data storage for anticipated events. In this research, the arrays were specifically designed to record energy conversions occurring at contact points between particles. Millions of collisions occurred during the mill simulation, therefore data pertinent to this study was given consideration.

ii. Time step calculation

The stability of a numerical algorithm is crucial for ensuring accurate and consistent results. Theoretically, algorithm stability is influenced by the selected time step (Cundall & Strack, 1979). In this study, the simulation time step was chosen to guarantee that each contact event contained at least twenty (20) time steps. To maintain numerical stability, the maximum allowable time step was determined by approximating the interacting elements as springs at their contact points, based on the spring-dashpot contact model.

iii. Simulation and interval sampling

The number of time steps, referred to as cycles, required for the simulation is determined by dividing the real-time duration, represented by the number of mill revolutions and the calculated time step. The cycles corresponding to sampling intervals for specific data outputs, such as power measurements and particle position frames, are calculated by dividing their respective real-time intervals by the simulation time step.

iv. Particle generation

In the experimental stirred mill, all the particles are initially settled at the bottom at the beginning of each run. For the simulation, the balls were generated in a box-bound space within the mill and allowed to settle by gravity. Settling was accelerated by initially using lower stiffness before gradually raising it to the normal value.

v. Mill rotation without data sampling

The simulation allowed the user to specify a predefined number of revolutions before data sampling commenced, ensuring that data collection only began once the mill reached a steady-state condition. The power behaviour and impact energy indicate that no two revolutions are ever identical, even under steady-state operation. To improve the accuracy of the analysed data, it is advisable to increase the number of sampling revolutions when time allows.

vi. Mill rotation with data sampling

This stage of the requires the most computational time. It entails identifying all particles interaction at every time step, performing the necessary computations, and storing the output data. Figure 3.6 illustrates the series of computations carried out during the process.

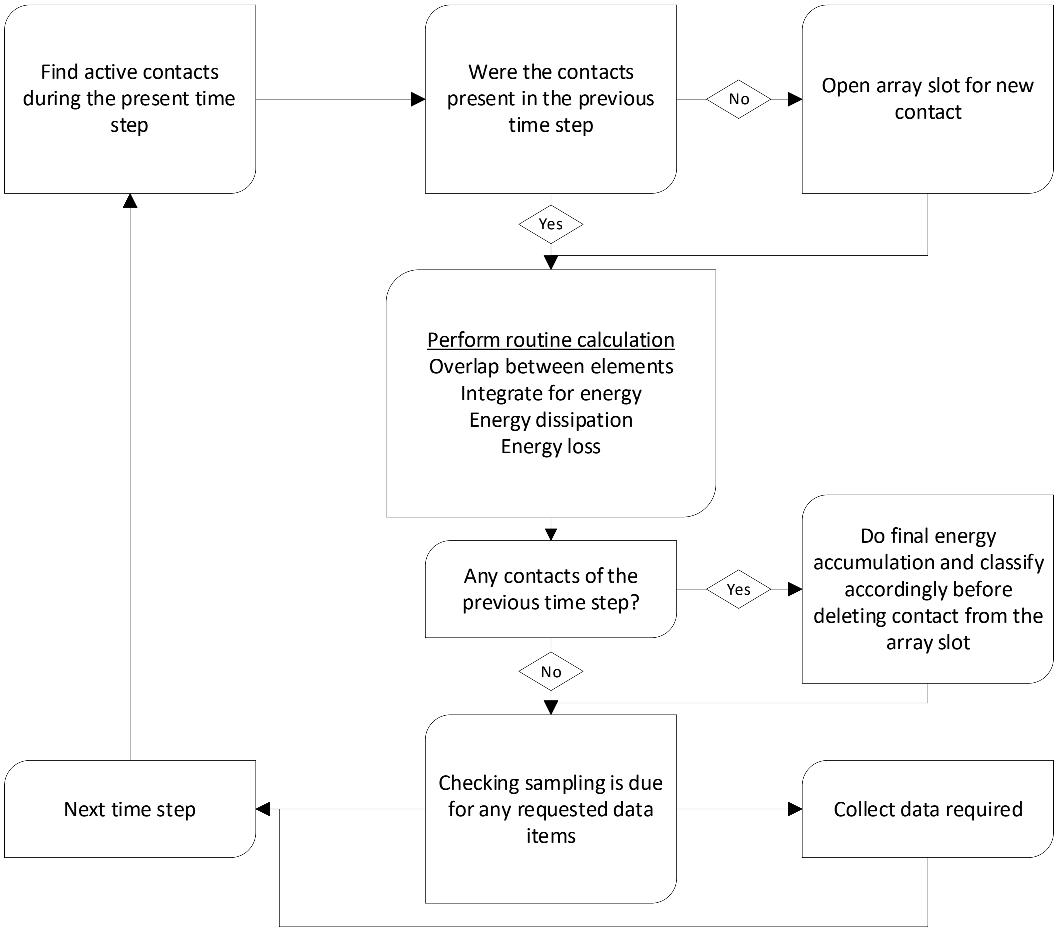

Figure 3.6. The DEM simulation computational procedure (reprinted from Bwalya, 2005).

3.3. 2 The simulation computational scheme

a) Overlap calculation

As discussed in Chapter 2, the DEM framework defines overlap as the minimal distance of penetration which happens when two particles touch or when a particle touches a wall. The overlap in DEM represents a mathematical concept that shows how particles deform when they collide. The contact stiffness and overlap values determine the normal contact force while tangential forces depend on surface friction and relative motion between contacting bodies. The DEM uses this method to precisely model particle interactions, energy transfer and collision dynamics at each simulation time step.

b) Dissipation energy

The energy dissipated during contact at time step i is determined using equation 3.2, as outlined by (Itasca Consulting Group, 1993).

$$E_i = \frac{2D(\Delta_i - \Delta_{i-1})}{\delta t}\sqrt{K_m} \qquad (3.2)$$

Where D is the damping ratio, K_m is the coefficient of stiffness for a particle of mass m, $\Delta_i$and Δ_{i-1} represent the overlap displacements at time steps i and $i-1$, respectively, and

δt is the time step interval. To account for the dissipated energy, the dissipated energy values are accumulated and consolidated at the end of the contact event. The energy is represented in an energy spectrum.

In order to increase the scheme's computational accuracy, care must be taken to account for the uncertainty in the precise times at which a contact starts or ends.

c) Strain energy

The strain energy absorbed by a particle at time interval i based on the contact forces provided by PFC, is determined through numerical integration as follows:

$$E_i = (F_i + F_{i-1})(\Delta_i - \Delta_{i-1})/2 \qquad (3.3)$$

where E represents the energy, F denotes the force, and Δ refers to the overlap distance between the contacting elements.

Energy accumulation occurs only when the overlap between elements increases, ensuring that only relevant contributions are considered. The user selects range of energy classes to utilise, and each contact event's maximum strain energy is logged into the appropriate energy class. An energy spectrum is produced at the conclusion of the simulation.

d) Frictional energy

Particles moves both perpendicularly and parallel to one another during the simulation, which causes frictional energy loss at the points of contact. From the PFC program, the frictional energy loss for a specific contact point at the present time step is also derived.

e) Data sampling

The simulation program makes it possible to gather many kinds of data over the course of the simulation. After the mill reaches a steady-state condition and the pre-sampling revolutions are finished, important data like power draw, impact energy, frictional energy, and the quantity of impact collisions are collected. A list of data that the simulation can produce is described in the following subsections.

i. Instantaneous mill power

Based on the torque produced by the balls in direct contact with the mill wall, the instantaneous input power is computed. This is sometimes called input power. The sample time intervals, such every second or every tenth of a second, are defined by the user in order to collect the necessary data.

ii. Frictional loss

This is the energy that is lost when two objects make contact, such as a ball and a wall, rub against one another.

iii. Simulation frames

Throughout the simulation, photographic frames of the mill contents are captured at user-specified intervals. These frames are then compiled at the end of the simulation to create an animation or video depicting the motion of the load. The animation can be visualized in the following ways:

- Stills – shows the balls' precise locations in a cross-sectional perspective at particular points throughout the simulation.
- Particle Paths – shows, in a single cross-sectional graphic, the path taken by each individual ball during mill rotation.
- Position Density Plots (PDPs) – gives a cross-sectional picture of the particle distribution by highlighting the areas that the balls occupy the most frequently throughout the mill diameter.

iv. Spectral energy data

The simulator monitors all collision events throughout the simulation and categorises them into established energy groupings. The user specifies the energy range to be utilised during the experiment. The simulator also offers the capability to record an impact energy spectrum for a defined particle size within the load.

v. Damping, normal and tangential energy loses

These energy losses arise from interactions between colliding elements during the simulation. Damping energy loss occurs due to the dissipation of energy through the damping mechanism, which absorbs impact forces and reduces kinetic energy. Normal energy loss is attributed to the deformation and restitution effects during collisions along the normal direction of impact. Tangential energy loss results from frictional forces acting parallel to the contact surface, contributing to slip and rolling resistance. These losses play a crucial role in understanding energy dissipation mechanisms within the mill and their effect on particle motion and grinding efficiency.

Before running the simulation, careful consideration should be given to the selection of data to be recorded, as excessive data collection can significantly reduce computational efficiency and slow down the simulation process (Samukute, 2019). For this research, only essential data were recorded, including spectral energy, normal and tangential energy losses, and power draw, to ensure a balance between data accuracy and simulation performance.

f) Simulation report

Upon completion of each simulation, a report is produced that includes the simulation data according to the parameters specified by the user before the simulation. This encompasses information such as power consumption, simulation frames, and energy spectra. A sample report is included in the Appendices.

3.3. 3 Contact model and simulation parameters selection criteria

Balancing simulation accuracy with computational efficiency is a recognized challenge in DEM simulations (Bwalya, 2005). A more comprehensive data sample can enhance the quantitative and qualitative representation of the simulated process but often demands greater computational resources and time. The selection of contact models and simulation parameters is influenced by several factors, including the desired accuracy, available computational resources, and the specific characteristics of the system under study.

a) Contact Model

The linear spring-dashpot (LSD) model is widely used in DEM simulations due to its simplicity and computational efficiency. This model effectively balances accuracy and computational demand, making it suitable for large-scale simulations involving numerous particles. Literature demonstrates the applicability of the LSD model in DEM simulations, highlighting its capability to reduce simulation runtime (Bwalya, 2005).

While the LSD model has certain limitations, such as generating large instantaneous forces at the onset of contact and negative forces before separation, these can be mitigated through model modifications. Crosley (1975) proposed adjusting the damping term to depend on both overlap and relative velocity at the contact point, resulting in more stable force behaviours during collisions. This approach helps address the noted drawbacks, enhancing the model's accuracy without significantly increasing computational costs.

While the linear spring-dashpot model offers simplicity and computational efficiency, other models provide alternative approaches that may better capture specific contact behaviours such as the Hertz-Mindlin and Johnson-Kendall-Roberts (JKR) Model which is an extension of the Hertz-Mindlin model (Johnson *et al.*, 1971; Mindlin, 1949).

In this study, the LSD model available within the DEM-PFC-3D program was used. According to Yeom *et al*. (2019) and Zhao *et al*. (2024), the LSD model remains one of the most robust and computationally efficient formulations in DEM, forming the foundation for more advanced models such as Hertz-Mindlin and JKR. Although these nonlinear models can represent contact deformation more accurately, they require substantially greater computational effort. Given the study's objectives and the need to simulate large numbers of media particles, the LSD model provided an optimal balance between physical representation and computational efficiency.

b) Simulation parameters

Selecting appropriate simulation parameters is crucial in DEM simulations to ensure accurate representation of particle interactions and realistic system behaviour. Key parameters include material stiffness, the coefficient of restitution, and the coefficient of friction. Material stiffness is essential for accurately determining the forces generated during particle interactions. The coefficient of restitution defines the material's damping characteristics and influences energy dissipation upon impact, while the coefficient of friction controls whether sliding occurs at points of contact (Mishra & Rajamani, 1992).

In simulations involving grinding media, these parameters directly affect collision dynamics, particle mobility, and overall energy distribution within the system. Since this study focuses on wear of grinding media, the dissipation of impact and shear energy is more relevant than individual force magnitudes, as wear is primarily driven by energy transfer during particle collisions. Tracking energy dissipation allows for a better understanding of wear mechanisms and predictions of grinding media degradation over time. Given that wear is directly influenced by energy dissipation, selecting appropriate parameter values ensures an accurate representation of particle interactions and wear mechanisms.

To ensure consistency with previous research and improve the reliability of the simulation, values for the coefficient of restitution and coefficient of friction were adopted from established studies (Bwalya, 2005; Mishra & Rajamani, 1992; Samukute, 2019; Jankovic, 2003). The selected parameters have been widely validated in similar milling environments and therefore provided a reliable basis for simulating particle-particle and particle-wall interactions within the stirred mill. While experimental calibration of these parameters can further improve accuracy, it was beyond the practical scope of this study.

i. Material stiffness

The stiffness of the material influences the force produced in the springs, which subsequently governs the energy transferred during ball impacts. The measurement can be conducted with a device referred to as an ultrafast load cell. For additional information regarding this measurement technique, refer to (Mishra & Rajamani, 1992).

The stiffness of ceramic grinding media, such as alumina and zirconia-based beads, typically falls within the range of $10^7 - 10^9\ N/m$. Higher stiffness values necessitate smaller time steps in DEM simulations to ensure numerical stability, which increases computational demand. To maintain a balance between accuracy and simulation efficiency, an appropriate stiffness value must be selected. Mishra and Rajamani (1992) reported contact stiffness values ranging between $10^5\ N/m$ and $10^8\ N/m$ depending on collision conditions, while Cleary *et al*. (2015) applied a normal stiffness of approximately $10^6\ N/m$ for stable overlap ratios in stirred mill simulations. In this study, $10^7\ N/m$ was chosen which was within these literature-validated ranges to maintain realistic particle overlap (< 1% of particle diameter) and ensure numerical stability of the simulation time step.

Bwalya (2005) noted that enhanced stiffness results in elevated particle vibrations without a corresponding increase in the total energy of the system. He also observed that collision events capable of causing fractures occur more frequently at reduced stiffness levels, indicating that employing an unreasonably low stiffness value may result in an overestimation of breaking.

To balance computational efficiency with realistic material behaviour, previous research has explored modelling approaches and measurement techniques for contact parameters. Given time constraints in this study, stiffness values higher than the order of $10^7\ N/m$ were not considered to ensure computational feasibility while maintaining reasonable accuracy.

ii. Coefficient of restitution

The coefficient of restitution for colliding bodies is mathematically defined as:

$$e = \frac{\int RdP}{\int PdP} \quad (3.4)$$

Where $\int RdP$ and $\int PdP$ represent the deformation and restitution impulses, respectively. Using this definition, for two discs moving in the same direction before and after impact, the coefficient of restitution is expressed as:

$$e = \frac{(V_b)_2 - (V_a)_2}{(V_a)_1 - (V_b)_1} \quad (3.5)$$

where V_a and V_b are the velocities of discs a and b with subscripts 1 and 2 referring to the velocities just before and after impact, respectively.

The coefficient of restitution is a material characteristic influenced by various parameters, including hardness, dimensions, morphology, and impact velocity of the colliding entities. The coefficient of restitution must be assessed under conditions that nearly mimic those present in the mill (Mishra & Rajamani, 1992).

In stirred mills, grinding media interactions are primarily governed by shear and attrition forces, rather than impact dominated collisions. The motion of grinding beads is influenced by stirrer design, rotational speed, and slurry viscosity, leading to intense particle - particle and particle - wall interactions. Unlike tumbling mills, where impact events can be directly measured, stirred mills involve predominantly rolling, sliding, and compression-driven contacts, making it difficult to directly determine the coefficient of restitution under realistic operating conditions.

Since direct measurement within the mill is challenging, researchers often rely on DEM calibration studies, where coefficient of restitution values are inferred by matching simulation outcomes with experimentally observed grinding performance. Studies have reported values within the range of 0.2 – 0.6, (Jayasundara *et al*., 2008; Ndimande *et al*., 2019), selected based on previous research and empirical adjustments to best replicate observed particle motion in stirred mill environments.

In this study, the coefficient of restitution was selected within the literature reported range of 0.2-0.6 and subsequently adjusted through iterative simulations to align the predicted power draw with experimental measurements. This calibration ensured that energy dissipation during particle collisions reflected realistic mill dynamics maintaining plausible physics of the contact interactions.

iii. Coefficient of friction

In stirred mills, the coefficient of friction is a key parameter that influences shear interactions, media flow behaviour, and energy dissipation. Unlike tumbling mills, where friction affects the height to which grinding media are lifted before impact, stirred mills operate under shear dominated conditions, where particle interactions involve rolling, sliding, and surface contact forces (Sinnott *et al*., 2006). The correct specification of friction is crucial for accurately modelling these interactions in DEM simulations.

Previous research on DEM simulations of stirred mills has employed different coefficient of friction values depending on material properties and calibration studies. Esteves *et al*. (2021) used a static friction coefficient of 0.3, while Liu *et al*. (2024) employed 0.15 for media - media interactions and 0.21 for media-wall interactions. Yang (2018) reported a coefficient of friction of 0.17, based on the Hertz-Mindlin contact model. Ford and Naude (2021) used a higher coefficient of friction of 0.45 in their DEM study of a fluidized stirred media mill, suggesting that friction values may vary based on mill design and operational conditions. These findings indicate that the selection of an appropriate coefficient of friction should be based on experimental validation to ensure realistic representation of media behaviour.

For this study, a coefficient of friction in the range of 0.10 – 0.30 was selected, aligning with values reported in previous DEM simulations of stirred media mills. This range ensured an accurate representation of shear interactions, particle mobility, and energy dissipation within the system while maintaining computational feasibility.

iv. Particle shape

Spheres were selected as the preferred particle shape of grinding media for this study since the DEM simulations included grinding media only, and the exclusion of feed particles meant that spherical elements could sufficiently represent the physical interactions occurring within the mill. DEM studies frequently use spheres as they simplify contact detection, reduce computational costs, and provide well-established calibration parameters.

Although PFC software allows for the creation of non-spherical particles such as ellipsoids, the effects of particle shape variation on grinding performance were not considered within the scope of this research. Studies have shown that non-spherical particles influence flow dynamics and collision behaviour, but incorporating these effects would introduce additional computational complexity and require extensive parameter calibration.

Given the focus of this research, spherical particles were used to represent the grinding media, ensuring consistency with previous DEM simulations of stirred mills and maintaining computational efficiency.

3.3. 4 Stirred media mill simulation set-up for the study

This section describes the stirred media mill setup used in the DEM simulations and the targeted simulation outputs relevant to grinding media wear. The study aimed to analyse the load behaviour of grinding media in a stirred media mill, focusing on key DEM parameters that best infer potential wear mechanisms. To ensure computational efficiency while maintaining relevance to grinding media wear, the analysis was limited to three primary DEM outputs; contact forces, collision energy spectra, and power dissipation in contacts. These parameters potentially infer wear mechanisms in stirred media mills.

The mill setup was designed to replicate the laboratory scale stirred media milling environment, ensuring controlled conditions for analysing grinding media behaviour. The interactions between the grinding beads, stirrer, and mill walls generate complex force distributions that directly affect media wear. Specifications of the mill and summary of simulation parameters as required for the DEM simulations is shown in Table 3.5 and Table 3.6 respectively.

Table 3.5. Specification of the laboratory scale stirred mill as required for the DEM simulations.

Parameter	**Description**
Rated Power	3 kW
Angular speed	404 rpm
Mill volume	5853 cm^3
Stirrer	Steel pins
Mill diameter	180 mm
Mill height	224 mm
Stirrer shaft diameter	26 mm
Pin diameter	17 mm
Pin radial length	120 mm
Pin spacing (single column)	24.5 mm

Table 3.6. Summary of DEM simulation parameters.

Parameter	**DEM simulation value**
Bead density	4000 g/cm^3
Bead diameter	6,5,4 mm
Stirrer velocity	404 rpm
Coefficient of restitution	0.2 – 0.6
Coefficient of friction	0.1 – 0.4

Quantitative prediction of wear using DEM was not feasible due to resource and time constraints, which prevented the material characterisation of the ceramic beads and resolving to separate tangential and normal forces. Material characterisation plays a crucial role in wear studies as it provides essential properties such as hardness, fracture toughness, and elasticity, which are required for developing quantitative wear models. Without these parameters, it is not possible to compute precise wear rates or establish direct numerical correlations between grinding media behaviour and material degradation.

As a result, this study focuses on experimental tests that correlates with DEM simulation tests. Instead of attempting to establish DEM model for predicting grinding media wear, the focus is on identifying dominant wear mechanisms based on DEM outputs such as contact forces, collision energy spectra, and power dissipation. This analysis provides insights into how different operating mill conditions influence grinding media wear behaviour. Although this approach does not yield numerical predictions of wear, it offers valuable information on the conditions that may lead to increased media degradation, which is essential for optimising stirred media milling processes.

3.4 Summary

This chapter described the experimental setup, materials, and modelling framework used in this research and highlighted the rationale behind selected parameters. Laboratory grinding tests were designed to provide representative operating conditions for stirred media milling, while DEM simulations replicated the same environment to study particle interactions. Selections such as the use of alumina beads, spherical particle representation, the linear spring-dashpot contact model, and parameter ranges for stiffness, restitution, and friction were made to balance physical reality with computational efficiency. Together, these methodological decisions establish a sound foundation for analysing grinding media behaviour and evaluating wear mechanisms in stirred media mills.

Chapter 4 Results and discussion

4.1 Introduction

Grinding is an energy intensive process, where the energy input plays a crucial role in achieving the desired product fineness and minimising media wear. As noted by Joost and Schwedes (1996), wear of media in stirred media mills is directly related to the energy dissipated within the grinding chamber. Specifically, the amount of energy input, relative to the volume of the mill, significantly impacts both grinding efficiency and media wear (Joost & Schwedes, 1996). This highlights the importance of specific energy, a key parameter that directly influences the degree of particle size reduction in stirred media mills, together with stress energy. Controlling specific energy input is often sufficient to achieve the desired product quality (Joost & Schwedes, 1996).

In this study, specific energy was the primary focus, wherein energy input was varied at three levels: 5, 10, and 20 kWh/t, to assess its impact on particle size distribution, power consumption, torque, and ceramic bead wear. Feed size was also investigated at two levels, from coarse to fine: -1180+850 µm and -600+425 µm. Although feed size is a crucial factor affecting grinding efficiency, it has not received the same level of coverage in stirred media milling literature as other parameters, such as solids concentration. This factor forms an important part of the study, to explore its influence on energy requirement and media wear.

4.2 Experimental results and discussions

4.2. 1 Overview of experimental work

This section provides a recap of the experimental setup used in the study, which involved a laboratory scale batch vertical stirred media mill. The mill, with a total volume of 5800 cm^3, was equipped with a pin stirrer driven by a 3 kW motor. The specific energy input was varied at three levels: 5, 10, and 20 kWh/t, and two distinct feed sizes were used: -1180+850 µm (coarse) and -600+425 µm (fine). This was to assess its influence on product fineness, energy consumption, and media wear. Power consumption and torque were monitored using integrated sensors, while ceramic media with a density of 4000 kg/m^3 and constant solids ratio of 50% was used in all tests to focus on the effects of energy input and feed size. Particle size distribution after each milling process was measured, and the mass loss of grinding media was also measured to calculate wear rate.

4.2. 2 Specific energy input

Specific energy input plays a crucial role in the grinding process, as it directly impacts both the size reduction of particles and wear of media. This parameter is widely recognized as the most important factor influencing grinding efficiency. In stirred media mills, specific energy controls how effectively particles are broken down, but it also accelerates media wear. As stated by Kwade and Schwedes (2007), finding the optimal energy input is critical to balancing milling efficiency and minimizing wear.

Specific energy input and product fineness

The relationship between specific energy input and product fineness was assessed by measuring the particle size distribution at varying energy levels. Figure 4.1 illustrates how increasing specific energy input led to finer particle sizes for both coarse and fine feed materials. This is consistent with the observations in previous studies, where higher energy input generally correlates with size reduction, as the grinding media imparts more kinetic energy to the particles (Becker *et al*., 2001; Rule *et al*., 2008). This result is further analysed in terms of characteristic values: D_{50} and D_{80}. D_{50} represents the median size, where 50% of the particles are smaller, and D_{80} is the size below which 80% of the particles fall. These values are commonly used to summarize the grinding results in terms of product fineness.

As specific energy input increased, both D_{50} and D_{80} values decreased for both feed sizes as given in Table 4.1 and illustrated in Figure 4.2. For the coarse feed, the D_{50} decreased from 964 µm at 5 kWh/t to 845 µm at 20 kWh/t, while D_{80} also decreased from 1094 µm to 1046 µm. Fine feed, exhibited a similar trend with D_{50} reducing from 415 µm to 81 µm, and D_{80} reducing from 526 µm to 448 µm as the energy input increased from 5 kWh/t to 20 kWh/t.

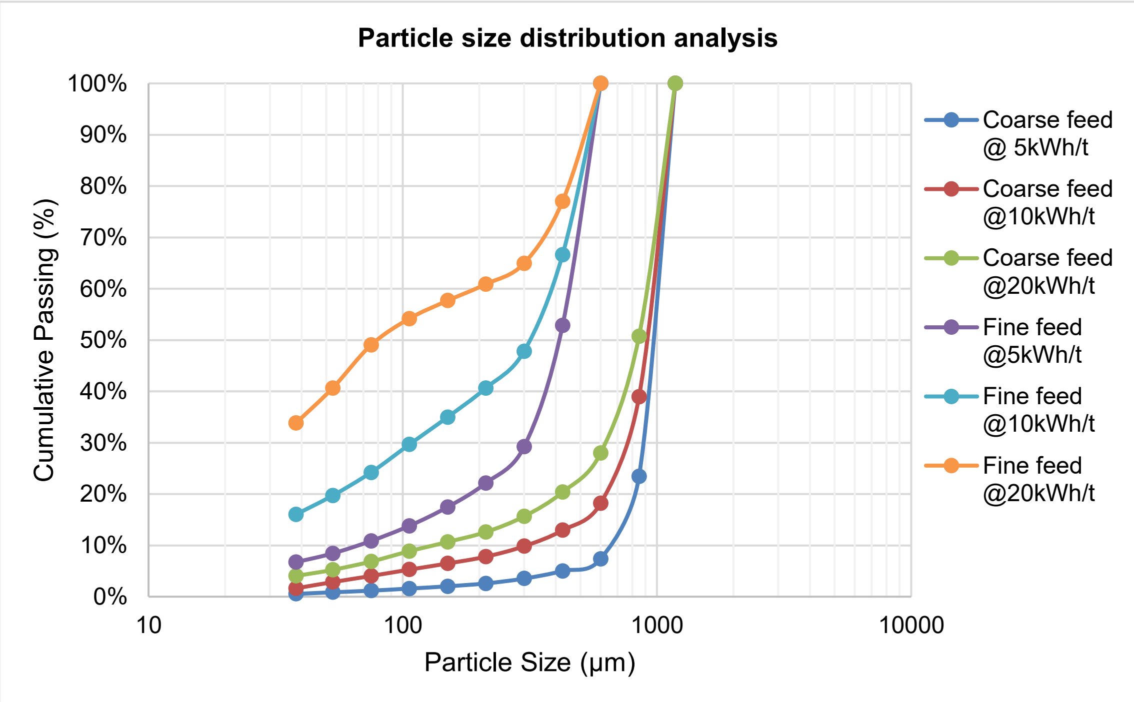

Figure 4.1. Effect of specific energy input on product fineness.

The grinding progress for fine feed at different energy levels shows a more efficient reduction in particle size compared to the coarse feed. At 5 kWh/t, D_{50} for fine feed was already 415 μm, significantly smaller than the D_{50} of coarse feed at 964 μm. As the energy input increased to 20 kWh/t, D_{50} for fine feed dropped dramatically to 81 μm, reflecting a substantial reduction in particle size. In contrast, the coarse feed showed a smaller reduction in size, with a D_{50} of 845 μm at 20 kWh/t, indicating slower grinding progression. The same was observed in the findings of Becker and Schwedes (1999), who discussed the challenges of reducing the size of coarser particles in stirred mills, especially when media sizes are not optimally matched to the feed size.

Table 4.1. Table shows the effect of specific energy input on product characteristic sizes.

Test Number	**Feed Size (μm)**	**Energy Input (kWh/t)**	**Product size, D_{50} (μm)**	**Product size, D_{80} (μm)**
1	-1180+850	5	964	1094
2	-1180+850	10	910	1072
3	-1180+850	20	845	1046
4	-600+425	5	415	526
5	-600+425	10	315	495
6	-600+425	20	81	448

This trend is clearly shown in Figure 4.2, where the fine feed graph demonstrates a more consistent, linear decrease in D_{50}, indicating a greater size reduction efficiency on the fine size class by the media size used. In contrast, the coarse feed graph exhibits a slight turn from 10 kWh/t to 20 kWh/t, which suggests that as time progressed, the rate of particle size reduction diminished. This behaviour indicates that the operational conditions were less favourable to the coarse feed, especially the size of the media used, which supports the fact that for every feed size class there is an optimum media size that facilitates efficient grinding. As highlighted by Rule *et al*. (2008), the selection of appropriate media, especially its size, plays a crucial role in maximising energy efficiency and minimising media wear. If the feed size is not properly matched to the media size, energy that should be used for actual grinding work end up getting consumed in other ways, such as excessive media wear. In such cases, wear is expected to be significant, as the mismatch leads to increased collision forces, causing more rapid degradation of the media (Hassall *et al*., 2016).

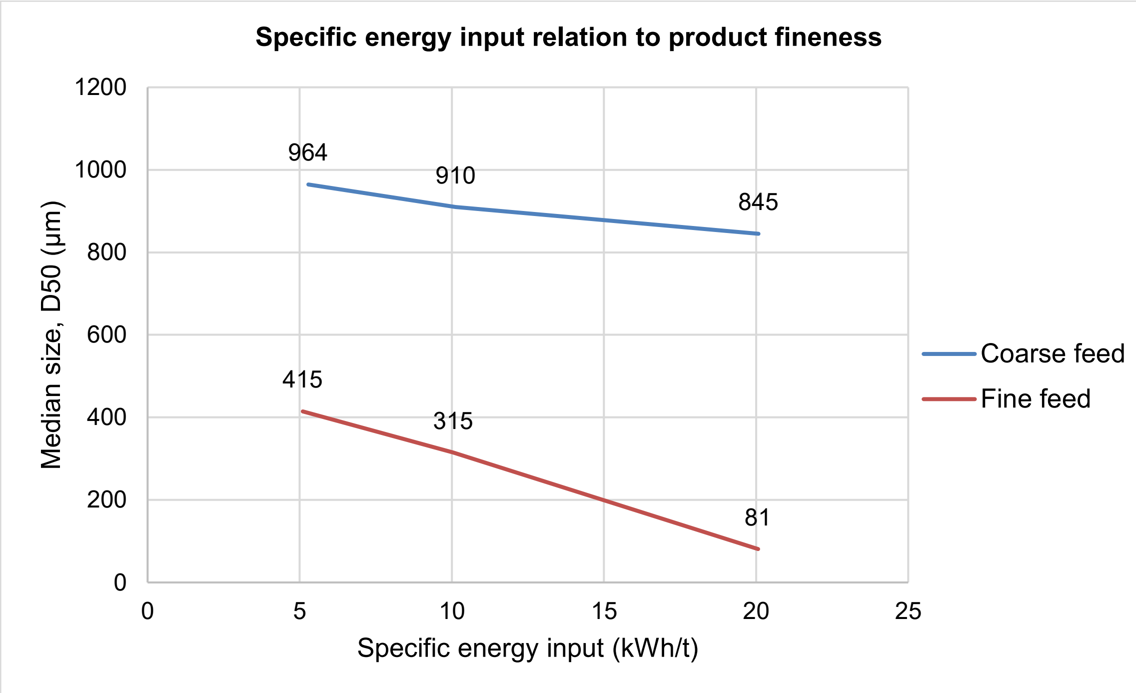

Figure 4.2. Relation between specific energy input and product characteristic size.

c) Specific energy input and milling time

The relationship between specific energy input and milling time was also examined, as the grinding process is influenced not only by energy input but also by residence time. Figure 4.3 illustrates the variation in milling time for both coarse and fine feed material as the specific energy input increases.

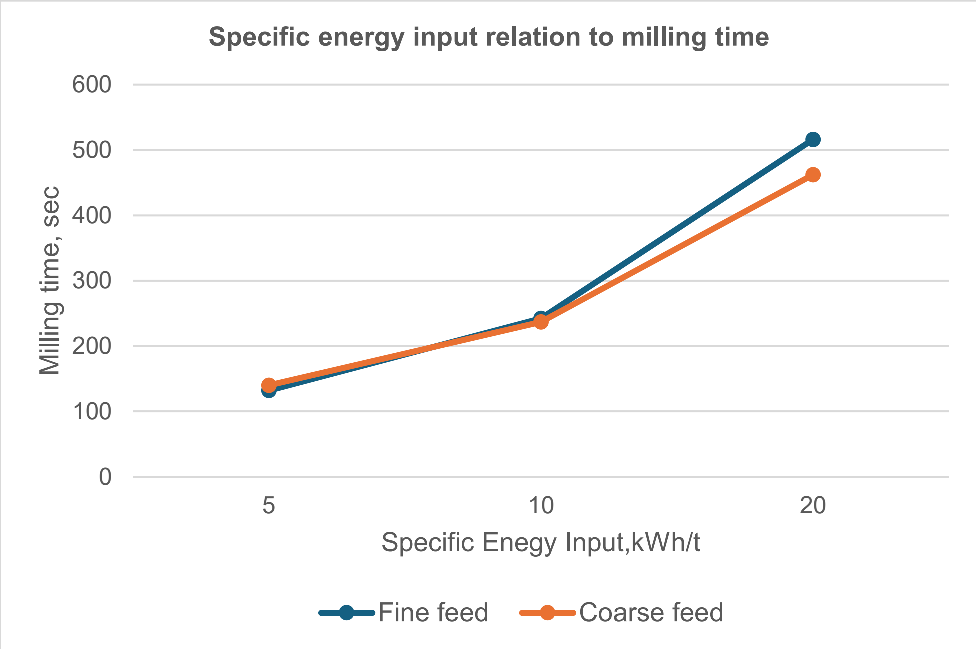

Figure 4.3. Relation of specific energy input, milling time and feed size.

As milling time increases so does specific energy input for both feed sizes. The coarse feed relatively required less milling time for the same energy input especially for high energy input. For instance, coarse feed reached 20 kWh/t at a lower milling time of 462 seconds compared to 516 seconds of fine feed. However, this difference is not evident at lower specific energy inputs, where both feed sizes show comparable milling times. This shows that the relative inefficiencies that arise with coarse feed becomes more pronounced under intensified grinding conditions. This means a significant portion of the energy was lost in non-productive events, such as media wear and other forces that do not directly impact particle size reduction.

As highlighted by Becker *et al.* (2001), coarse feeds are particularly susceptible to inefficiency when media size is not optimized for the feed size, causing excessive energy dissipation into wear and abrasion of grinding media. This further supports the need for careful matching of media size and feed size to ensure that the energy is effectively utilised for grinding rather than dissipated into non-productive processes.

4.2. 3 Power draw

Power draw is a crucial parameter in stirred media mills, representing the energy required to maintain the motion of the grinding media within the mill. Rather than directly indicating particle size reduction, it reflects the energy input necessary to create the mechanical forces that induce stress in the particles, causing them to break and reduce in size. As described by Kwade and Schwedes (2007), power draw in stirred media mills is related to the energy needed for the continuous motion of the grinding media, which then transfers energy to the feed material through collisions, impacts, and friction. According to Cleary *et* *al*, (2015), power draw is also a useful indicator of the mill's energy efficiency, providing insights into how effectively the energy is being transferred to the particles.

In this study, power draw was recorded continuously using sensors integrated into the mill system, allowing real-time tracking of energy consumption during the grinding process. Power draw is typically calculated by summing the forces acting on the mill chamber wall. The power draw was then derived from equation (3.1). An instantaneous power draw report was generated at the end of each test run, and a sample of this report is provided in the appendices. Analysis of power draw is presented from Figure 4.4 to Figure 4.6. Figure 4.4 presents the instant power time variation for both fine and coarse feed at different specific energy inputs. Graphs for 10 kWh/t fine and 10 kWh/t coarse feeds are presented for analysis and discussion purposes (refer to appendices for an illustration of all the graphs generated). The graph highlights the distinct behaviour of the power draw throughout the duration of the tests.

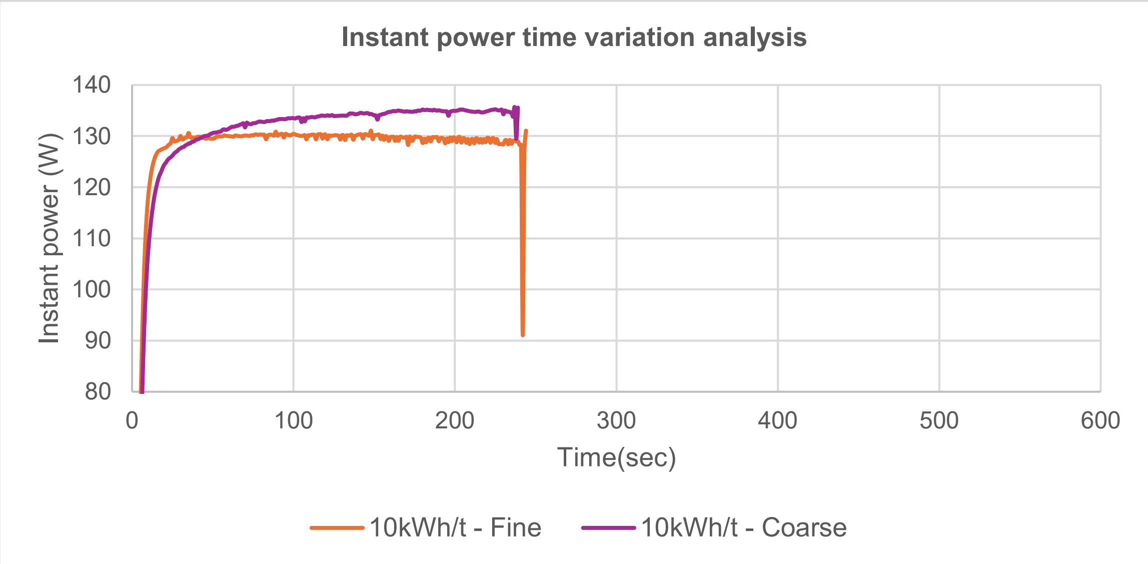

Figure 4.4. Instant power time variation analysis for different feed sizes at distinct specific energy input.

For both feed sizes, the power draw exhibits a steep increase, however fine feed tests reached peak power relatively quicker than coarse feed test. For instance, it took 10 seconds for fine feed test to reach 107 kW power compared to 16 seconds of the corresponding coarse feed. After a steep ascend, fine feed tests exhibit a relatively steeper downward turn before stabilising opposed to a relatively gradual descend shown by the coarse feed tests. This trend suggests that the grinding process is highly dynamic in the early stages for fine feed tests and in contrast, coarse feed displays a slower descent to a steady value suggesting a more consistent energy consumption pattern throughout the milling process.

Generally, coarse feed exhibits a higher instantaneous power draw than fine feed across the different energy inputs, except for the 5 kWh/t test as highlighted in Figure 4.5 and Figure 4.6 in form of average and maximum power. However, as the test progresses, the difference between the two feed sizes decreases, with the gap gradually closing. This suggests that the initial higher power draw for fine feed at 5 kWh/t test, might be related to the specific interactions between the fine particles and grinding media, which could have a different response to energy input compared to other fine feed tests.

The 10 kWh/t fine feed graph shows relatively high fluctuations in power draw compared to the corresponding 10 kWh/t coarse feed. These fluctuations may be attributed to the varying dynamics between the fine feed and the grinding media. It is important to note that the mill reached a peak rotational speed of 406 rpm for fine feed, as opposed to the 403 rpm recorded for all other tests. This increased rotational speed likely contributed to the higher fluctuations in power draw observed for fine feed at this energy level test. This is further highlighted by average and maximum power recorded for the 10 kWh/t fine feed test which is relatively higher than all the other fine feed tests as shown in Figure 4.5 and Figure 4.6. This finding underscores the influence of stirrer speed to grinding performance which is an area that is extensively covered in literature (Cleary *et al.*, 2015; Jankovic, 2004; Sinnott *et al*., 2006).

As the test progressed, graphs revealed a slight decrease in power draw. This is particularly evident in the 20 kWh/t tests, where both fine and coarse feeds show a slight drop in power. However, the fine feed graph exhibits a relatively more pronounced decline compared to the coarse feed. This drop may be due to several factors, which may include feed particles becoming finer and rounder and exhibiting less friction resistance hence relatively low energy is required to compensate the power losses. Wear of media cannot be attributed to this phenomenon since at 20 kWh/t media mass loss is expected to be insignificant.

This decreasing power draw over time is in agreement with the findings of Becker *et al*. (2001) and Becker and Schwedes (1999), who observed that as media wear increases, the efficiency of the grinding process decreases, leading to an increase in energy dissipation rather than size reduction.

Figure 4.5. Instant power averages for different feed classes at distinct specific energy input.

Figure 4.6. Recorded maximum instant power for different feed classes at distinct specific energy input.

Figure 4.5 and Figure 4.6 provide additional insights into the instantaneous power draw, as already noted in the preceding passages, by presenting the average instantaneous power and the maximum recorded instantaneous power respectively. These figures complement the time variation analysis from Figure 4.4, presenting a clearer understanding of the overall power consumption trends. Figure 4.5 indicates that coarse feed generally requires a slightly higher average power draw than fine feed across all energy levels except for the 5 kWh/t tests**.** The same is noted on the maximum power recorded for all the tests. Generally, coarse feed recorded higher maximum power.

Although fluid viscosity was not directly measured in the tests, it plays an important role in influencing grinding efficiency. Its influence can be inferred from the observed power draw trends. As shown in Figure 4.6, coarse size consistently recorded slightly higher maximum instantaneous power than fine feed, particularly at 10 kWh/t and 20 kWh/t. This suggests greater resistance within the slurry, likely due to increased apparent viscosity associated with larger particle sizes and less uniform patterns. At the same solids concentration, coarse particles tend to increase interparticle friction and impact fluid mobility, effectively raising the hydrodynamic resistance in the mill. Ultimately, more energy is required to sustain the same grinding conditions.

These increased viscous forces consume a portion of the total power draw, leading to a decrease in grinding efficiency. Power draw in stirred media mills is influenced not only by the media motion and particle breakage but also by the slurry's viscosity, which impacts the energy required to overcome resistance in the fluid (Becker & Schwedes, 1999).

Cleary *et al*. (2015) discussed how higher viscosity increases the power required to move the grinding media and achieve particle size reduction. This could be a contributing factor to the higher power draw observed for coarse feed in the tests. When the slurry viscosity increases, energy is diverted away from particle breakage and instead used to overcome the resistance of the thicker fluid, contributing to inefficiency in the grinding process. This is important because it suggests that, in addition to media size and feed size, the viscosity of the slurry plays a critical role in determining the overall power consumption in stirred media mills.

4.2. 4 Torque

Mill torque is directly related to the power draw in stirred media mills as defined by equation (3.2). Both parameters reflect the mechanical energy required to sustain the motion of the grinding media and transfer energy to the particles. Torque in stirred mills is a measure of the rotational resistance of the system and is influenced by factors such as stirrer speed, media characteristics, and the feed material. Cleary *et al*. (2015) and Kwade and Schwedes (2007) highlighted that changes in torque reflect the energy dissipation patterns during grinding and can be used to assess the milling process performance.

In this study, torque was continuously measured using sensors integrated into the lab - scale stirred media mill system, as described in Chapter 3. These sensors allowed for real-time tracking of torque during the grinding process, providing continuous data on the resistance encountered by the stirrer as it moved the grinding media. At the end of each test, an instantaneous torque report was generated, summarizing the recorded torque data for that specific run.

Figure 4.7 presents the mill torque time variation for both fine and coarse feed materials at different specific energy input levels. Similar to the power draw trend, torque exhibits an initial sharp increase for both feed sizes**.** Fine feed reaches peak torque relatively faster than coarse feed, which aligns with the observed power draw behaviour from Figure 4.4. For instance, fine feed reaches peak torque more quickly, with a rapid ascent in the early seconds of the test before stabilising, whereas coarse feed takes a more gradual path to reach steady-state torque.

The torque profiles also show that coarse feed generally requires higher torque than fine feed across the different energy inputs, similar to the trends seen in the power draw analysis. However, for the 5 kWh/t tests (Figure 5.5), fine feed initially shows a higher torque value, but as the test progresses, the gap between the feed types gradually reduces. This suggests that the dynamic interactions between fine particles and grinding media in the early stages of grinding might have caused a higher torque requirement at this specific energy input level, but this difference diminishes as the grinding process continues.

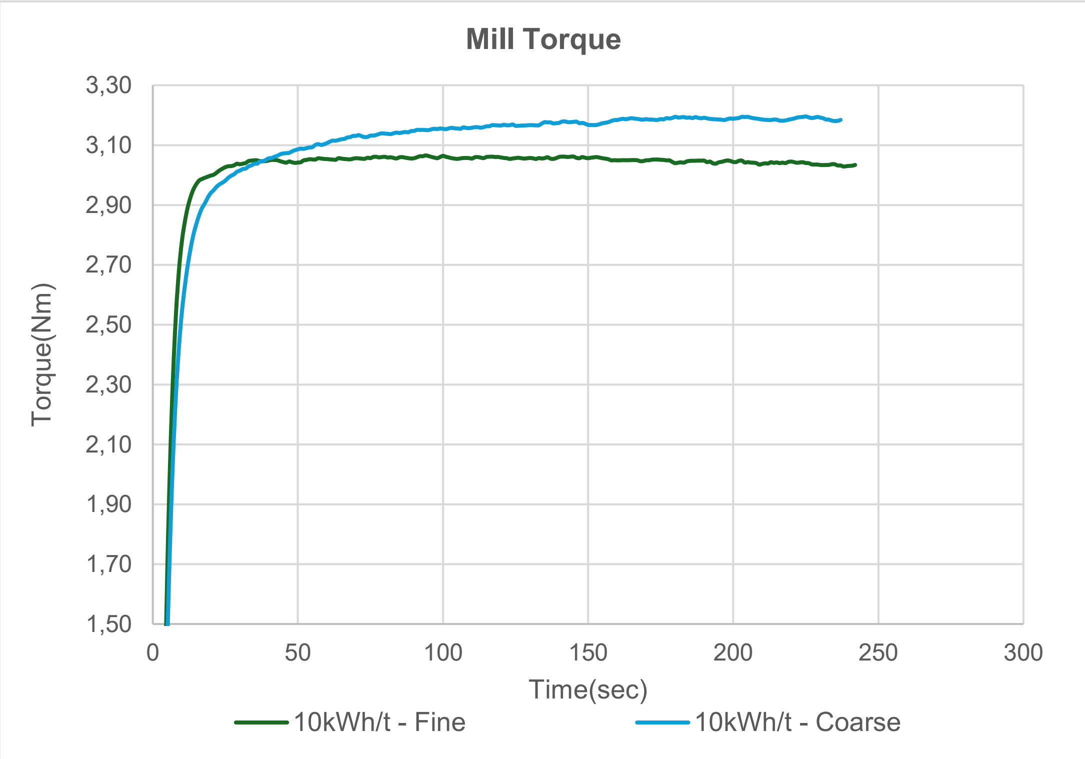

Figure 4.7. Mill torque time variation analysis for different feed sizes and distinct specific energy input.

Figure 4.8 shows the average torque for both feed sizes at different specific energy input levels. As with the power draw, coarse feed generally shows a higher average torque than fine feed, except for 5 kWh/t fine feed test. The trends observed here mirror the power draw averages in Figure 4.4. Figure 4.9 presents the maximum recorded torque for each test. The maximum torque follows a similar trend to the average torque, with coarse feed generally showing higher peak values compared to fine feed across the different specific energy levels. This aligns with the maximum power trends observed, where coarse feed consistently requires higher peak values for both power and torque.

Higher torque is typically associated with higher energy dissipation (Kwade & Schwedes, 2007), especially in the early stages of grinding when the particle size is larger, and more energy is needed to break the particles. The initial higher torque for fine feed can be attributed to the complex interactions between the fine particles and the grinding media, requiring additional energy to facilitate breakage in the initial phase. As the grinding continues and the particle size reduces, the torque required to move the media and grind the material decreases, aligning with the observed results in Figure 4.7 and Figure 4.8.

Figure 4.8. Average torque analysis for different feed sizes at distinct specific energy input.

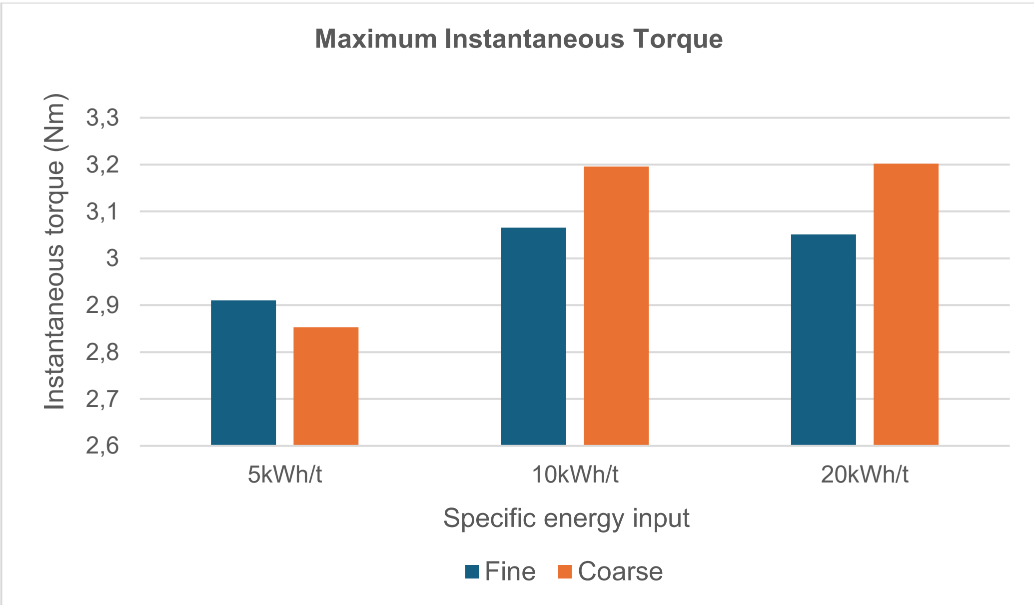

Figure 4.9. Maximum torque recorded for different feed sizes at distinct specific energy input.

The analysis of torque supports the findings from the power draw analysis, as expected due to their relationship. Both parameters exhibit similar trends, with coarse feed consistently requiring relatively high torque.

4.2. 5 Energy input

Energy input represents the total energy supplied to the system during the grinding process. It is a combination of two main components: the energy dissipated through collisions, friction, and shear forces within the mill, and the energy absorbed by the grinding media and the product particles. Energy input directly correlates with power draw, as power is the rate at which energy is supplied to the mill system. The energy that is dissipated does not contribute directly to particle size reduction but rather to maintaining the dynamics of the grinding process, whereas the absorbed energy is used for actual size reduction of the particles (Becker & Schwedes, 1999; Kwade & Schwedes, 2007; Sinnott *et al*., 2006).

Figure 4.10 presents the time variation of instantaneous energy for both fine and coarse feed materials at different specific energy input levels. As with power draw, the instantaneous energy increases rapidly at the beginning of the test, with fine feed reaching peak energy values more quickly than coarse feed. Finer particles have a greater surface area exposed to the grinding media, leading to more frequent interactions and thus higher initial energy consumption. This is in agreement with the study by Sinnott *et al*. (2006) who highlighted that finer particles tend to consume more energy during the early stages of grinding due to their increased surface area, which leads to more particle-media interactions.

Over time, the energy consumption stabilises, with a slight decrease observed toward the end of the grinding process. This reduction can be attributed to the decreasing efficiency of the mill as particle size reduction slows, and energy dissipation becomes more dominant, a trend observed by Hassall *et al*. (2016), who emphasized that as media wear increases, less energy is available for actual grinding.

Figure 4.11 and Figure 4.12 shows the average and maximum instantaneous energy respectively for different feed sizes at various energy input levels. Similar to the trends observed in power draw and torque, coarse feed generally exhibits slightly higher average energy consumption than fine feed across all energy input levels. This trend suggests that coarse particles require more energy for grinding, which aligns with the findings of Cleary *et al*. (2015), who observed that coarser feed tends to require more energy for initial breakage, as the particles are larger and more resistant to fracture.

Energy input, as measured in this study, provides crucial insight into the energy efficiency of the grinding process. The trends observed demonstrate how energy is distributed throughout the milling process and how different feed sizes, and energy levels impact the overall energy consumption. The relationship between energy input and the efficiency of size reduction is complex, and understanding these trends helps in optimising the milling process and reduce media wear.

Figure 4.10. Time variation analysis of instant energy at different feed sizes and distinct specific energy input.

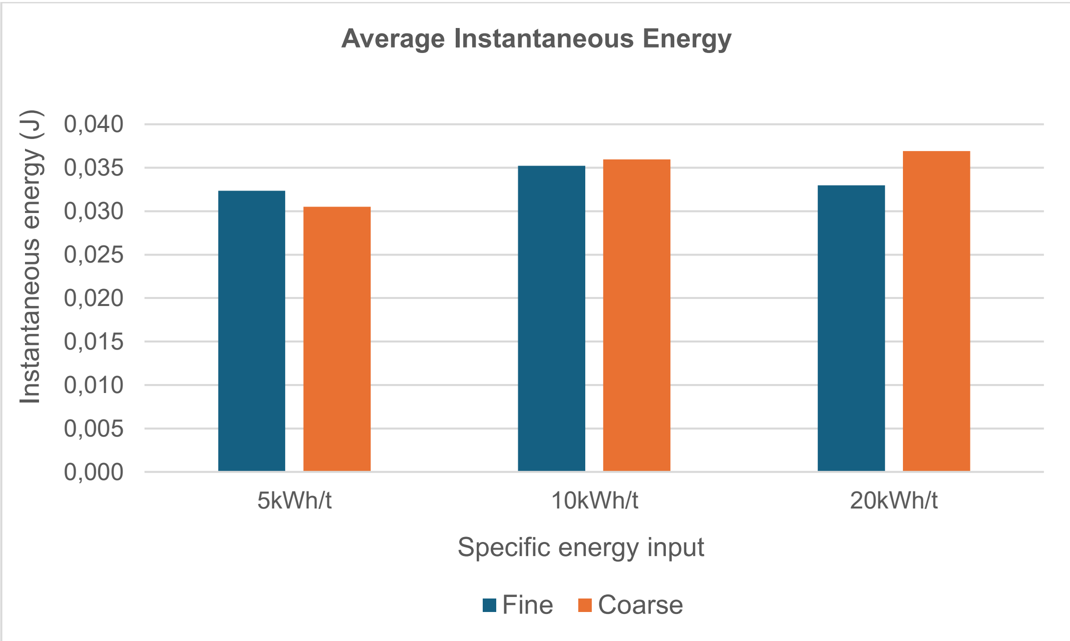

Figure 4.11. Average instant energy for different feed sizes and distinct specific energy input.

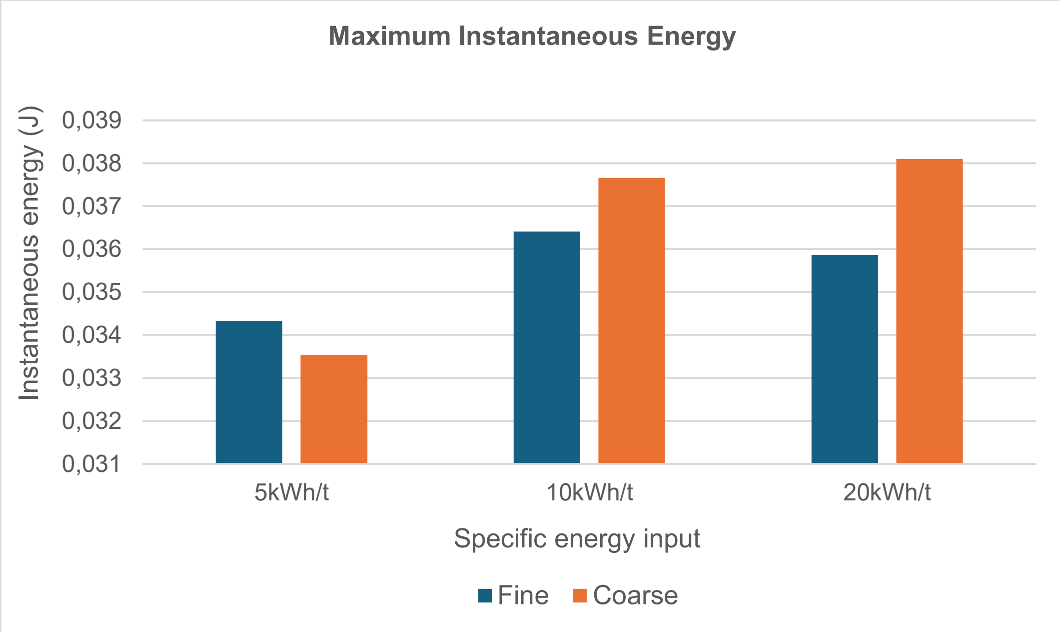

Figure 4.12. Maximum instant energy recorded for different feed sizes and distinct specific energy input.

4.2. 6 Media wear test

This section describes and discusses the findings of the wear tests that were conducted as part of the grinding tests. Coarse size class was selected as feed material and other parameters were kept constant as given in Chapter 3, i.e. mill speed, solids concentration, media sizes, fill ratio and mill geometry. The tests were allowed to run for approximately two and four hours with measurements taken after every test i.e. mass loss according to equation 2.3. A milling performance report was also generated at the end of every grinding test (see appendices for reference).

Figure 4.13 presents the time variation analysis of specific energy input during the wear test with coarse feed i.e. Test 2. Over the duration of the test, which lasted approximately four hours, the specific energy input showed a linear variation over time which is consistent with findings from the grinding tests. This indicates a steady, proportional increase in the energy supplied to the system as grinding progressed.

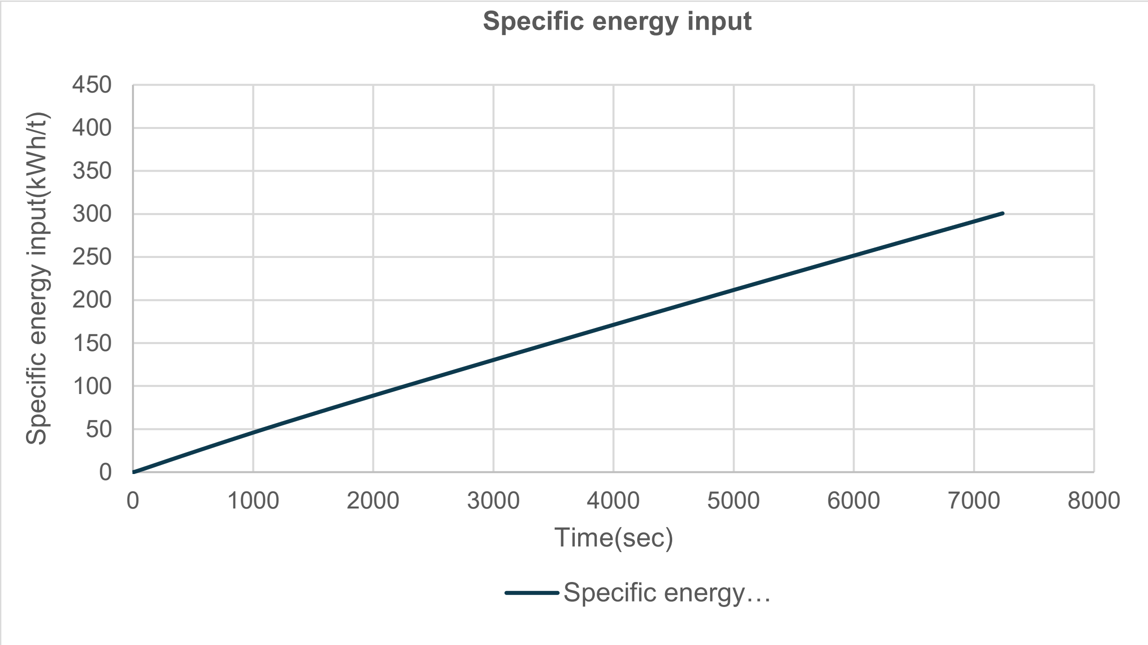

Figure 4.13. Time variation analysis of specific energy input of wear test run conducted with coarse feed size with other parameters constant.

Figure 4.14 presents time variation of mill power over the duration of the four-hour wear test period for Test 2. Power draw reached a peak 146 W and achieved an average of 130 kW. The average power is consistent with what was observed in the grinding tests with coarse feed. Maximum power, on the hand, is slightly higher than what was observed in the grinding tests. This can be explained by a relatively higher average stirrer speed recorded at 408 rpm against 404 rpm observed for the grinding tests. Overall, the wear test power draw parameters were in good agreement with grinding tests under the same conditions.

The power draw graph exhibits a steady decrease with time, which was also noted in the grinding tests. This can be attributed to several factors, such as media wear, in this case wear can be considered due to the extended time of the test as opposed to the initial size reduction tests, and the reduction in grinding efficiency as the process progresses. According to Kwade and Schwedes (2007), power draw typically decreases over time in stirred media mills due to the ongoing wear of the media, which causes the grinding environment to become less effective at transferring energy to the feed material. As the grinding media become smoother and more worn, they experience less resistance, which results in a reduction in the required power to maintain the same stirrer speed (Cleary *et al.*, 2015).

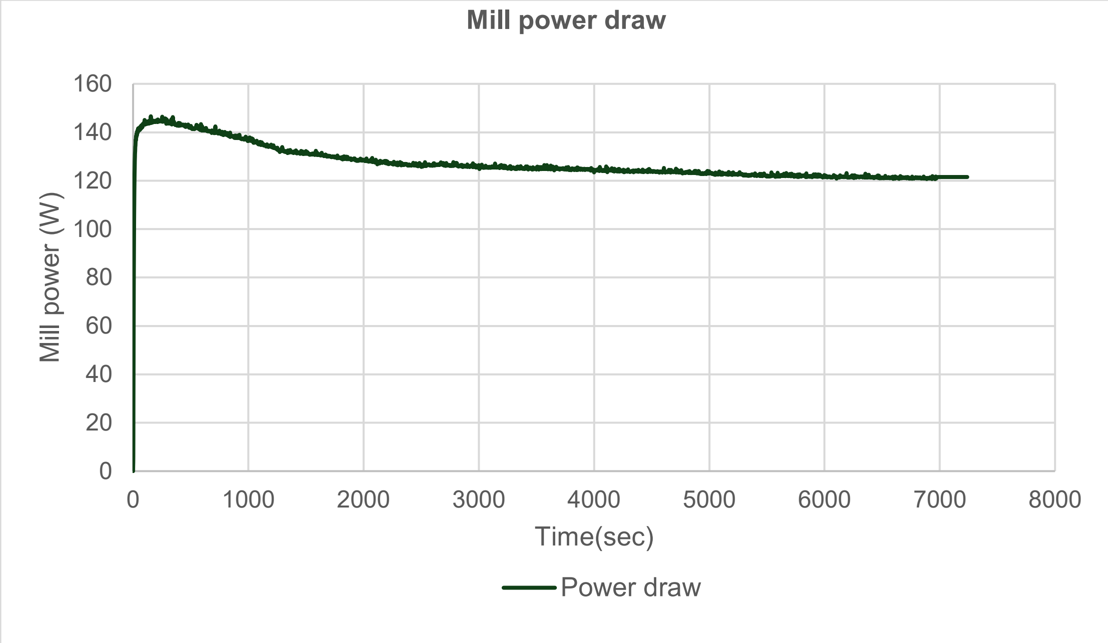

Figure 4.14. Time variation analysis of mill power of the media wear test conducted with coarse feed size with other parameters constant.

Table 4.2 presents the maximum values observed for the parameters studied in the media wear test. The key parameters considered are specific energy, mill power, instant energy, and mill speed. From Table 4.2, the specific energy input in Test 2 (300.68 kWh/t) is double that of Test 1 (145.58 kWh/t). This aligns with the time variation analysis of specific energy input presented earlier which suggests a linear relationship between specific energy and time for the conditions tested in this study.

Table 4.2. Maximum values observed for the parameters studied in the media wear test.

	Specific energy (kWh/t)	**Time(sec)**	**Mill power (W)**	**Instant Energy (J)**	**Mill Speed (rpm)**
Test 1	145,58	3624	130,64	0,036	408,86
Test 2	300,68	7238	146,60	0,041	411,31

Figure 4.15 and Table 4.3 present the media wear loss analysis during the wear tests conducted with coarse feed, where other parameters were held constant. It is important to note that only coarse feed was considered for the wear tests to obtain measurable media wear responses of media for meaningful analysis. The data highlights a clear trend showing that media wear increases as time progress. This trend is consistent with findings from time variation analysis of specific energy input. As specific energy input doubled, wear also doubled, suggesting a direct relationship between the energy applied in the grinding process and the rate of media degradation. The relationship between specific energy and wear is in alignment with findings from Kotze and Bedesi (2015), who suggested that wear

in stirred media mills is directly related to energy input, where higher energy inputs typically result in increased wear rates. The work of Kwade and Schwedes (2007) also suggested that media wear in stirred media mills is primarily influenced by the energy input, which accelerates wear through repeated mechanical collisions and abrasion between the media and particles.

Table 4.3 also shows an apparent increase in the mass of the - 5 mm size fraction after wear tests. This reflects mass loss from +5 mm size class, as worn media particles reduced in size and subsequently entered the – 5 mm size fraction at the end of the wear test.

Table 4.3. Mass loss for different media sizes.

	4 hr Wear Test (-1180+850 µm)				2 hr Wear Test (-1180+850 µm)			
Mass (g)	**6 mm**	**5 mm**	**-5 mm**	**Total**	**6 mm**	**5 mm**	**-5 mm**	**Total**
M1	2336,37	2336,49	2336,55	7009,41	2336,69	2336,75	2336,51	7009,95
M2	2333,4	2207,46	2458,96	6999,82	2327,42	2241,97	2435,83	7005,22
ΔM	2,97	129,03	-122,41	9,59	9,27	94,78	-99,32	4,73

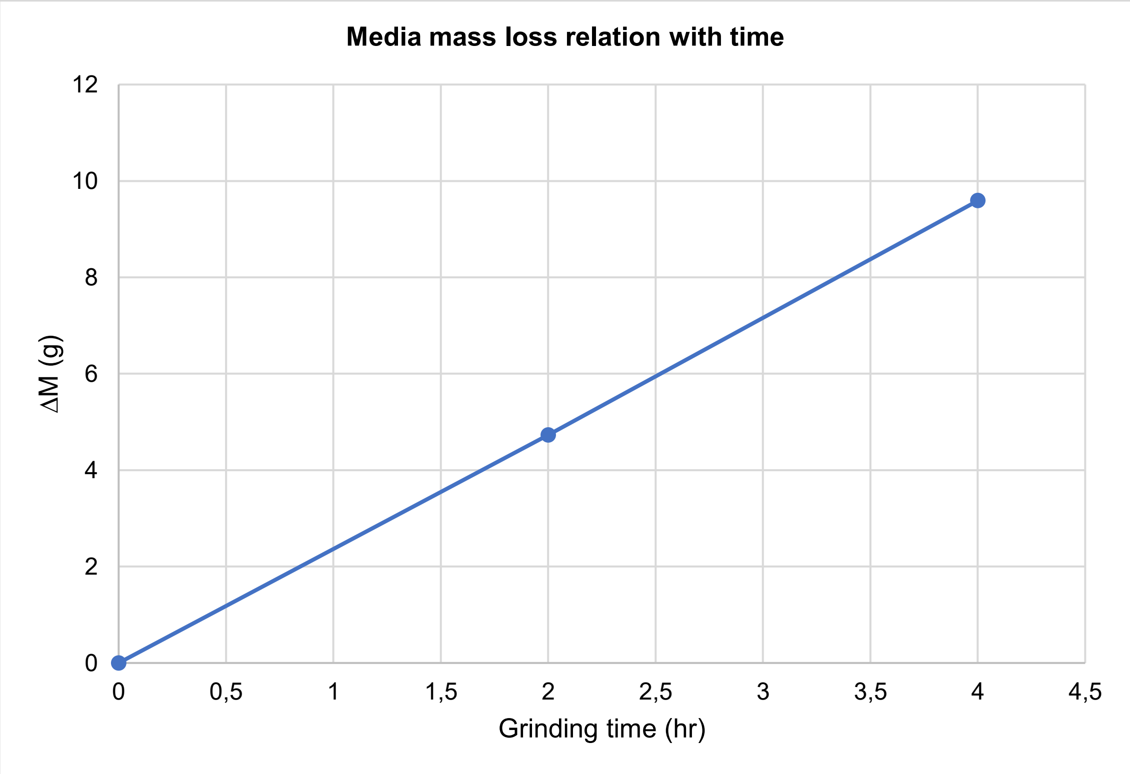

Figure 4.15. Media wear loss analysis with coarse feed and other parameters constant.

In conclusion, the wear loss data from these wear tests aligns with the literature, confirming the relationship between specific energy input and media wear in stirred media mills. Further, it underscores the importance of energy control and monitoring in optimising milling performance and minimising media consumption during grinding.

4.2. 7 Summary of experimental results

The experimental study highlighted influence of key input parameters such as specific energy input and feed size on grinding performance in the laboratory-scale stirred media mill. Increasing energy input led to finer particle sizes for both coarse and fine feed materials, with finer particles being reduced more efficiently highlighting the importance of closely matching feed material to media sizes. The coarse feed required less milling time for the same energy input, suggesting its relative inefficient grinding compared to fine feed.

The impact of stirrer speed was also observed, as an increase in speed contributed to higher fluctuations in power draw and torque for all feed sizes. Also impact of slurry viscosity was observed, which increased with feed size, playing a crucial role in energy consumption: larger feed particles increased the viscous forces, reducing the overall grinding efficiency. These findings indicate that for coarse feed, more energy was lost to non-productive events such as media wear, further confirming the need for optimal media size matching to feed size.

In terms of output parameters, both power draw and torque exhibited trends that aligned with the input parameters, showing that coarse feed generally required higher torque and power. This supports the idea that relatively more energy was dissipated in frictional losses and media wear rather than contributing to particle size reduction. The findings from the wear test, where coarse feed was used, revealed a direct relationship between energy input and wear rate: coarser feed produced more significant wear, which is ideal for studying the wear process. The results underscore that higher energy input accelerates media wear, particularly in the case of coarse feed, reinforcing the importance of balancing energy input with feed size and media selection to minimise wear and improve grinding efficiency.

4.3 Simulation results and discussion

4.3. 1 Overview of simulation work

A description of the simulation procedure was given in Chapter 3. The simulation part of the research leveraged the PFC DEM simulation code. The primary objective of the simulations was to analyse the behaviour of grinding media to explain grinding results observed in grinding tests with a particular focus on wear. Key metrics such as power draw energy spectra and spatial distributions of particles and their velocities provide insights into the grinding process which then provide avenues for both energy and wear optimisation.

Notwithstanding the power and flexibility of the current version of PFC code available at the Department, the work was presented with some challenges. Notably, the PFC code could not separate normal and tangential energy losses as per configuration, which resulted in only total power loss being available for analysis. This was a setback for the research work as information of power loss split into tangential and normal provides insight into the type of dominant forces present in stirred mils. Another limitation was on selection of media size. Smaller sizes proved to take long man hours to generate which resulted in use of size double the size of experimental tests sizes to reduce the computational burden while still maintaining relevant simulation conditions. These limitations could be addressed in future work through use of more advanced DEM programs such as RockyDEM or EDEM. These codes incorporate more sophisticated contact models and energy-tracking capabilities that can separately quantify normal and tangential energy dissipation during collisions. This would allow for a more detailed analysis of energy transfer mechanisms, especially in relation to wear and impact forces. The enhanced computational efficiency available in RockyDEM can support simulations with smaller media sizes and larger particle counts, thereby reducing the need to scale up media size while maintaining realistic milling conditions.

Given these constraints, the simulations focused on three primary outputs: power draw, collision energy spectra, capturing simulation frames. These metrics still offer valuable insights into the grinding process. Analysis of results and insights drawn are presented in the following passages.

Table 4.4 presents simulation input and output data, in the form of coefficient of friction and restitution and power draw, which was recorded as total power loss from the report generated by the simulator (refer to appendices). Other input parameters were matched with grinding tests configurations except for media sizes and exclusion of slurry phase as mentioned earlier, also refer to appendices for the parameters input report.

Table 4.4. A summary of the simulations undertaken including input and output parameters.

Simulation ID	**Coefficient of friction**	**Coefficient of restitution**	**Particle size (mm)**	**Mill speed (rpm)**	**Media mass (g)**	**Media density (g/cm³)**	**Av. Power Draw (W)**
Sim 1	0.1	0.2	16,14	404	7010	4000	103,9765215
Sim 2	0.3	0.2	16,14	404	7010	4000	100,3896752
Sim 3	0.1	0.6	16,14	404	7010	4000	82,82778984

The selection of the coefficient of friction and coefficient of restitution in DEM simulations is typically achieved by a combination of theoretical values and empirical calibration. Literature provides initial estimates for these parameters, derived from experimental observations in similar system. In this study, both the coefficient of friction and coefficient of restitution were selected by calibrating the simulation program to match experimental power draw data. The process involved adjusting the values of these coefficients iteratively, running simulations, and comparing the simulated power draw with the actual experimental results until a close match was achieved. This calibration ensured more realistic simulation of the grinding process conditions.

It is important to note the impact of the coefficient of friction and coefficient of restitution on power draw as these parameters offers insights into the media properties. The findings from Jayasundara *et al*. (2008) provide valuable insights. Their study showed that increasing the particle/particle sliding friction coefficient led to changes in particle flow dynamics, with higher friction resulting in a more stratified flow and fewer high-energy collisions. But this adjustment had a negligible effect on the power draw of the system, which is consistent with the current result, as the friction coefficient primarily governs the interactions between particles without significantly influencing the overall energy consumption.

Their study also showed that that higher restitution coefficients resulted in more frequent and energetic collisions, improving grinding performance in terms of collision frequency and energy. Despite these increases in collision activity, the power draw remained almost constant. In contrast, in this study, an increase in coefficient of restitution to 0.6 resulted in a decrease in power draw. This drop could be attributed to the reduced energy dissipation during collisions, as higher restitution allows particles to retain more kinetic energy. This results in less energy being absorbed by the system, reducing the power input required to sustain the grinding action. It suggests that, beyond a certain point, increased restitution at may lead to a more energy-efficient system, potentially reducing the overall power demand.

4.3. 2 Simulation power draw

When average power draw between the experimental tests and the simulation is compared in Figure 4.16, the simulation displays a lower power draw. This is to be expected as the simulation model does not include the slurry phase, and slurry is known to play a major role in energy dissipation through viscous forces. Simulations only recorded energy dissipation from media-media and media-mill geometry collisions because the slurry was excluded, which resulted in a lower total power draw than the experimental tests that included this extra slurry dissipation.

Table 4.5 shows % deviation between simulated and experimental average power draw values for both fine and coarse feeds. Percentage deviations ranged from approximately 14 % to 33 %. The deviations were consistently higher for the coarse feed, reflecting the greater influence of slurry-particle interactions in coarse feed grinding, which were not present in the dry DEM simulations.

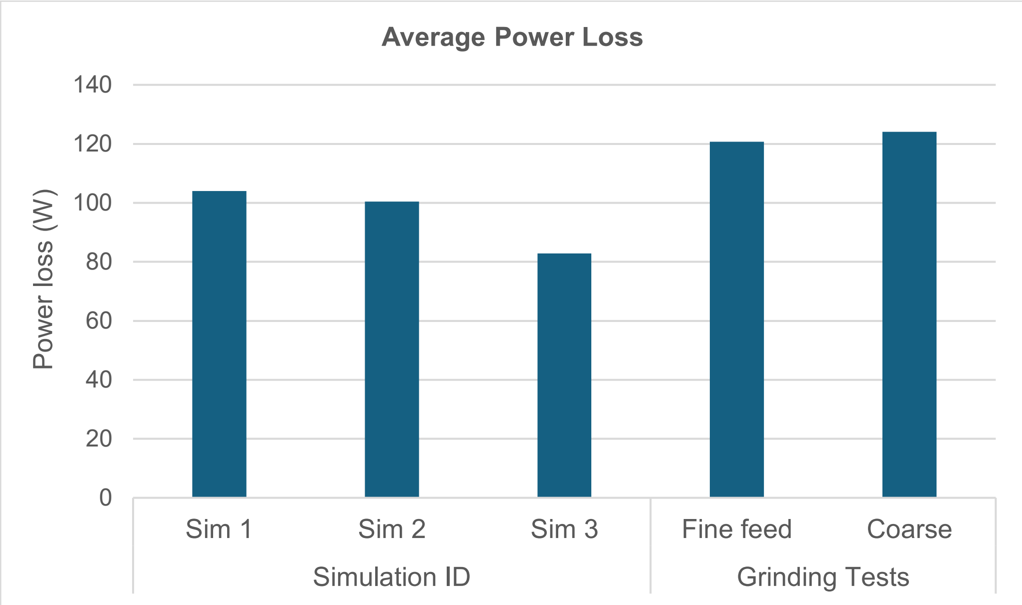

Figure 4.16. Average power loss for simulation and experimental tests.

Table 4.5. Deviation between average simulated and experimental power draw.

Simulation ID	Experimental Test Feed	Average Experimental Power Loss (W)	Average Simulation Power Loss (W)	% Deviation = ((Exp – Sim)/Exp) x 100
Sim 1	Fine	120.68	103.98	13.84
	Coarse	124.09		16.21
Sim 2	Fine	120.68	100.39	16.81
	Coarse	124.09		19.10
Sim 3	Fine	120.68	82.83	31.36
	Coarse	124.09		33.25

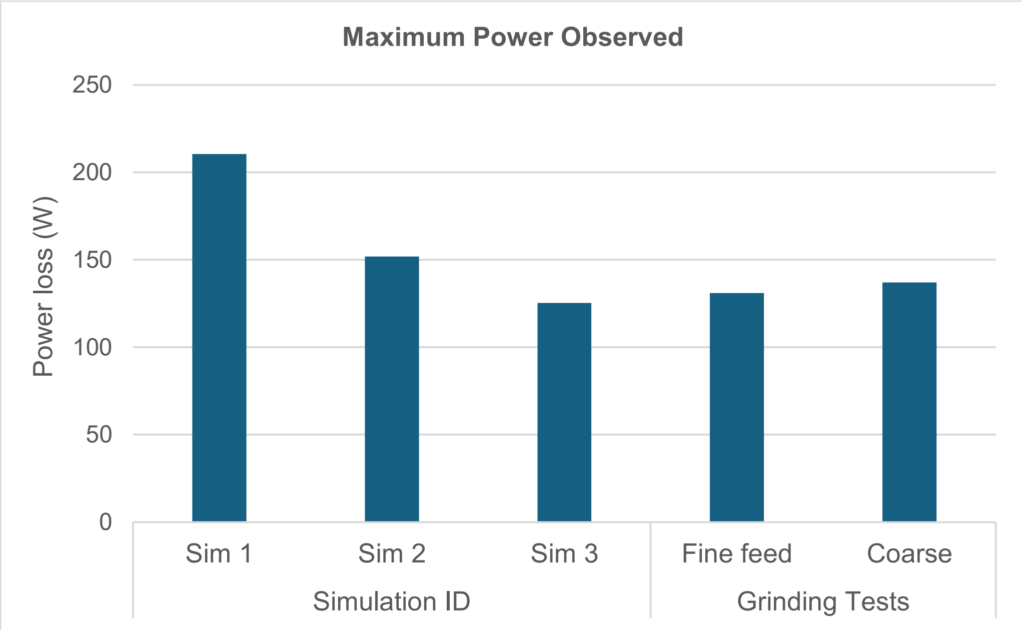

Figure 4.17. Maximum power observed for both simulation and experimental tests.

The simulations' maximum power draw, Figure 4.17, in a similar fashion, was likewise less than the experimental data. Again, since slurry adds to the resistance and power requirements during grinding, this discrepancy is probably explained by the simulation's absence of the slurry phase. Slurry can contribute up to 34% of the system's power dissipation because it adds resistance through viscosity (Ndimande *et al.*, 2019). Notwithstanding these variations, the simulation model nevertheless offers a fairly accurate depiction of the grinding process, especially when it comes to media-media interactions. The simulation well captured the basic energy dissipation mechanisms, making the model a valuable tool for examining the dynamics of core grinding, even though slurry would increase the overall power consumption.

Figure 4.18. Simulation power time variation.

The simulation's power-time variation is displayed in Figure 4.18, which demonstrates an intriguing and noteworthy degree of power draw fluctuation over time. This power fluctuation can be a sign of possible grinding process inefficiencies. It is a topic that merits more research because figuring out the fundamental reasons behind these variations may open more optimisation possibilities. Such erratic power fluctuations in many systems frequently indicate that some process elements are not operating as well as they could. An important improvement in energy efficiency and overall mill performance may result from determining and resolving the causes of these oscillations.

4.3. 3 Collision energy spectra

The distribution of energy levels during particle collisions in the mill is depicted by the collision energy spectra in Figure 4.19, where low-energy hits are more common. These results are consistent with findings of Ndimande *et al*. (2019), Larsson *et al*. (2020) and Sinnott *et al*. (2006) which all revealed comparable energy spectra in stirred medium mills.

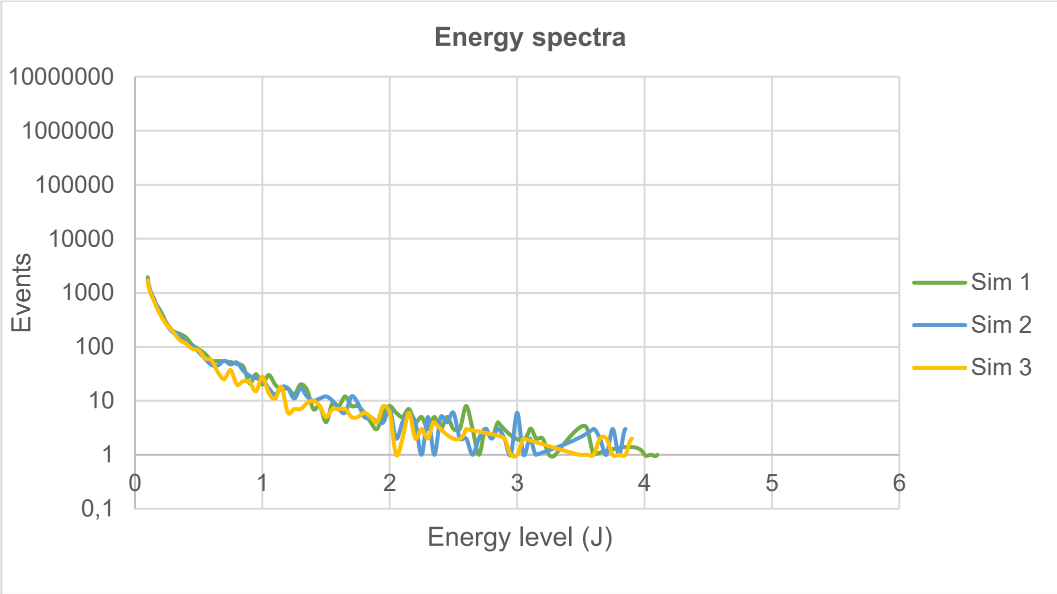

Figure 4.19. Simulation collision energy spectra.

The energy spectra offer a useful tool for forecasting feed particle breakage and wear. We can forecast how feed particles will break depending on the energy levels they encounter during collisions by merging the energy spectra with the breakage probability models such as one proposed by Bwalya and Chimwani (2020).A similar prediction can be made in terms of grinding media wear by incorporating energy based wear models such one created by Xie and Zhao (2022).

4.3. 4 Summary of simulation work

Despite difficulties encountered, the simulation program used in this study turned out to agree with the grinding tests outcome of power draw. The simulation program's inability to provide separate normal and tangential energy losses was one of the main drawbacks, which prevented the availability of comprehensive power loss data. Some experimental settings were also changed including exclusion of slurry phase and larger media sizes due to the low computational power of the current version of the code.

Notwithstanding these difficulties, the simulation produced a promising power draw estimate, and the calibrated coefficients of friction and restitution produced outcomes in line with experimental observations. Significantly, power draw decreased when the coefficient of restitution was adjusted to 0.6. This suggests that higher restitution lowers energy dissipation and may increase energy efficiency after a certain point, providing information about how to optimise grinding processes.

The models' power-time variation revealed fluctuations, this offers an intriguing direction for future study. Knowing the underlying causes of these power oscillations may help identify areas for optimisation since they may indicate inefficiencies in the grinding process. Also, the simulation's collision energy spectrum agreed with results from previous studies which demonstrated a preponderance of low-energy collisions. The study nevertheless offers a strong basis for future research, despite the exclusion of the slurry phase and difficulties with the simulation code preventing more thorough examination. Incorporating wear and breakage models into a more potent DEM tool will enable a thorough comprehension of the grinding process, including media wear and size reduction mechanisms, ultimately enhancing grinding efficiency optimisation.

Chapter 5 Conclusions and recommendations

5.1 Conclusions

This study investigated the wear behaviour of ceramic grinding media in stirred media mills through combined experimental and numerical (DEM) approaches. The aim was to understand how operating conditions, energy input, and media interactions influence energy transfer, power draw, and ultimately, wear behaviour. The work provided key insights into both the potential and the limitations of the DEM program used for simulating the milling process, as well as valuable findings from the experimental tests. The following paragraphs outline the key findings of the study.

Separate normal and tangential contact-force components could not be extracted due to functionality limitations within the DEM platform. However, analysis of the collision-energy spectra revealed a predominance of low impact energy events, consistent with previous studies (Cleary *et al.*, 2015), indicating that attrition and abrasion were the dominant wear mechanisms under the simulated conditions. DEM predicted power draw values were approximately 13 - 34% lower than experimental measurements, primarily due to the exclusion of the slurry phase, which contributes up to approximately 34% of total power draw in similar systems (Ndimande *et al.*, 2019). Increasing the coefficient of restitution from 0.2 to 0.6 produced a marked decrease in power dissipation, also in agreement with earlier findings, as less energy was lost per collision and the power required to sustain continuous particle motion decreased. Similarly, increasing the coefficient of friction from 0.1 to 0.3, while holding restitution constant at 0.2, reduced the power draw from 103 W to 100 W, which inferred that a relatively higher friction diminished particle mobility and reduces energy transfer efficiency. These results confirmed that DEM could reproduce realistic energy transfer trends and revealed the sensitivity of power draw to material contact parameters.

Although the DEM software supported the function of resolving stress and energy distribution data, multiple attempts to execute the required post processing script were unsuccessful. These technical issues prevented the generation of reliable stress mapping outputs, restricting the analysis to global energy and power responses only. As a result, the direct identification of localised wear prone regions could not be performed. Future work should therefore revisit this aspect using improved computational setups or updated scripts to enable extraction and visualisation of stress fields for detailed mapping of potential wear zones.

Grinding experiments conducted at specific energy inputs of 5, 10, and 20 kWh/t demonstrated that higher energy input produced progressively finer product sizes, confirming the direct relationship between energy input and grinding efficiency. Feed size was found to have a marked influence on mill power draw and energy consumption. The coarse feed (-1180 + 850 μm) exhibited consistently higher power draw and torque than the fine feed (-650 + 425 μm), reflecting increased resistance to motion with increased feed size at constant grinding media size. For the same milling duration, the coarse feed consumed more energy than the fine feed, primarily due to heightened energy losses associated with non-size reduction interactions and increased viscous resistance. Increasing mill speed further elevated both power draw and specific energy input, illustrating the sensitivity of energy demand to operating speed and feed characteristics.

Wear tests performed on the coarse feed condition for 2 h and 4 h revealed a clear increase in the mass of the -5 mm size fraction, highlighting measurable bead degradation due to wear. The wear rate profile showed an approximately linear relationship with milling time under the tested conditions. Although fine feed wear tests were deliberately excluded, the observed linear trend suggests that feed size, in combination with mill speed and specific energy input, directly governs both the rate and mechanism of wear in stirred media mills.

Collectively, these findings demonstrate that DEM is a valuable tool for exploring energy-transfer mechanisms and their link to grinding media wear behaviour. Notwithstanding simplifications and technical constraints, the study established fundamental relationships between energy input, contact parameters, and power dissipation, which provide a foundation for developing more predictive and experimentally validated wear models in stirred media milling.

5.2 Recommendations

The following suggestions are made for further study in light of the encouraging findings and the noted limitations.

5.2. 1 Enhance DEM simulations

Incorporating the slurry phase into the simulations is advised since it will yield a more comprehensive representation of the grinding environment. Incorporating energy dissipation related to the slurry would probably increase the power draw forecasts' accuracy and provide further information about the slurry's function in grinding media wear.

5.2. 2 Material characterization

The material characterisation of ceramic beads, particularly hardness and fracture toughness, should be the main emphasis of future research. These characteristics should be included in more complex wear models since they are essential for comprehending the behaviour of media wear.

5.2. 3 Integration of wear and breakage models

For a more comprehensive understanding of the grinding process, future work should aim to integrate both wear and breakage models in the DEM simulations. This would provide a holistic view of the milling process, considering both the mechanical degradation of grinding media and the size reduction of feed particles.

References

Altun, O., Benzer, H., & Enderle, U. (2013). Effects of operating parameters on the efficiency of dry stirred milling. *Minerals Engineering, 43-44*, 58-66.

Altun, O., Benzer, H., & Enderle, U. (2014). The effects of chamber diameter and stirrer design on dry horizontal stirred mill performance. *Minerals Engineering, 69*, 24-28.

Altun, O., Darılmaz, Ö., Karahan, E., Sert, T., Altun, D., Toprak, A., & Hür, A. (2023). Understanding HIGMill operation at copper regrind application; operating parameters, wear and mineral liberation. *Minerals Engineering, 191*, 1-15.

Becker, M., & Schwedes, J. (1999). Comminution of ceramics in stirred media mills and wear of grinding beads. *Powder Technology, 105*, 374-381.

Becker, M., Kwade, A., & Schwedes, J. (2001). Stress intensity in stirred media mills and its effect on specific energy requirement. *International Journal of Mineral Processing, 61*, 189-208.

Blecher, L., Kwade, A., & Schwedes, J. (1996). Motion and stress intensity of grinding beads in a stirred media mill. Part 1: Energy density distribution and motion of single grinding beads. *Powder Technology, 86*(1), 59-68.

Boikov, A., Savelev, R., Payor, V., & Potapov, A. (2021). Universal Approach for DEM Parameters Calibration of Bulk Materials. *MDPI*.

Bwalya, M. (2005). Using the Discrete Element Method to Guide the Modelling of Semi and Fully Autogenous Milling. Johannesburg: University of the Witwatersrand.

Bwalya, M., & Chimwani, N. (2020). Development of a more descriptive particle breakage probability model. *Minerals, 10*(8).

Cayirli, S., Gokcen, H. S., & Yuce, N. (2024). The impact of different stirrer designs and mill orientations on the grinding efficiency. *Powder Technology, 438*, 1-11.

Cleary, P. W. (1998). Predicting charge motion, power draw, segregation and wear in ball mills using discrete element methods. *Minerals Engineering, 11*(11), 1061-1080.

Cleary, P. W. (2001). Modelling comminution devices using DEM. *International Journal for Numerical and Analytical Methods in Geomechanics, 25*(1), 83-105.

Cleary, P. W., Sinnott, M. D., & Morrison, R. (2006). Analysis of stirred mill performance using DEM simulation: Part 2 - Coherent flow structures, liner stress, and wear, mixing and transport. *Minerals Engineering, 19*(15), 1551-1572.

Cleary, P. W., Sinnott, M. D., & Pereira, G. G. (2015). Computational prediction of performance for a full scale Isamill: Part 1 - Media motion and energy utilisation in a dry mill. *Minerals Engineering, 79*, 220-238.

Cundall, P. A. (1988). Formulation of a three-dimensional distinct element model: Part I. A scheme to detect and represent contacts in a system composed of many polyhedral blocks. *International Journal of Rock Mechanics and Mining Sciences & Geomechanics Abstracts, 25*(3), 107-116.

Cundall, P. A., & Strack, O. D. (1979). A discrete numerical model for granular assemblies. *Géotechnique, 29*(1), 47-65.

Curry, D. C., & Clermont, B. (2005). Improving the efficiency of fine grinding - Developments in ceramic media technology. *Minerals Engineering*, 1333-1338.

Dogan, C. P., & Hawk, J. A. (1999). Role of composition and microstructure in the abrasive wear of high-alumina ceramics. *Wear*, 1050-1058.

Edwards, G. C. (2016). Investigation of operating parameters in a vertical stirred mill. Cape Town: University of Cape Town.

Esteves, P. M., Mazzinghy, D. B., Galéry, R., & Machado, L. C. (2021). Industrial Vertical Stirred Mills Screw Liner Wear Profile Compared to Discrete Element Method Simulations. *Minerals, 11*(3).

Feng, Y. T. (2021). An energy-conserving contact theory for discrete element modelling of arbitrarily shaped particles: Contact volume based model and computational

issues. *Computational Methods in Applied Mechanics and Engineering, 373*, 113493.
Ford, E., & Naude, N. (2021). Investigating the effect on power draw and grinding performance when adding a shell liner to a vertical fluidised stirred media mill. *Minerals Engineering, 160*, 1-10.
Fraige, F. Y., Langston, P. A., & Chen, G. Z. (2008). Distinct element modelling of cubic particle packing and flow. *Powder Technology, 186*, 224-240.
Guo, W., Han, Y., Gao, P., & Tang, Z. (2022). Effect of operating conditions on the particle size distribution and specific energy input of fine grinding in a stirred mill: Modeling cumulative undersize distribution. *Minerals Engineering, 176*, 1-9.
Hassall, P., Nonnet, E., Keikkala, V., Komminaho, T., & Kotila, L. (2016). Ceramic bead behavior in ultra fine grinding mills. *Minerals Engineering, 98*, 232-239.
Jankovic, A. (2003). Variables affecting the fine grinding of minerals using stirred mills. *Minerals Engineering, 16*(3), 337-345.
Jayasundara, C. T., Yang, R. Y., Yu, A. B., & Curry, D. (2008). Discrete particle simulation of particle flow in IsaMill-Effect of grinding medium properties. *Chemical Engineering Journal, 135*(1), 103-112.
Johnson, K. L., Kendall, K., & Roberts, A. D. (1971). Surface energy and the contact of elastic solids. *Proceedings of the Royal Society of London A: Mathematical, Physical and Engineering Sciences, 324*, 301-313.
Joost, B., & Schwedes, J. (1996). Comminution of white fused alumina and wear of grinding beads in stirred media mills: Part II. Effect of operational parameters, grinding chamber geometry and beads hardness on the wear of grinding beads. *Ceramic Forum International, 73*, 69-76.
Kotzé, H. (2012). Selecting ceramic grinding media: Part 1 - Theory. *Chemical Engineering & Technology, 35*(11), 2051-2057.
Kotzé, H., & Bedesi, N. (2015). Selecting ceramic media: Part 2 - Evaluating the wear. *International Journal of Mineral Processing, 136*, 45-49.
Kwade, A., & Schwedes, J. (2007). Wet grinding in stirred media mills. In *Handbook of Powder Technology (Volume 12)* (pp. 253-381). Amsterdam: Elsevier.
Kwade, A., Blecher, L., & Schwedes, J. (1996). Motion and stress intensity of grinding beads in a stirred media mill. Part 2: Stress intensity and its effect on comminution. *Powder Technology, 81*(1), 69-76.
Lane, J. E., Metzger, P. T., & Wilkinson, R. A. (2010). A review of discrete element method (DEM) particle shapes and size distributions for lunar soil. Washington, D.C.: NASA.
Larsson, S., Pålsson, B. I., Parian, M., & Jonsén, P. (2020). A novel approach for modelling of physical interactions between slurry, grinding media, and mill structure in wet stirred media mills. *Minerals Engineering, 148*, 1-11.
Larsson, S., Rodríguez Prieto, J. M., Heiskari, H., & Jonsén, P. (2021). A novel particle-based approach for modeling a wet vertical stirred media mill. *Minerals, 11*(1), 1-19.
Lehto, H., Musuku, B., Keikkala, V., Kurki, P., & Paz, A. (2016). Developments in stirred media milling testwork and industrial scale performance of Outotec HIGmill. *Proceedings of the XXVII International Mineral Processing Congress* (pp. 1-19). Vancouver: Elsevier.
Lin, X., & Ng, T. T. (1997). A three-dimensional discrete element model using arrays of ellipsoids. *Geotechnique, 47*(2), 319-329.
Lisso, M. (2013). Evaluating the effect of operating variables on energy consumption in stirred mills. Cape Town: University of Cape Town.
Liu, Z., & Zhao, Y. (2020). Multi-super-ellipsoid model for non-spherical particles in DEM simulation. *Powder Technology, 361*, 190-202.
Liu, Z., Wang, S., Zhang, H., Chen, Z., Guo, J., Wu, S., . . . Huang, Q. (2024). Performance analysis of vertical stirred mill based on multi-coupling method. *Advanced Powder Technology, 35*.
Lu, G., Third, J. R., & Müller, C. R. (2015). Discrete element models for non-spherical particle systems: From theoretical developments to applications. *Chemical Engineering Science, 127*, 425-465.

Magamatha, K. A., Mulaba-Bafubiandi, A. F., Randigwane, A., Bolha, W., & Anyimadu, A. (2014). Evaluation of ceramic media wear characteristics on the M100 Isa Mill. *International Journal of Research in Chemical, Metallurgical and Civil Engineering, 1*(1), 66-70.

Mankosa, M. J., Adel, G. T., & Yoon, R. H. (1986). Effect of media size in stirred ball mill grinding of coal. *Powder Technology, 49*(1), 75-82.

Massola, C. P., Chaves, A. P., & Albertin, E. (2016). A discussion on the measurement of grinding media wear. *Journal of Materials Research and Technology, 5*(3), 282-288.

Mindlin, R. D. (1949). Compliance of elastic bodies in contact. *Journal of Applied Mechanics, 16*, 259-268.

Mishra, B. K. (2003). A review of computer simulation of tumbling mills by the discrete element method. *International Journal of Mineral Processing, 71*(1-2), 95-112.

Mishra, B. K., & Rajamani, R. K. (1992). The discrete element method for the simulation of ball mills. *Applied Mathematical Modelling, 16*(11), 598-604.

Moema, J. S., Papo, M. J., Slabbert, G. A., & Zimba, J. (2009). Grinding media quality assurance for the comminution of gold ores. *World Gold Conference* (pp. 27-34). Johannesburg: The Southern African Institute of Mining and Metallurgy.

Ndimande, C. B., Cleary, P. W., Mainza, A. N., & Sinnott, M. D. (2019). Using two-way coupled DEM-SPH to model an industrial scale Stirred Media Detritor. *Minerals Engineering, 137*, 259-276.

Nezami, E. G., Hashash, Y. M., Zhao, D., & Ghaboussi, J. (2004). A fast contact detection algorithm for 3-D discrete element method. *Computers and Geotechnics, 31*(6), 575-587.

Ohenoja, K., Illikainen, M., & Niinimäki, J. (2013). Effect of operational parameters and stress energies on the particle size distribution of TiO2 pigment in stirred media milling. *Powder Technology, 234*, 91-96.

Ohenoja, K., & Illikainen, M. (2015). Effect of operational parameters and stress energies on stirred media milling of talc. *Powder Technology, 283*, 254-259.

Radziszewski, P. (2002). Exploring total media wear. *Minerals Engineering, 15*(12), 1073-1087.

Radziszewski, P. (2013). Assessing the stirred mill design space. *Minerals Engineering, 41*, 9-16.

Reed, J. S. (1995). *Principles of Ceramics Processing* (2nd ed.). New York: John Wiley & Sons, Inc.

Rule, C. M., Knopjes, L., Clermont, B., & Philippe, C. (2008). Fine grinding-Developments in ceramic media technology and resulting improved plant performance at Anglo Platinum. *Third International Platinum Conference 'Platinum in Transformation'* (pp. 53-62). The Southern African Institute of Mining and Metallurgy.

Sadler, L. Y., Brooks, D. R., & Stanley, D. A. (1975). Attrition mill operating characteristics. *Powder Technology, 12*(1), 19-28.

Samukute, O. (2019). Using the DEM to relate Drop Ball Tests to Semi-Autogenous Grinding Mills. Johannesburg: University of the Witwatersrand.

Sinnott, M. D., Cleary, P. W., & Morrison, R. (2006). Analysis of stirred mill performance using DEM simulation: Part 1 - Media motion, energy consumption, and collisional environment. *Minerals Engineering, 19*(15), 1537-1550.

Taylor, L., Skuse, D., Blackburn, S., & Greenwood, R. (2020). Stirred media mills in the mining industry: Material grindability, energy-size relationships, and operating conditions. *Powder Technology, 369*, 1-16.

Theuerkauf, J., & Schwedes, J. (1999). Theoretical and experimental investigation on particle and fluid motion in stirred media mills. *Powder Technology, 105*, 406-412.

Toraman, Ö. Y., Teymen, A., Ersoy, O., & Köse, H. (2019). The effect of ceramic grinding media on stirred milling and experimental testing of media wear. *6th International Conference on Materials Science and Nanotechnology For Next Generation (MSNG 2019)* (pp. 241-244). Niğde: Niğde Ömer Halisdemir University.

Weber, U., & Langlois, D. (2010). The effect of grinding media performance on milling and operational behaviour. *The Journal of The Southern African Institute of Mining and Metallurgy, 110*(3), 147-154.

Williams, J. R., & O'Connor, R. (1995). A linear complexity intersection algorithm for discrete element simulation of arbitrary geometries. *Engineering Computations, 12*(2), 185-201.

Wills, B. A., & Napier-Munn, T. (2006). *Wills' mineral processing technology: An introduction to the practical aspects of ore treatment and mineral recovery* (7th ed.). Oxford: Butterworth-Heinemann.

Wu, T., Zhou, J., Wu, B., & Liu, J. (2016). Effect of rare-earth Lu2O3 on the wear resistance of alumina ceramics for grinding media. *Powder Technology, 303*, 27-32.

Wu, T., Zhou, J., Wu, B., & Xiong, Y. (2016). Effect of Y2O3 additives on the wet abrasion resistance of an alumina-based grinding medium. *Wear, 356-357*, 9-16.

Xie, C., & Zhao, Y. (2022). Investigation of the ball wear in a planetary mill by DEM simulation. *Powder Technology, 398*, 1-12.

Xie, C., Song, T., & Zhao, Y. (2020). Discrete element modeling and simulation of non-spherical particles using polyhedrons and super-ellipsoids. *Powder Technology, 368*, 253-267.

Yang, Y. (2018). A study of fine particle grinding in vertically stirred media mills via positron emission particle tracking technology and the discrete element method. Birmingham: University of Birmingham.

Yang, Y., Rowson, N. A., Tamblyn, R., & Ingram, A. (2017). Effect of operating parameters on fine particle grinding in a vertically stirred media mill. *Separation Science and Technology, 52*(6), 1143-1152.

Yeom, S. B., Ha, E.-S., Kim, M.-S., Jeong, S. H., Hwang, S.-J., & Choi, D. H. (2019). Application of the Discrete Element Method for Manufacturing Process Simulation in the Pharmaceutical Industry. *MDPI*.

Zhao, Y., Ma, H., Xu, L., & Zheng, J. (2017). An erosion model for the discrete element method. *Particuology, 34*, 81-88.

Zhao, Y., Xu, L., Umbanhowar, P. B., & Lueptow, R. M. (2019). Discrete element simulation of cylindrical particles using super-ellipsoids. *Particuology, 46*, 55-66.

Zhao, Z., Wu, M., & Jiang, X. (2024). A Review of Contact Models' Properties for Discrete Element Simulation in Agricultural Engineering. *MDPI*.

Appendices

APPENDIX A Experimental work

Additional information gathered during the course of the experimental work is presented in this section. Figure 5.1 shows images of the ceramic media utilised in the grinding tests.

Figure 5.1. Ceramic media used in the grinding tests.

Figure 5.2 presents the results of sieve analysis conducted on the dried sample after grinding test runs

	Grinding Result - Seive Analysis (mass retained,g)													
Test Numbe	Feed Size (µm)	Energy Input (kWh/t)	1180µm	850µm	600µm	425µm	300µm	212µm	150µm	106µn	75µm	53µm	38µm	Under 38µm
1	Mono-sized Tests -1180+	5,29	0,00	229,13	48,12	7,06	4,44	2,83	1,68	1,32	1,22	0,94	0,95	1,62
2	Mono-sized Tests -1180+	10,13	0,00	182,83	62,21	15,70	9,32	6,10	3,96	3,59	3,71	3,55	3,66	4,86
3	Mono-sized Tests -1180+	20,08	0,00	147,49	68,22	22,78	14,12	9,13	5,78	5,42	6,02	4,83	3,54	12,11
4	Mono-sized Tests -600+4	5,10	0,00	0,00	0,00	141,06	70,64	21,15	13,95	10,98	8,76	7,26	5,09	20,11
5	Mono-sized Tests -600+4	10,04	0,00	0,00	0,00	99,86	56,17	21,51	16,86	15,98	16,24	13,44	11,02	47,89
6	Mono-sized Tests -600+4	20,07	0,00	0,00	0,00	68,65	35,98	12,16	9,57	10,47	15,37	24,99	20,37	100,96

Figure 5.2. Sieve analysis results of the individual tests.

Figure 5.3 presents a sample of the grinding performance report that was generated by the stirred mill program at the end of grinding tests. This copy was for the coarse feed run at 5 kWh/t.

Date and Time	Relative time (sec)	Mill Torque_raw	Mill Torque_filtered	Mill Speed	Mass kg	Mill Power - instant	Energy - instant	Energy - Acc	Specific Energy - instant	Specific Energy - Acc
2024/02/28 08:25	2156,122	0,166314	0,017513	142	0,85	0,260523	0,000072	0,000072	0,000085	0,000085
2024/02/28 08:25	2157,122	2,498708	0,044486	281,551724	0,85	1,312152	0,000364	0,000437	0,000429	0,000514
2024/02/28 08:25	2158,123	2,691633	0,489361	401,517241	0,85	20,584344	0,005718	0,006155	0,006727	0,007241
2024/02/28 08:25	2159,123	2,465446	0,888926	266,862069	0,85	24,851686	0,006903	0,013058	0,008121	0,015362
2024/02/28 08:25	2160,123	2,119512	1,1747	188,517241	0,85	23,199658	0,006444	0,019502	0,007582	0,022944
2024/02/28 08:25	2161,123	2,622447	1,345966	362,344828	0,85	51,092769	0,014192	0,033695	0,016697	0,039641
2024/02/28 08:25	2162,123	3,102763	1,577352	403,965517	0,85	66,753866	0,018543	0,052237	0,021815	0,061456
2024/02/28 08:25	2163,123	2,944431	1,853862	401,517241	0,85	77,980329	0,021661	0,073899	0,025484	0,08694
2024/02/28 08:25	2164,123	2,884558	2,051549	403,965517	0,85	86,821957	0,024117	0,098016	0,028373	0,115313
2024/02/28 08:25	2165,123	2,845973	2,202548	403,965517	0,85	93,212258	0,025892	0,123908	0,030462	0,145774
2024/02/28 08:25	2166,123	2,794083	2,319181	403,965517	0,85	98,148199	0,027263	0,151172	0,032075	0,177849
2024/02/28 08:25	2167,123	2,746184	2,405266	403,965517	0,85	101,79134	0,028275	0,179447	0,033265	0,211114
2024/02/28 08:25	2168,123	2,724896	2,467064	403,965517	0,85	104,406642	0,029002	0,208449	0,03412	0,245234
2024/02/28 08:25	2169,123	2,696955	2,513801	403,965517	0,85	106,384562	0,029551	0,238	0,034766	0,28
2024/02/28 08:25	2170,123	2,673006	2,547001	403,965517	0,85	107,789603	0,029942	0,267942	0,035225	0,315225
2024/02/28 08:25	2171,123	2,675667	2,569842	403,965517	0,85	108,756228	0,03021	0,298152	0,035541	0,350767
2024/02/28 08:25	2172,123	2,662362	2,589025	403,965517	0,85	109,568048	0,030436	0,328587	0,035807	0,386573
2024/02/28 08:25	2173,123	2,65704	2,602319	403,965517	0,85	110,13064	0,030592	0,359179	0,03599	0,422564
2024/02/28 08:25	2174,123	2,646396	2,612238	403,965517	0,85	110,550426	0,030708	0,389888	0,036128	0,458691
2024/02/28 08:25	2175,123	2,65837	2,61843	403,965517	0,85	110,812461	0,030781	0,420669	0,036213	0,494904
2024/02/28 08:25	2176,124	2,642404	2,62567	403,965517	0,85	111,118861	0,030866	0,451535	0,036313	0,531218
2024/02/28 08:25	2177,124	2,65837	2,628706	403,965517	0,85	111,247354	0,030902	0,482437	0,036355	0,567573
2024/02/28 08:25	2178,124	2,65837	2,634083	403,965517	0,85	111,474921	0,030965	0,513402	0,03643	0,604003
2024/02/28 08:25	2179,124	2,63176	2,638486	403,965517	0,85	111,661237	0,031017	0,544419	0,036491	0,640493
2024/02/28 08:25	2180,124	2,626438	2,637267	403,965517	0,85	111,609642	0,031003	0,575422	0,036474	0,676967
2024/02/28 08:25	2181,124	2,627769	2,635304	403,965517	0,85	111,526573	0,03098	0,606402	0,036447	0,713414

Figure 5.3. A sample copy of grinding performance report.

Figure 5.4 to Figure 5.6 presents the time variation plots of all the tests conducted.

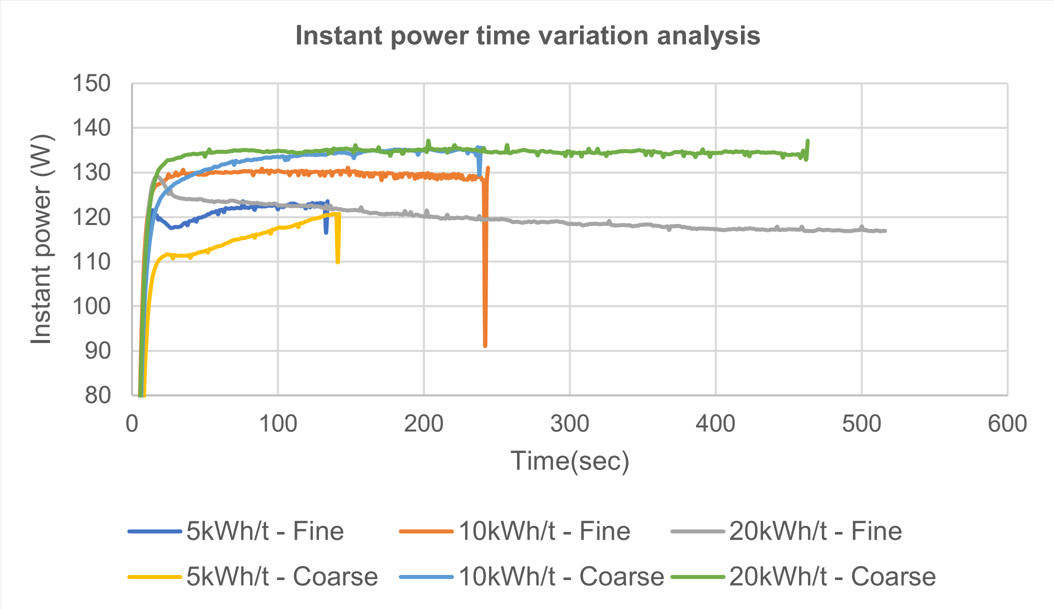

Figure 5.4. Instant power plots for all tests.

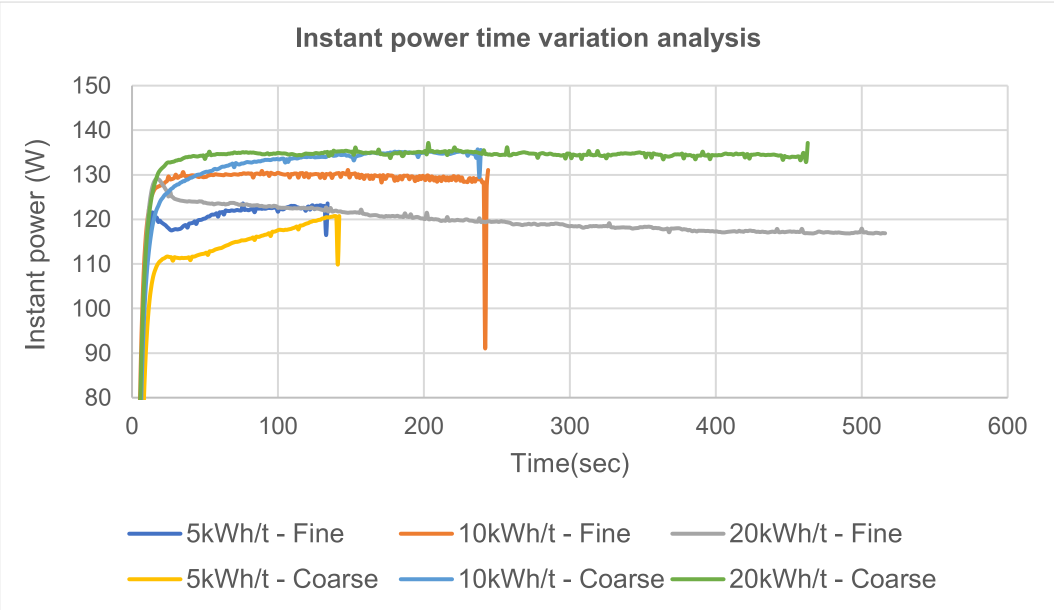

Figure 5.5. Instant torque plots for all tests.

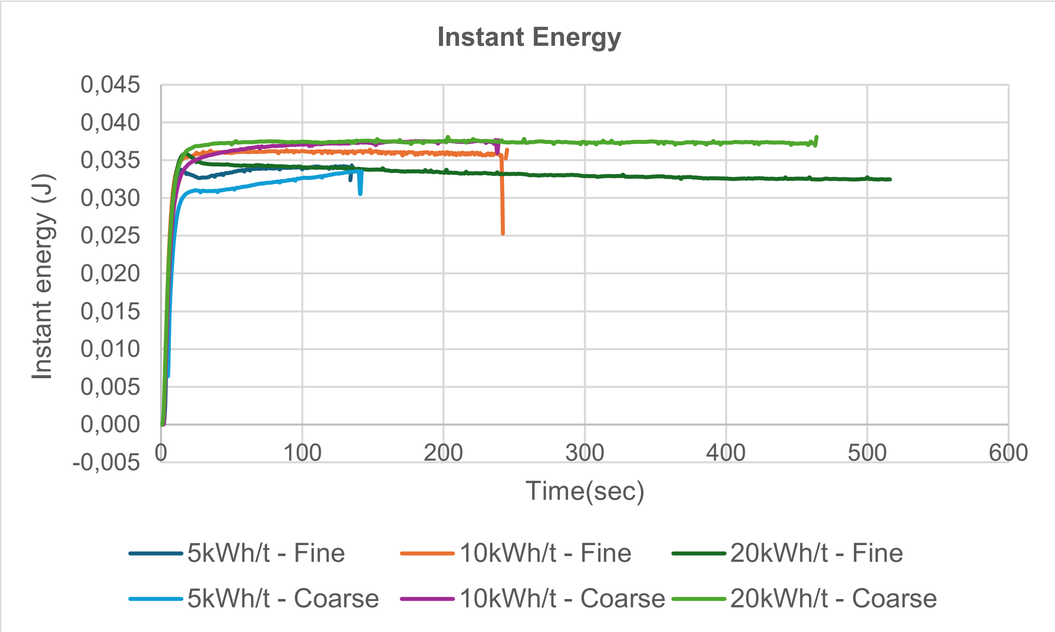

Figure 5.6. Instant energy plots for all tests.

APPENDIX B Simulation work

Figure 5.7 presents a sample of the simulation input script file defined by the user. The energy-sampling rate denotes the frequency at which energy values are sampled. The frame sampling rate determines the frequency at which frames are captured for the production of the animation video.

```
.180 ;Crusher diameter
0.224 ;Crusher height
0.026  ;Shaft diameter
0.186  ;Shaft length
0.12 ;Pin length
0.017 ;Pin diameter
4 ;Number of Pins
0.08325 ;Distance of uppermost pin from top
0.0245; Space distance between pin centres
90; Pin phase angle difference
404; Rotation Speed
7; Media mass
1.7; Feed sample mass
.006;.0132; Upper Media diameter
.004;.0112; Lower Media diameter
4000; Media density
.016;.0132; Upper Particle diameter
.014;.0112; Lower Particle diameter
2670; Particle density
0.05; Energy_scale
0.5 ;  Energy_Sampling rate( every sec)
0.5  ; Frame sampling rate ( every sec)
30   ;Expt Run Time in seconds
0.2  ; General coefficent of restitution
0.4     ;Ballfric
0.4      ;Wallfric
StirrExp1 ; fILE NAME
0     ; Type 0 for Demo and then 1 for actual simulation
```

Figure 5.7. DEM simulator input script file.

Figure 5.8 shows an example of the output file that records all collisions involving each ball, categorised into standard energy classifications. The data extracted from the output files can be loaded into MS Excel or other spreadsheet for analysis. Figure 5.9 depicts a sample of the generic file which captures energy class and number events.

```
Report for size,0.01600,0.01400,Speed,4.04000000000e+002,Speed,0


Delta Energy =,6.22473978119e-001

Time(s),Power(W),Totlss(W),Damplss(W),Frclss(W),Normlss(W),Tanglss(W)
1.00000000000e+000,3.40154485884e+000,9.95811828050e+001,9.95811828050e+001,0.00000000000e+000,9.95811828050e+001,0
2.00000000000e+000,2.90867211952e+000,7.97776977891e+001,7.97776977891e+001,0.00000000000e+000,7.97776977891e+001,0
3.00000000000e+000,3.20570596367e+000,7.36062811104e+001,7.36062811104e+001,0.00000000000e+000,7.36062811104e+001,0
4.00000000000e+000,3.19287887411e+000,9.53211400137e+001,9.53211400137e+001,0.00000000000e+000,9.53211400137e+001,0
5.00000000000e+000,3.95471026221e+000,7.61231502642e+001,7.61231502642e+001,0.00000000000e+000,7.61231502642e+001,0
6.00000000000e+000,4.28834911490e+000,7.57553798354e+001,7.57553798354e+001,0.00000000000e+000,7.57553798354e+001,0
7.00000000000e+000,2.93251319567e+000,1.00727777046e+002,1.00727777046e+002,0.00000000000e+000,1.00727777046e+002,0
8.00000000000e+000,3.91544578647e+000,6.71406604950e+001,6.71406604950e+001,0.00000000000e+000,6.71406604950e+001,0
9.00000000000e+000,2.76402363263e+000,6.57269598930e+001,6.57269598930e+001,0.00000000000e+000,6.57269598930e+001,0
1.00000000000e+001,2.62258496352e+000,7.52949901360e+001,7.52949901360e+001,0.00000000000e+000,7.52949901360e+001,0
1.10000000000e+001,3.98931304993e+000,1.25281584090e+002,1.25281584090e+002,0.00000000000e+000,1.25281584090e+002,0
1.20000000000e+001,3.22463536631e+000,6.44615974011e+001,6.44615974011e+001,0.00000000000e+000,6.44615974011e+001,0
1.30000000000e+001,3.22279964519e+000,6.84911971261e+001,6.84911971261e+001,0.00000000000e+000,6.84911971261e+001,0
1.40000000000e+001,2.93006823554e+000,7.70301670513e+001,7.70301670513e+001,0.00000000000e+000,7.70301670513e+001,0
1.50000000000e+001,2.70215406986e+000,8.18792211585e+001,8.18792211585e+001,0.00000000000e+000,8.18792211585e+001,0
1.60000000000e+001,3.15600625467e+000,9.67527258662e+001,9.67527258662e+001,0.00000000000e+000,9.67527258662e+001,0
1.70000000000e+001,3.23499002135e+000,8.42581347427e+001,8.42581347427e+001,0.00000000000e+000,8.42581347427e+001,0
1.80000000000e+001,4.19110163981e+000,8.36903702305e+001,8.36903702305e+001,0.00000000000e+000,8.36903702305e+001,0
```

Figure 5.8. Detailed output file.

```
joules ,Events
0,0
5.00000000000e-002,6548544
1.00000000000e-001,1693
1.50000000000e-001,695
2.00000000000e-001,386
2.50000000000e-001,252
3.00000000000e-001,188
3.50000000000e-001,133
4.00000000000e-001,114
4.50000000000e-001,91
5.00000000000e-001,86
5.50000000000e-001,61
6.00000000000e-001,56
6.50000000000e-001,34
7.00000000000e-001,25
7.50000000000e-001,37
8.00000000000e-001,20
8.50000000000e-001,23
9.00000000000e-001,22
9.50000000000e-001,15
1.00000000000e+000,28
1.05000000000e+000,14
1.10000000000e+000,11
1.15000000000e+000,18
1.20000000000e+000,6
1.25000000000e+000,7
1.30000000000e+000,7
```

Figure 5.9. Simulation generic file.